AD-A093 101 FLORIDA STATE UNIV TALLAHASSEE MESOSCALE AIR-SEA INT--ETC F/G 8/3
MIXING, CONVECTION, AND ADVECTION IN THE UPPER OCEAN.(U)
NOV 80 B CUSHMAN-ROISIN N00014-75-C-0201
UNCLASSIFIED 171 NL

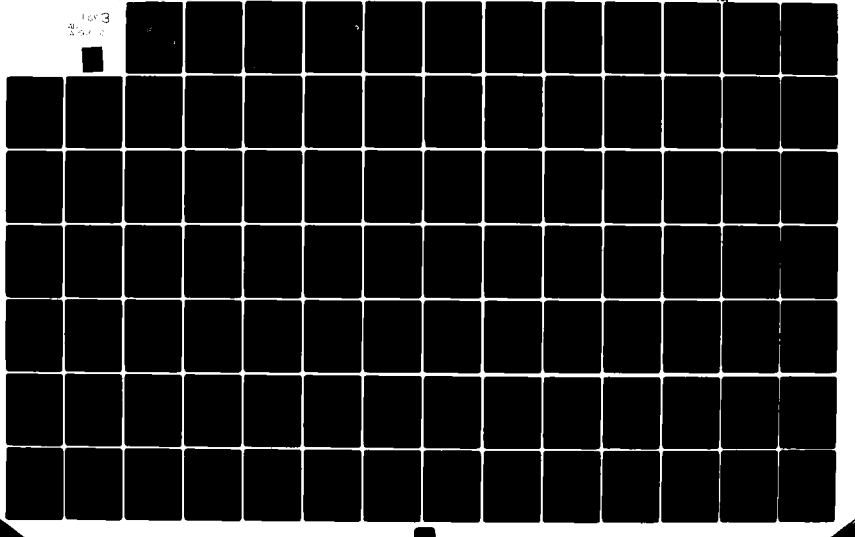

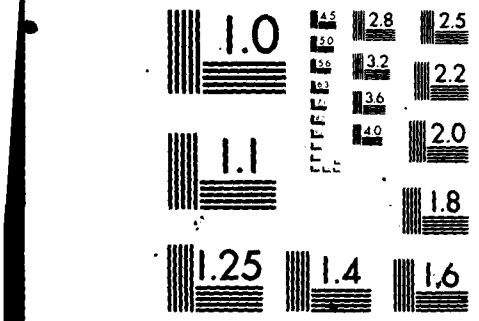

MICROCOPY RESOLUTION TEST CHART
NATIONAL BUREAU OF STANDARDS-1963-A

SECURITY CLASSIFICATION OF THIS PAGE (When Data Entered)

REPORT DOCUMENTATION PAGE

READ INSTRUCTIONS BEFORE COMPLETING FORM

1. REPORT NUMBER: 171
2. GOVT ACCESSION NO.: AD-A093 101
3. RECIPIENT'S CATALOG NUMBER: Doctoral Thesis

4. TITLE (and Subtitle): Mixing, Convection, and Advection in the Upper Ocean
5. TYPE OF REPORT & PERIOD COVERED: Technical Report
6. PERFORMING ORG. REPORT NUMBER:

7. AUTHOR(s): Benoit Cushman-Roisin
8. CONTRACT OR GRANT NUMBER(s): N00014-75-C-0201, N00014-80-C-0076

9. PERFORMING ORGANIZATION NAME AND ADDRESS: Florida State University, Departments of Meteorology and Oceanography, Tallahassee, Florida 32306
10. PROGRAM ELEMENT, PROJECT, TASK AREA & WORK UNIT NUMBERS: NR 083-231

11. CONTROLLING OFFICE NAME AND ADDRESS: Office of Naval Research, Code 481, NSTL Station, Mississippi 39529
12. REPORT DATE: November 1980
13. NUMBER OF PAGES: 195

14. MONITORING AGENCY NAME & ADDRESS (if different from Controlling Office)
15. SECURITY CLASS. (of this report): UNCLASSIFIED
15a. DECLASSIFICATION/DOWNGRADING SCHEDULE

LEVEL II

16. DISTRIBUTION STATEMENT (of this Report)

APPROVED FOR PUBLIC RELEASE. DISTRIBUTION OF THIS REPORT IS UNLIMITED.

17. DISTRIBUTION STATEMENT (of the abstract entered in Block 20, if different from Report)

DTIC ELECTE DEC 19 1980 S D

18. SUPPLEMENTARY NOTES

19. KEY WORDS (Continue on reverse side if necessary and identify by block number)

Convection, mixing, upper ocean
Thermals, mixed layer, thermocline,
Frontogenesis.

20. ABSTRACT (Continue on reverse side if necessary and identify by block number)

Convection, mixing and advection in the upper ocean may be thought of as the motion of two interacting fluids of different properties: the sinking fluid parcels generated near the surface and transmitting surface information downward, and the compensating rising return flow. A general theory based on this concept is developed and applied to various cases, including deepening of the wind-mixed layer, penetrative convection due to surface cooling, and upper ocean frontogenesis due to horizontal advection.

DD FORM 1 JAN 73 1473 EDITION OF 1 NOV 65 IS OBSOLETE S/N 0102-LF-014-6601

SECURITY CLASSIFICATION OF THIS PAGE (When Data Entered)

AD A093101

DTIC FILE COPY

SECURITY CLASSIFICATION OF THIS PAGE (When Data Entered)

20. ABSTRACT (Contd.)

Equations of the general theory are written for two interacting Boussinesq fluids in a rotating frame. Interaction terms are parameterized in order to apply the theory to geophysical situations. Considerable simplification is obtained by assuming that the response time of turbulence is much less than the time scale of evolution of the overall system. This assumption is realized in all geophysical situations and is a generalized statement based upon approximations invoked previously by various authors. The study of deepening of the wind-mixed layer and of penetrative convection due to surface cooling are straightforward applications of the general theory. The analytical treatment of the equations is simplified using the observations that the mixed layer is quasi-homogeneous in its physical properties and that the thermocline is a thin layer of large gradients. The solution is analytical and simple. Its agreement with observations is excellent and comparable to sophisticated numerical models capable of resolving small-scale turbulence. Advection and its interaction with mixing are studied in a case of frontogenesis. Interactions result in important cross-front asymmetries in properties such as mixed-layer depth, thermocline strength and/or mixed-layer density. Results also show that there exists a critical time scale within which mixing dominates and beyond which advection controls the upper ocean. For a mixed layer about one hundred meters thick, this time scale is of the order of one month. In the presence of strong mixing, frontolysis can ensue.

Although the applications focus on the upper ocean, the theory ~~is general~~ also applies to the lower atmosphere.

12

Mesoscale Air-Sea Interaction Group

Technical Report

MIXING, CONVECTION, AND ADVECTION IN THE UPPER OCEAN

BY

BENOIT CUSHMAN—ROISIN

Geophysical Fluid Dynamics Institute

Florida State University

Tallahassee, Florida 32306

NOVEMBER 1980

ONR Contract N00014-75-C-0201

ONR Contract N00014-80-C-0076

12

Mixing, Convection, and Advection

In the Upper Ocean

by

Benoit Cushman-Roisin

Geophysical Fluid Dynamics Institute
Florida State University
Tallahassee, Florida 32306

Technical Report
Mesoscale Air-Sea Interaction Group

November 1980

ONR Contract N00014-75-C-0201 and

ONR Contract N00014-80-C-0076

FOREWORD

The problem of predicting the deepening of a turbulent, weakly-stratified fluid has significant applications in oceanography and meteorology. Both the atmospheric boundary layer and the upper ocean can deepen due to convective penetration. The action of the windstress on the ocean can deepen the mixed layer. The literature in these problems is vast and complicated.

In this Ph.D. dissertation, an unusual but fruitful approach is adopted. Two interacting fluids are envisioned. This formulism allows the analytical interpretation of the penetrative convection problem and the wind mixing problem. The comparison of the results with laboratory experiments is very encouraging. The detailed profiles of turbulent fluxes need to be compared to actual field measurements. Some data are available but were not accessible to us. The theoretical results in this report are a major advance in understanding the physics of the ocean.

Ocean modellers have continually ignored the influence of horizontal structure on the dynamics of convective fluids. A small step forward has been accomplished in the final problem where the wind mixing occurs in the vicinity of an oceanic front. The conclusions are useful for understanding ocean variability due to wind mixing on ocean fronts.

Finally, the reader will find a tremendous amount of redundancy in this report. This was my decision. The report is written such that each major chapter is written as a separate paper for subsequent submission to a journal.

James J. O'Brien
Director
Mesoscale Air-Sea Interaction Group

ABSTRACT

MIXING, CONVECTION, AND ADVECTION
IN THE UPPER OCEAN

Convection, mixing and advection in the upper ocean may be thought of as the motion of two interacting fluids of different properties: the sinking fluid parcels generated near the surface and transmitting surface information downward, and the compensating rising return flow. A general theory based on this concept is developed and applied to various cases, including deepening of the wind-mixed layer, penetrative convection due to surface cooling, and upper-ocean frontogensis due to horizontal advection.

Equations of the general theory are written for two interacting Boussinesq fluids in a rotating frame. Interaction terms are parametrized in order to apply the theory to geophysical situations. Considerable simplification is obtained by assuming that the response time of turbulence is much less than the time scale of evolution of the overall system. This assumption is realized in all geophysical situations and is a generalized statement based upon approximations invoked previously by

various authors. The study of deepening of the wind-mixed layer and of penetrative convection due to surface cooling are straightforward applications of the general theory. The analytical treatment of the equations is simplified using the observations that the mixed layer is quasi-homogeneous in its physical properties and that the thermocline is a thin layer of large gradients. The solution is analytical and simple. Its agreement with observations is excellent and comparable to sophisticated numerical models capable of resolving small-scale turbulence. Advection and its interaction with mixing are studied in a case of frontogenesis. Interactions result in important cross-front asymmetries in properties such as mixed-layer depth, thermocline strength and/or mixed-layer density. Results also show that there exists a critical time scale within which mixing dominates and beyond which advection controls the upper ocean. For a mixed layer about one hundred meters thick, this time scale is of the order of one month. In the presence of strong mixing, frontolysis can ensue.

Although the applications focus on the upper ocean, the theory is general and also applies to the lower atmosphere.

à Mary,

pour son intarissable support

Entends le son des vagues.
Ecoute le message de la mer:
Turbulence et calme se succèdent,
Mais le navire arrivera à bon port.

ACKNOWLEDGEMENTS

This work was supported by the Office of Naval Research, Ocean Science and Technology Branch, under contract No. N00014-80-C-0076. Partial support was provided by the Belgian American Educational Foundation through a CRB Fellowship.

The author wishes to express his deep gratitude to Dr. James J. O'Brien for serving as major professor and without whom this dissertation would not have been a reality. His support, encouragements, and comments were appreciated throughout the course of this research. Sincere thanks go to Drs. Albert Barcilon, Phil Hsueh, David Loper, and Christopher Tam for their helpful suggestions and comments and for serving on the doctoral committee.

The author also wishes to thank Drs. Willem Malkus, Pearn Niiler, Steven Piacsek, and Gunnar Roden, with whom he had fruitful discussions. Thanks are extended to the audiences of talks presented by the author at various oceanographic institutions, from which emerged helpful remarks.

Profound gratitude goes to Mary Cushman-Roisin who commented on the text during its preparation. Sincere appreciation is extended to Ms. Pat Heaton, who typed the manuscript, and to Mr. Dewey Rudd, who drafted the figures. Thanks go to Mrs. Ruth Pryor for her typing assistance during the final phase of manuscript completion.

TABLE OF CONTENTS

LIST OF TABLES

LIST OF ILLUSTRATIONS

Figure 14. Sketch of penetrative convection in the upper ocean due to surface cooling by an imposed heat flux Q. In the mixed layer, the mean temperature $\bar{T}$ is almost constant, while the convective heat flux $\overline{wT}$ decreases with depth. In the thermocline, $\bar{T}$ varies sharply, while $\overline{wT}$ increases rapidly. The neutral level is the level where thermals and anti-thermals have the same temperature. The dotted curve is the mean-temperature profile at a later time, showing the cooling in the mixed layer and the heating in the thermocline.

Figure 15. Plots of the coefficients ϵ and A defined by (50) and (58), ϵ is the ratio $\bar{T}/(-\Gamma h)$, and A is the ratio $-(\overline{wT})_{-h}/Q$.

Figures 16a and b (a) Dimensionless vertical velocity variance and (b) dimensionless vertical turbulent flux of vertical heat flux near the surface, for $(1-mD)/\kappa m=5$ and $2m=0.64$. Dots correspond to atmospheric observations presented by Wyngaard, *et al.* (1971).

Figure 17. Vertical profile of the rms vertical velocity, scaled by $-w_*$.

Figure 18. Vertical profiles of the vertical-velocity variance, $\overline{w^2}$, scaled by w_*^2. The solid curve is the solution of the present model. The dashed curve is the numerical solution of Zeman and Lumley (1976). The dots represent the data of Willis and Deardorff (1974), run S1.

Figure 19. Vertical profiles of the vertical flux of turbulent kinetic energy, $-\frac{1}{2}\overline{ww^2}$, scaled by w_*^3. The solid curve is the solution of the present model. The dashed curve is the numerical solution of Zeman and Lumley (1976). The dots represent the data of Willis and Deardorff (1974), run S1.

Figure 20. Vertical profiles of the temperature variance, $\overline{(T-\bar{T})^2}$, scaled by $(u_*/Q)^2$. The solid curve is the solution of the present model. The dashed curve is the solution of Zeman and Lumley (1976). The dots represent the data of Willis and Deardorff (1974), run S1.

Figure 21. Vertical profile of the mean temperature, $\bar{T}$, scaled by Γh.

LIST OF SYMBOLS

Symbol	Meaning	Dim.	Remark
a	Any physical quantity (Chap.2)	-	
	or Mixing parameter (Chap.5)	1	>0
A	Ratio of heat flux at the bottom of the mixed layer to surface heat flux	1	>0
b	Buoyancy: $b = g(-\alpha T+\beta S)$	LT^{-2}	
b_o	Reference buoyancy	LT^{-2}	constant
b_-	Buoyancy in the stratified fluid	LT^{-2}	
B	Total mixed-layer buoyancy (Chap.3 & 4)	L^2T^{-2}	
	or Scale for $\bar{b}-b_o$ and b_--b_o (Chap.5)	LT^{-2}	
$\mathcal{B}$	Maximum vertical buoyancy flux	L^2T^{-3}	
c	Any physical quantity	-	
D	Rate of dissipation (Chap.3)	ML^2T^{-3}	
	or Dissipation coefficient (Chap.4)	1	>0
DIM	Dynamic Instability Model	-	
E	Volume exchange (Chap.2)	T^{-1}	>0 or <0
	or Dimensionless rate of entrainment (Chap. 3 & 4)	1	
E_m	Mass exchange	$ML^{-3}T^{-1}$	>0 or <0
f	Fraction of area occupied by thermals to the total area	1	0<f<1
f_o	Coriolis parameter	T^{-1}	
F_s	TKE flux at the surface	ML^2T^{-3}	
F_h	TKE flux at the bottom of thermocline	ML^2T^{-3}	
g	Acceleration of gravity	LT^{-2}	constant
h	Mixed-layer depth	L	

h_o	Initial mixed-layer depth	L
$\dot{h}$	Rate of entrainment of stratified fluid in the mixed layer	LT^{-1}
H	Scale for the mixed-layer depth and z	L
$\underset{\sim}{k}$	Vertical unit vector, pointing upward	1
KE	Total Kinetic Energy	ML^2T^{-2}
ℓ	Monin-Obukov length: $\ell=u_*^3/\kappa B$	L
L	Horizontal length scale	L
m	$m = \frac{1}{2}(1-2f)\left(f(1-f)\right)^{\frac{1}{2}}$	1
MKE	Total Mean Kinetic Energy	ML^2T^{-2}
$\underset{\sim}{n}$	Horizontal components of the outward unit normal to Σ	1
n_z	Vertical component of the outward unit vector to Σ	1
N	Brunt-Väisälä frequency in the stratified fluid: $N^2=\alpha g\Gamma$	T^{-1}
p	Pressure	$ML^{-1}T^{-1}$
PE	Total Potential Energy	ML^2T^{-2}
Q	Kinematic surface heat flux: $Q=\overline{wT}\|_{surf}$	KLT^{-1} >0 upward
Ri	Frictional Richardson number $Ri=B/u_*^2$ (Chap.3), $Ri=B/w_*^2$ (Chap.4)	1
Ro	Rossby number: $Ro=V/f_oL$ (Chap.5)	1
Rv	Overall Richardson number $Rv=B/(U^2+V^2)$ (Chap.3)	1
S	Sum of contributions to TKE budget (Chap.2)	ML^2T^{-3}
	or Salinity (Chap.5)	S
t	Time variable	T
T	Temperature, as in $T', T'', \overline{T}, T_{rms}$	K
	or Depth-independent part of $\overline{T}/\Gamma$	L

T_o	Reference temperature	K	constant
$\tilde{T}$	T_{rms}/Γ	L	
TEM	Turbulent Erosion Model	-	
TKE	Total Turbulent Kinetic Energy	ML^2T^{-2}	
u	Horizontal velocity in the x-direction, as in $u', u'', \bar{u}, u_{rms}$	LT^{-1}	
u_*	Friction velocity	LT^{-1}	>0
$\tilde{u}$	u_{rms}	LT^{-1}	
U	Depth-independent part of $\bar{u}$ (Chap.3)	LT^{-1}	
	or Scale for $\bar{u}$ (Chap.5)	LT^{-1}	
U_*	Scale for u_*	LT^{-1}	
v	Horizontal velocity in the y-direction	LT^{-1}	
$\tilde{v}$	v_{rms}	LT^{-1}	
V	Total volume of the system (Chap.2)	L^3	
	or Depth-independent part of $\bar{v}$ (Chap.3)	LT^{-1}	
	or Scale for $\bar{v}$ (Chap.5)	LT^{-1}	
w	Vertical velocity, as in $w', w'', \bar{w}, w_{rms}$	LT^{-1}	
w_{Ek}	Ekman vertical velocity in stratum	LT^{-1}	
$\tilde{w}$	$-w_{rms}$	LT^{-1}	
W	Scale for $\bar{w}$ and w_{Ek}	LT^{-1}	
x	(Long-front) horizontal coordinate	L	
y	(Cross-front) horizontal coordinate	L	
z	Vertical upward coordinate	L	
α	Coefficient of thermal expansion	K^{-1}	
β	Coefficient of salinity contraction	S^{-1}	
Γ	Vertical temperature gradient in the stratified fluid	KL^{-1}	

Γ_2	Initial horizontal buoyancy gradient	T^{-2}	
Γ_3	Initial vertical buoyancy gradient	T^{-2}	
δ	Friction force in the vert. mom. eqn.	LT^{-2}	
$\delta\xi$	Dimensionless thickness of thermocline	1	
ΔT	Temperature jump across the thermocline	K	
$\Delta\rho$	Density jump across the thermocline	ML^{-3}	
$\underset{\sim}{\nabla}_H$	Two-dimensional gradient operator	L^{-1}	
ε	Coefficient of proportionality between T and h: $T=\varepsilon h$	1	
η	Similarity coordinate near surface: $\eta=-z/\ell$	1	$\eta \geq 0$
κ	Von Kármán constant	1	constant
ν_T	Eddy heat diffusivity	L^2T^{-1}	
ν_u	Eddy viscosity in the x-direction	L^2T^{-1}	
ν_v	Eddy viscosity in the y-direction	L^2T^{-1}	
ξ	Similarity variable: $\xi=-z/h$	1	$0 \leq \xi \leq 1$
ρ	Density	ML^{-3}	
ρ_o	Reference density	ML^{-3}	constant
Σ	The closed surface bounding the system	-	
τ	Dimensionless τ_x	1	
τ_x	Wind-stress in the x-direction	$ML^{-1}T^{-2}$	
τ_y	Wind-stress in the y-direction	$ML^{-1}T^{-2}$	
$(...)'$	Quantity refering to thermals	-	
$(...)''$	Quantity refering to anti-thermals	-	
$\overline{(...)}$	Mean quantity	-	
$(...)_{rms}$	Root-mean-square fluctuation	-	>0 or <0

CHAPTER ONE

INTRODUCTION

Air-sea interactions cannot be successfully modelled without a deep knowledge of the upper-ocean dynamics and thermodynamics. The currents and variations of temperature and salinity in the upper ocean are induced and controlled by surface atmospheric conditions, oceanic lateral advection, and deep oceanic conditions. The complexity of the situation can, however, be somewhat simplified by classifying the various processes which take place in the upper ocean. They are: turbulent mixing by wind stirring or mean current shear, convection, penetrative convection, entrainment of stratified fluid, and re-stratification. All these processes involve small-scale turbulent motions, in space as well as in time. In this work, the resulting fine structure is studied in order to achieve a better knowledge of the dynamics and thermodynamics in the upper ocean.

Upper-ocean processes can be thought of as the relative motion of two interacting fluids: the sinking fluid parcels generated near the surface and transmitting surface information downward and the rising fluid parcels forming the return flow. The former play the active role in mixing and convection, and are called *thermals*. The latter play the alternate passive role and are called *anti-thermals*. A general theory based on this concept is developed and applied to various cases, including deepening of the wind-mixed layer, penetrative convection due to surface cooling, and upper-ocean frontogenesis due to horizontal advection.

The work is divided into several chapters (Chapters 2 to 5), each of them being a discrete and independent entity. As an advantage, the reader interested in one specific topic may limit his/her reading to a particular chapter without facing problems understanding symbols or basic ideas. Despite advantages, this presentation leads to some unavoidable repetition, for which the author apologizes.

Chapter two is the development of the general theory of mixing and convection, based on the concept of a two-fluid system. It is an application of the dynamical theory of interacting continua proposed by Kelly (1964), developed by Green and Naghdi (1965), and generalized by Truesdell (1969). The equations are written for two interacting Boussinesq fluids in a rotating frame. Interaction terms are parametrized for the purpose of geophysical situations. Pairs of governing equations are derived for thermals and anti-thermals. Each pair meets an Invariance Principle as a consequence of reciprocity in the roles played by thermals and anti-thermals. Considerable simplification is obtained by assuming that the response time of turbulence is much less than the time scale of evolution of the overall system. This assumption is realized in all geophysical situations. Each pair of governing equations is transformed into an average equation for which interaction terms cancel, combined with a very simple equation linking the two fluid properties. An important parameter of the model is the fraction, f, of area occupied by thermals. Since a closure assumption is needed, a dynamic saturation equilibrium between thermals and anti-thermals is assumed. This implies a constant value of f throughout the convective layer.

Chapter three is the application of the theory to the deepening of the wind-mixed layer. In view of simple algebra, the model is one-dimensional, frictionless, and neglects the turbulence production by the mean-flow shear in the thermocline. Hence, the increase in potential energy required for deepening is supplied by the turbulence input at the surface. The analytical treatment of the equations is simplified using the well-known facts that the mixed layer is quasi-homogeneous and that the thermocline is a thin layer of large gradients. The vertical structure throughout the mixed layer and thermocline is given by an analytical solution. Vertical profiles of mean velocity components, mean temperature, and vertical fluxes of momentum and heat are then plotted. The solution also yields bulk formulae predicting the rate of deepening, the thermocline thickness, and the mean surface temperature. As the mixed layer deepens, the thermocline shallows, vertical profiles, therefore do not remain similar to themselves in time. The analytical solution is not self-similar.

Chapter four is the application of the theory to penetrative convection due to surface cooling, as it occurs past mid-fall and during winter. The model is still one-dimensional, but includes dissipation. Wind stirring plays an important role when the convective layer is shallow, but rapidly convection dominates the process. Thermal instability itself supplies the kinetic energy required for stirring and deepening. Wind stirring is therefore ignored in that section. Assuming a quasi-homogeneous mixed layer and a sharp thermocline, a single non-similar analytical solution is found. Vertical profiles of mean values and vertical fluxes

are plotted for the mixed layer and the thermocline. The solution also yields bulk formulae predicting the rate of deepening, the mean surface temperature, the heat flux at the bottom of the mixed layer and the thermocline thickness. Although the results presented here focus on convection in the upper ocean forced by surface cooling, they also apply directly to convection in the atmospheric boundary layer above a heated ground.

Chapter five is a study of advective effects and their interactions with wind-mixing effects. A case of frontogenesis is chosen in order to include lateral variations in advection and mixing and in order to understand better frontal dynamics of the large-scale oceanic fronts in the central North Pacific. Interactions between advection and mixing result in important cross-front asymmetries in properties such as mixed-layer depth, pycnocline strength, and/or mixed-layer density. Two cases are treated separately: the case of convergence (when the water masses downwell at the front) and the case of confluence (when the water masses form a long-front current).

CHAPTER TWO

A GENERAL THEORY OF MIXING AND CONVECTION: MODELLING BY TWO BUOYANT INTERACTING FLUIDS

1. INTRODUCTION

Convection may be caused by either an initially unstable situation or by a continuously-applied external forcing. In most geophysical convective situations, convection is of the latter kind and is maintained by a forcing which is almost invariably applied along one boundary rather than within the fluid. The theory developed here attempts to model convection when convective motions are driven under such circumstances. Convection of air above a heated ground, mixing of the upper ocean under the action of wind stress and/or surface cooling, and penetrative convection in stars are some examples.

Along the boundary where the forcing is applied, fluid particles coming from the interior are altered; their velocity components and/or temperature are modified. The same particles thus leave the boundary with new properties. As a consequence of this mechanism, convection can be thought of as the relative motion of two different fluids: the fluid particles coming from the interior toward the boundary, and the altered fluid particles leaving that boundary with different properties. The latter play the active role in convection and will be called *thermals*. This name was adopted by glider pilots for masses of warm air rising from hot ground. Ever since, this word has been widely used in the field of convection. The other fluid parcels play an alternate passive role and will be called *anti-thermals*.

The model presented here does not require interpreting thermals and anti-thermals as discrete elements. Particles will not be numbered nor will they be assigned a volume. The two fluids may be considered like plumes, puffs or other forms (Scorer, 1978). However, the terminology of thermals and anti-thermals is used for convenience because discrete elements are more easily perceived. As a formal extension, the word thermal will be even assigned arbitrarily to non-buoyant fluid having an excess of momentum.

Priestley (1959) has shown how one can obtain information about the mean properties and the fluctuations in air over a heated ground by considering it as the superposition of many closely-spaced convecting elements. However, his approach is limited to environmental lapse rate constant with height and does not allow the elements to grow or decrease as they migrate vertically.

The model developed here is an extension of the dynamical theory of interacting continua proposed by Kelly (1964) and Green and Naghdi (1965), and extended by Truesdell (1969). For the present purpose, equations are written for a two-fluid continuum in a rotating frame. The Boussinesq approximations are made (Spiegel and Veronis, 1960), and interaction terms are parametrized in view of geophysical situations.

The forcing along the boundary generates thermals at the expense of anti-thermals, whereas interactions between the two fluids in the interior progressively transform thermals back to anti-thermals. Thermals are directly driven by the external forcing, while anti-thermals are driven by reaction to the thermals

(continuity of mass, conservation of momentum and heat). The two fluids have different properties; their relative motion is thus a mechanism capable of transferring heat, momentum, energy, or any other constituent, through the convective layer.

2. FRACTION OF AREA OCCUPIED BY THERMALS

At a given level, any horizontal surface is crossed by thermals and anti-thermals. At a given time, a given horizontal area A is occupied partly by thermals and partly by anti-thermals (Figure 1). From a hypothetical instant infra-red picture detecting warm and cold regions, one may compute the fraction of area occupied by thermals for that surface at that time. That value inevitably varies in a certain range, and a theoretical ensemble average yields, in a statistical sense, a local instantaneous mean value. If one evokes the hypothesis of ergodicity, this averaging process is equivalent to an average over horizontal distances and time intervals short compared to lateral and temporal scales of variation characterizing the whole system. The resulting quantity, noted as f, is dimensionless, positive and less than unity (Manton, 1975). As a direct result, the fraction of area available to anti-thermals is (1-f). Although it is anticipated that f will be assumed to be a constant, the governing equations derived hereafter are written in a general framework, allowing local and temporal variations of f.

The observed mean value of any quantity is a combination of contributions due to the two fluids in the ratio of their respective

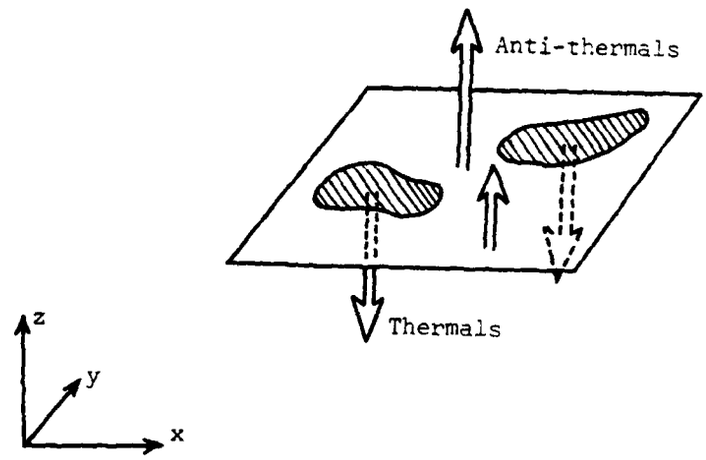

Figure 1. The fraction of area occupied by thermals at any level is the instantaneous local value, averaged over horizontal distances and time intervals short compared to lateral and temporal scales of variation of the overall system.

available areas:

horizontal velocity $\overline{u} = fu' + (1-f)u''$, (1)

$\overline{v} = fv' + (1-f)v''$, (2)

vertical velocity $\overline{w} = fw' + (1-f)w''$, (3)

pressure $\overline{p} = fp' + (1-f)p''$, (4)

density $\overline{\rho} = f\rho' + (1-f)\rho''$, (5)

temperature $\overline{T} = fT' + (1-f)T''$, (6)

where primed and double-primed quantities refer to thermals and anti-thermals, respectively. The bar thus represents an operator averaging over short horizontal distances and short time intervals in the sense defined previously. It indirectly assumes that each fluid is characterized by single values rather than by distribution functions of their properties.

The above relations, rather than a definition of mean values, constitute the mathematical expression of the average operator:

$$\overline{a} = fa' + (1-f)a'',$$

where a represents any physical quantity. The application of this operator may also define momentum, heat and energy fluxes. In the context of Boussinesq approximations, the vertical fluxes of horizontal momentum (Reynolds stresses divided by ρ_o, the reference density) are:

$$-\overline{uw} = -fu'w' - (1-f)u''w'', \quad (7)$$

$$-\overline{vw} = -fv'w' - (1-f)v''w'', \quad (8)$$

the kinematic vertical convective heat flux (heat flux divided by $\rho_o C_p$) has the form:

$$\overline{wT} = fw'T' + (1-f)w''T'', \tag{9}$$

and the vertical flux of turbulent kinetic energy reads:

$$\begin{aligned} &\tfrac{1}{2}\,\overline{w\left((u-\bar{u})^2+(v-\bar{v})^2+(w-\bar{w})^2\right)} \\ &= \tfrac{1}{2}fw'\left((u'-\bar{u})^2+(v'-\bar{v})^2+(w'-\bar{w})^2\right) \\ &+ \tfrac{1}{2}(1-f)w''\left((u''-\bar{u})^2+(v''-\bar{v})^2+(w''-\bar{w})^2\right). \end{aligned} \tag{10}$$

Other fluxes may be defined in an analogous way but are not of primary importance to geophysical convection problems.

Finally, the averaging operator may also be used to define root-mean-square (rms) quantities, measuring departures from mean values. If a represents any physical quantity, the rms fluctuation is defined as:

$$a_{rms} = \pm\,\overline{(a-\bar{a})^2}^{\,\frac{1}{2}}, \tag{11}$$

i.e.,
$$a_{rms}^2 = f(a'-\bar{a})^2 + (1-f)(a''-\bar{a})^2. \tag{12}$$

Simple calculations yield:

$$a_{rms} = \left(\frac{f}{1-f}\right)^{\frac{1}{2}}(a'-\bar{a}) = -\left(\frac{1-f}{f}\right)^{\frac{1}{2}}(a''-\bar{a}) \tag{13}$$

$$= \left(f(1-f)\right)^{\frac{1}{2}}(a'-a''). \tag{14}$$

The sign is selected as to yield a positive value when the thermals quantity a' exceeds the mean value $\bar{a}$. The rms fluctuation is directly proportional to the difference between thermals and anti-thermals values, and is zero when these values are equal and do not

differ from the mean.

3. MASS AND VOLUME EXCHANGES BETWEEN THERMALS AND ANTI-THERMALS

Thermals and anti-thermals continuously exchange mass and, consequently, momentum, heat, and energy. At any moment and at any location, either thermals or anti-thermals lose some of their mass to the other. The exchange is controlled by E_m, the *mass* exchange per unit time and total volume of fluid (kg $m^{-3}s^{-1}$). However, in the Boussinesq framework, that quantity is advantageously replaced by the *volume* exchange, E, per unit time and total volume (s^{-1}) defined as:

$$E = \frac{E_m}{\rho_o} , \qquad (15)$$

where ρ_o is the reference density close to the actual densities of thermals and anti-thermals, ρ' and ρ'', respectively. By definition, the mass exchange, E_m, is chosen to be positive if anti-thermals lose mass to thermals and is negative if thermals lose mass to anti-thermals.

In subsequent sections, it will be assumed that heat and momentum are transferred exclusively through this mass exchange, thus excluding transfer by diffusion or collision. However, this assumption may be questionable for highly turbulent clouds, where momentum exchange between air masses can occur without mass exchange, as in a collision.

4. INVARIANCE PRINCIPLE

From a semantic point of view, thermals and anti-thermals play reciprocal roles: what is lost by one is gained by the other. Thermals may be labelled anti-thermals and vice-versa. Their dynamics and thermodynamics are therefore to be governed by corresponding equations and the following Invariance Principle must hold:

Principle: All the governing equations must be invariant under the transformation:

primed quantity	$\longleftrightarrow$ double-primed quantity
f	$\longleftrightarrow$ $1-f$
E	$\longleftrightarrow$ $-E$
rms fluctuation	$\longleftrightarrow$ -rms fluctuation.

It may easily be seen that any mean quantity such as $\overline{u}$, $-\overline{uw}$, $\overline{wT}$, ... is invariant under that transformation, and equations for mean values will thus automatically meet the Invariance Principle.

5. GOVERNING EQUATIONS

The dynamics and thermodynamics of two interacting fluids are parts of the mathematical theory of mixtures. This latter theory aims to represent exchanges of mass, momentum, heat, and energy. Particular cases are theories of diffusion and chemical homogeneous reactions and kinetic theories of heterogeneous continua. A general framework for all such theories has been laid down by Kelly (1964),

Green and Naghdi (1965), and Truesdell (1969, Lecture 5) so as to include magnetohydrodynamic and other effects. Here, the governing equations are written for a two-fluid Boussinesq rotating continuum. Moreover, interaction terms are parametrized in view of geophysical situations.

a) Preliminary remark:

Thermals and anti-thermals have relatively large vertical velocities. Due to these sinking or rising motions, they do not have time nor do they go far enough laterally to be affected by temporal and horizontal variations in the overall system. As a result, in any equation, operators such as

$$\frac{\partial}{\partial t}(fa'),\ \frac{\partial}{\partial x}(fu'a'),\ \frac{\partial}{\partial y}(fv'a'),\ \frac{\partial}{\partial x}\left((1-f)u''a''\right),\ \ldots$$

lead to terms which are negligible compared to those involving the vertical operators applied to the same quantities:

$$\frac{\partial}{\partial z}(fw'a'),\ \frac{\partial}{\partial z}\left((1-f)w''a''\right),$$

i.e., vertical advection is the dominant part of the substantial time derivative. (See Appendix A for a detailed mathematical treatment.)

However, it will be seen in the treatment of the continuity equations that, in the case of zero global vertical motion, w' and w'' almost exactly balance each other, so that, in the equations for average variables, operators such as

$$\frac{\partial}{\partial t}\bar{a},\ \frac{\partial}{\partial x}(\overline{ua}),\ \frac{\partial}{\partial y}(\overline{va})$$

lead to terms comparable to those yielded by the vertical flux

operator:

$$\frac{\partial}{\partial z}(\overline{wa}) \ .$$

These conclusions are equivalent to stating that the response time of the two interacting fluids is much less than the time scale of evolution of the overall convective system.

The system is thus characterized by two time scales: time variations of the whole system will be resolved at the long time scale, by assuming a quasi-instantaneous response of the fluctuations at the short time scale.

b) Equation of state:

If salinity or other density variable effects are unimportant, and if density variations do not exceed a few percent, the equation of state may be adequately represented by a linear dependence upon the temperature only:

for thermals: $$\rho' = \rho_o \left(1 - \alpha(T'-T_o)\right), \qquad (16)$$

for anti-thermals: $$\rho'' = \rho_o \left(1 - \alpha(T''-T_o)\right), \qquad (17)$$

where α is the coefficient of thermal expansion ($\alpha=3.5\times10^{-3}\ ^oC^{-1}$ for air at 15^oC, $\alpha=10^{-4}\ ^oC^{-1}$ for pure water at 10^oC), and T_o is the reference temperature. The mean density is related to the mean temperature by:

$$\overline{\rho} = \rho_o \left(1 - \alpha(\overline{T}-T_o)\right). \qquad (18)$$

This latter result is obtained simply by summing (16) and (17) pre-

multiplied by f and (1-f), respectively. (If density is a linear function of salinity , an equation similar to (18) may be derived.)

c) Continuity equation:

In the Boussinesq framework, the variations of density are small, and the continuity equation is equivalent to the law of conservation of volume (Spiegel and Veronis, 1960). The equations become:

for thermals:

$$\frac{\partial}{\partial t} f + \frac{\partial}{\partial x}(fu') + \frac{\partial}{\partial y}(fv') + \frac{\partial}{\partial z}(fw') = E, \qquad (19)$$

for anti-thermals:

$$\frac{\partial}{\partial t}(1-f) + \frac{\partial}{\partial x}\left((1-f)u''\right) + \frac{\partial}{\partial y}\left((1-f)v''\right) + \frac{\partial}{\partial z}\left((1-f)w''\right) = -E, \qquad (20)$$

where E is the volume exchange between the two fluids, per unit time and volume, and is positive if anti-thermals lose mass to thermals (positive divergence of the thermals velocity field). It may be easily shown that the above two equations meet the Invariance Principle.

Summing (19) and (20), an averaged continuity equation is obtained:

$$\frac{\partial}{\partial x}\overline{u} + \frac{\partial}{\partial y}\overline{v} + \frac{\partial}{\partial z}\overline{w} = 0. \qquad (21)$$

As stated in the preliminary remark, the term $\partial\overline{w}/\partial z$ of this equation is the sum of the dominant terms in the left-hand sides of (19) and (20). The two other terms, $\partial\overline{u}/\partial x$ and $\partial\overline{v}/\partial y$, are the sum of negligible terms. Therefore, the two contributions to $\partial\overline{w}/\partial z$ almost cancel each other, and one may write:

$$\frac{\partial \overline{w}}{\partial z} = 0,$$

i.e., the mean vertical velocity is z-independent. Since, in most cases, there is no mean upwelling or downwelling, this mean velocity ought to be zero everywhere, leading to a relationship between w' and w":

$$\overline{w} = fw' + (1-f)w'' = 0. \tag{22}$$

To the same level of approximations, equations (19) and (20) reduce to:

$$E = \frac{\partial}{\partial z}(fw') = -\frac{\partial}{\partial z}\left((1-f)w''\right). \tag{23}$$

In the regions where variations of f are unimportant, $E=f\partial w'/\partial z$, i.e., thermals grow ($E > 0$) when they accelerate ($\partial w'/\partial z > 0$), and decrease in size ($E < 0$) when they decelerate ($\partial w'/\partial z < 0$). Note that E has not been parametrized in any manner.

d) Heat conservation equation:

In the context of Boussinesq approximations, the heat conservation equations are:

for thermals:

$$\frac{\partial}{\partial t}(fT') + \frac{\partial}{\partial x}(fu'T') + \frac{\partial}{\partial y}(fv'T') + \frac{\partial}{\partial z}(fw'T') = \frac{1}{2}E(T'+T''), \tag{24}$$

for anti-thermals:

$$\frac{\partial}{\partial t}\left((1-f)T''\right) + \frac{\partial}{\partial x}\left((1-f)u''T''\right) + \frac{\partial}{\partial y}\left((1-f)v''T''\right) + \frac{\partial}{\partial z}\left((1-f)w''T''\right) = -\frac{1}{2}E(T'+T''), \tag{25}$$

where molecular diffusivity and internal source of heat are neglected, since they are unimportant for most geophysical convective situ-

ations. The heat exchange between thermals and anti-thermals is modelled by a transfer of mass at the mean temperature (T'+T")/2. A justification of this parametrization and a discussion of a more general formulation is presented in Appendix B.

The above equations, which meet the Invariance Principle, could also have been written in terms of the buoyancies

$$b' = -\alpha g(T'-T_o), \quad b'' = -\alpha g(T''-T_o).$$

The sum of equations (24) and (25) yields the global heat conservation equation:

$$\frac{\partial}{\partial t}\overline{T} + \frac{\partial}{\partial x}\overline{uT} + \frac{\partial}{\partial y}\overline{vT} + \frac{\partial}{\partial z}\overline{wT} = 0, \tag{26}$$

which expresses that the time rate of change of the mean temperature $\overline{T}$ is equal to the negative of the divergence of the convective heat flux. In the case of horizontal homogeneity on scales much larger than the one of thermals, the reduced equation is:

$$\frac{\partial}{\partial t}\overline{T} = -\frac{\partial}{\partial z}\overline{wT}, \tag{27}$$

where the vertical convective heat flux $\overline{wT}$ is defined by (9).

Subtracting from (24) and (25) the continuity equations (19) and (20) pre-multiplied by T' and T", respectively, and assuming that thermals and anti-thermals do not have time to see lateral and temporal variations (preliminary remark), one obtains:

$$fw'\frac{\partial T'}{\partial z} = \frac{1}{2}E(T''-T'), \tag{28}$$

$$(1-f)w''\frac{\partial T''}{\partial z} = \frac{1}{2}E(T''-T'). \tag{29}$$

By use of (22), the difference of these two equations leads to:

$$\frac{\partial}{\partial z}(T' + T'') = 0 \ , \tag{30}$$

stating that vertical variations of temperatures are inversely correlated. This last equation is remarkable by its simplicity. As one may expect, similar results will be obtained from the treatment of the horizontal momentum equations, and these will greatly facilitate further computations.

e) Horizontal momentum equation:

In the context of Boussinesq approximations, the horizontal momentum equations on a rotating f_o-plane are:

for thermals:

$$\frac{\partial}{\partial t}(f\underset{\sim}{u}') + \frac{\partial}{\partial x}(fu'\underset{\sim}{u}') + \frac{\partial}{\partial y}(fv'\underset{\sim}{u}') + \frac{\partial}{\partial z}(fw'\underset{\sim}{u}') + ff_o\underset{\sim}{k}\times\underset{\sim}{u}'$$
$$= -\frac{1}{\rho_o}\nabla_{\underset{\sim}{H}}(fp') + \frac{1}{2}E(\underset{\sim}{u}'+\underset{\sim}{u}'') + \frac{1}{2}(1-2f)E(\underset{\sim}{u}'-\underset{\sim}{u}''), \tag{31}$$

for anti-thermals:

$$\frac{\partial}{\partial t}\left((1-f)\underset{\sim}{u}''\right) + \frac{\partial}{\partial x}\left((1-f)u''\underset{\sim}{u}''\right) + \frac{\partial}{\partial y}\left((1-f)v''\underset{\sim}{u}''\right) + \frac{\partial}{\partial z}\left((1-f)w''\underset{\sim}{u}''\right)$$
$$+ (1-f)f_o\underset{\sim}{k}\times\underset{\sim}{u}'' = -\frac{1}{\rho_o}\nabla_{\underset{\sim}{H}}\left((1-f)p''\right) - \frac{1}{2}E(\underset{\sim}{u}'+\underset{\sim}{u}'') - \frac{1}{2}(1-2f)E(\underset{\sim}{u}'-\underset{\sim}{u}''), \tag{32}$$

where $\underset{\sim}{u}'=(u',v',0)$, $\underset{\sim}{u}''=(u'',v'',0)$ are the horizontal velocity components of thermals and anti-thermals, respectively, $\underset{\sim}{k}=(0,0,1)$ the vertical unit vector pointing upward, $\nabla_{\underset{\sim}{H}}$ the two-dimensional gradient operator $(\frac{\partial}{\partial x},\frac{\partial}{\partial y},0)$, and f_o is the Coriolis parameter. Thermals and anti-thermals are subjected to two different pressures (Truesdell, 1969). Viscous forces are neglected since they are unimportant for most geophysical convective situations. The exchange of momentum is modelled by a transfer of mass at the mean

horizontal velocity $(\underset{\sim}{u}'+\underset{\sim}{u}'')/2$, analogous to the heat transfer. It may be shown that this form of exchange is the only one that conserves total kinetic energy in the horizontal motion. The last term of each equation represents a kinetic energy exchange, which is converted to kinetic energy in the vertical motion (See section about energetics). Finally, it may be seen that the pair of equations meets the Invariance Principle.

The sum of equations (31) and (32) yields an equation governing the mean horizontal momentum $\overline{\underset{\sim}{u}}=(\overline{u},\overline{v},0)$:

$$\frac{\partial}{\partial t}\overline{\underset{\sim}{u}} + \frac{\partial}{\partial x}\overline{u\underset{\sim}{u}} + \frac{\partial}{\partial y}\overline{v\underset{\sim}{u}} + \frac{\partial}{\partial z}\overline{w\underset{\sim}{u}} + f_o\underset{\sim}{k}\times\overline{\underset{\sim}{u}} = -\frac{1}{\rho_o}\nabla_H\overline{p}. \qquad (33)$$

In the particular case of horizontal homogeneity at large scales, the two components of equation (33) reduce to:

$$\frac{\partial\overline{u}}{\partial t} - f_o\overline{v} = -\frac{\partial}{\partial z}\overline{uw}, \qquad (34)$$

$$\frac{\partial\overline{v}}{\partial t} + f_o\overline{u} = -\frac{\partial}{\partial z}\overline{vw}, \qquad (35)$$

where the Reynolds stresses $-\overline{uw}$ and $-\overline{vw}$ are defined by (7) and (8).

Subtracting from (31) and (32) the continuity equations (19) and (20) pre-multiplied by $\underset{\sim}{u}'$ and $\underset{\sim}{u}''$, respectively, and assuming that the vertical advection terms dominate (preliminary remark), one obtains:

$$w'\frac{\partial}{\partial z}\underset{\sim}{u}' = E(\underset{\sim}{u}''-\underset{\sim}{u}'), \qquad (36)$$

$$w''\frac{\partial}{\partial z}\underset{\sim}{u}'' = E(\underset{\sim}{u}''-\underset{\sim}{u}'). \qquad (37)$$

By use of (22), the difference of these two equations leads to:

$$(1-f)\frac{\partial}{\partial z}\underset{\sim}{u}' + f\frac{\partial}{\partial z}\underset{\sim}{u}'' = 0, \tag{38}$$

which is comparable to (30).

f) Vertical momentum equation:

In the context of Boussinesq approximations (Spiegel and Veronis, 1960), densities may be approximated by the reference density ρ_o everywhere except in the buoyancy terms where actual values have to be kept. For two interacting fluids, the vertical momentum equations are:

for thermals:

$$\frac{\partial}{\partial t}(fw') + \frac{\partial}{\partial x}(fu'w') + \frac{\partial}{\partial y}(fv'w') + \frac{\partial}{\partial z}(fw'w')$$
$$= -\frac{1}{\rho_o}\frac{\partial}{\partial z}(fp') - \frac{g}{\rho_o}f\rho' + \frac{1}{2}E(w'+w''), \tag{39}$$

for anti-thermals:

$$\frac{\partial}{\partial t}\left((1-f)w''\right) + \frac{\partial}{\partial x}\left((1-f)u''w''\right) + \frac{\partial}{\partial y}\left((1-f)v''w''\right) + \frac{\partial}{\partial z}\left((1-f)w''w''\right)$$
$$= -\frac{1}{\rho_o}\frac{\partial}{\partial z}\left((1-f)p''\right) - \frac{g}{\rho_o}(1-f)\rho'' - \frac{1}{2}E(w'+w''). \tag{40}$$

The sum of these two equations yields an equation for mean quantities:

$$\frac{\partial}{\partial t}\overline{w} + \frac{\partial}{\partial x}\overline{uw} + \frac{\partial}{\partial y}\overline{vw} + \frac{\partial}{\partial z}\overline{ww} = -\frac{1}{\rho_o}\frac{\partial\overline{p}}{\partial z} - \frac{g}{\rho_o}\overline{\rho}. \tag{41}$$

The main balance consists of the terms on the right-hand side, i.e., the hydrostatic balance. The fourth term dominates the left-hand side, because w' and w'' do not cancel their effect in the correlation $\overline{ww}$ and vertical advection dominates. Using (13) and (22), the Reynolds stress $\overline{ww}$ is found to be equal to w_{rms}^2, and (41) may be

rewritten as:

$$\frac{1}{\rho_o}\frac{\partial \bar{p}}{\partial z} = -\frac{g}{\rho_o}\bar{\rho} - \frac{\partial}{\partial z} w^2_{rms}, \tag{42}$$

which simply is the hydrostatic relation corrected by the Reynolds stress divergence. To obtain an equation governing the vertical motions, this equation will be sutracted from (39), and this correction will become of the same order as the remaining terms.

A vertical velocity equation is needed in order to predict vertical motions through the convective layer. That equation, obtained by subtracting (42) multiplied by f from equation (39), using (13), (22), (23), and assuming once again that vertical advection is the dominant term of the total time derivative (preliminary remark), is:

$$3m\, w_{rms}\frac{\partial w_{rms}}{\partial z} + \frac{2m}{1-2f}\left(\frac{\bar{p}+mp_{rms}}{\rho_o} - (1+m^2)\, w^2_{rms}\right)\frac{\partial f}{\partial z}$$
$$= \alpha g\, T_{rms} - \frac{1}{\rho_o}\frac{\partial}{\partial z} p_{rms}, \tag{43}$$

where m is a coefficient dependent on f only, defined by:

$$m = \frac{1-2f}{2\left(f(1-f)\right)^{\frac{1}{2}}}. \tag{44}$$

This diagnostic equation controls the vertical motion of thermals and anti-thermals. It relates the vertical acceleration to the buoyancy. The pressure term allows an exchange of kinetic energy between horizontal and vertical motions. The equation finally includes a correction term due to eventual changes in f.

g) Need for a closure hypothesis:

In the above set of governing equations, the unknown variables are u', u", $\bar{u}$, v', v", $\bar{v}$, w', w", $\bar{w}$, T', T", $\bar{T}$, p', p", $\bar{p}$, f, and E. There are thus 17 variables for which 17 equations are needed.

The definitions of mean values $\bar{u}$, $\bar{v}$, $\bar{w}$, $\bar{T}$, and $\bar{p}$ [(1), (2), (3), (4), and (6)] yield 5 equations. The two continuity equations (19) and (20) may be equivalently replaced by (22) and (23). The heat conservation equations (24) and (25) may be replaced by (26) and (30), the horizontal momentum equations (31) and (32) by (33) and (38), the vertical momentum equations (39) and (40) by (42) and (43). Since the horizontal momentum are two-dimensional, there are 5+2+2+4+2 = 15 independent definitions and governing equations. One needs thus two extra equations to solve the problem for the 17 variables. A closure hypothesis will provide the first one, while an examination of the energetics will provide the second one.

6. CONSERVATION OF FRACTION OF AREA OCCUPIED BY THERMALS

Where thermals accelerate, they tend to separate vertically and to grow by entraining surrounding fluid (Turner, 1973, Chap. 6 and 7; Scorer, 1978, Chap. 8). Isolated thermals may grow freely, but in presence of many others, they grow until they feel a strong return flow more and more confined to a reduced fraction of area. This return flow will tend to erode the thermals, preventing them form growing any further, and a saturation equilibrium takes place. Inversely, the same equilibrium state does occur in regions where

thermals decelerate: there, they tend to accumulate, restricting the area available for the return flow and are therefore eroded. Anti-thermals now grow so that saturation of area is reached.

This saturation equilibrium leads to assigning a constant value to the fraction of horizontal area occupied by thermals. This assumption of a constant value of f is supported by atmospheric observations. Direct measurements were carried out by Grant (1965), while data obtained by Warner and Telford (1967) were used by Manton (1975) to evaluate values of f. Both sources show a narrow range of variation. The assumption was successfully used by Manton (1975) in an attempt to model convection in the atmospheric boundary layer below the inversion and by Roisin (1979) in a study of penetrative convection with application to upper ocean surface cooling. The encouraging results presented in subsequent papers support the validity of this assumption for both geophysical and laboratory applications.

The expression of the volume exchange between thermals and anti-thermals (23) is compatible with this assumption. Indeed, in regions where the fraction of area occupied by thermals is constant, equation (23) reduces to:

$$E = f \frac{\partial w'}{\partial z} , \qquad (45)$$

i.e., when thermals accelerate ($\partial w'/\partial z > 0$) and would normally separate if there were no exchanges, they grow ($E > 0$) and thus tend to avoid separation. The same conclusion holds when thermals decelerate ($\partial w'/\partial z < 0$, $E < 0$). This remark does not prove the assumption

of constant f, but rather affirms that if saturation equilibrium occurs, it is a stable equilibrium state.

Although the fraction f of area is expected to be constant for a given convective situation, it might differ from one case to another, depending upon the way thermals are produced. The value to be assigned to f depends upon the average size and rate of production of thermals along the boundary where the forcing is applied. For example, small scale convection by surface stress in laboratory experiments (Kato and Phillips, 1969; Kantha, Phillips and Azad, 1977) is not expected to yield the same value of f as oceanic convection in the upper ocean due to surface cooling (Kraus and Turner, 1967; Roisin, 1979). In the oceanic wind-mixed layer and in the corresponding laboratory experiments (Chapter three), the value of f is of the order of 10% (see Table 1). In the case of penetrative convection in the lower atmosphere, a reasonable range of values is 30%-40% (see Chapter four). On the other hand, large-scale horizontal variations in the forcing may lead to some lateral variations of f.

Aside from those possible lateral variations and from restricted regions where saturation equilibrium is not yet reached, the fraction of area occupied by thermals to the total area is assumed to be constant. It will therefore appear parametrically in the model. This assumption is stated at this early stage of the early stage of the modelling of convection, and its effects are anticipated to be unimportant.

As a consequence, equations (30) and (38) may be rewritten as:

$$\frac{\partial}{\partial z}(\bar{T} + mT_{rms}) = 0, \qquad (46)$$

$$\frac{\partial}{\partial z}(\bar{u} + 2m\, u_{rms}) = 0, \qquad (47)$$

where m is defined by (44) and rms quantities by (14). Since f is constant, these two equations are linear. The vertical momentum equation (43) becomes:

$$3m\, w_{rms} \frac{\partial}{\partial z} w_{rms} = \alpha g\, T_{rms} - \frac{1}{\rho_o} \frac{\partial}{\partial z} p_{rms}. \qquad (48)$$

7. ENERGETICS

In this section, exchanges of kinetic energy between mean and turbulent flow as well as conversion to potential energy are examined in detail. The last equation required by the model will result as a direct consequence of the statement that the response time of turbulent motions is much less than the time scale of variation of the overall convective system (preliminary remark).

The total kinetic energy (KE) may be divided in two parts, the kinetic energy in the mean flow (MKE) and the kinetic energy in the turbulent motions (TKE):

$$KE = \frac{1}{2} \rho_o \int_V \left(\overline{u^2} + \overline{v^2} + \overline{w^2}\right) dV$$

$$= \frac{\rho_o}{2} \int_V \left(\bar{u}^2+\bar{v}^2+\bar{w}^2\right) dV + \frac{\rho_o}{2} \int_V \left(u_{rms}^2+v_{rms}^2+w_{rms}^2\right) dV$$

$$= \quad MKE \quad + \quad TKE, \qquad (49)$$

where V is the total volume of the system. Equation (13) was used to separate means and fluctuations. The potential energy is defined

by:

$$PE = - \alpha g \rho_o \int_V z\, \overline{T}\, dV, \tag{50}$$

where z is the vertical coordinate, positive upward.

a) Mean Kinetic Energy Budget:

The time rate of change of the kinetic energy in the mean flow results from (33). An integration over the entire volume yields:

$$\begin{aligned} \frac{d}{dt} MKE &= -\rho_o \int_V (\underset{\sim}{\overline{u}} . \frac{\partial}{\partial z} \underset{\sim}{\overline{u}}\,\overline{u} + \underset{\sim}{\overline{u}} . \frac{\partial}{\partial y} \underset{\sim}{\overline{v}}\,\overline{u} + \underset{\sim}{\overline{u}} . \frac{\partial}{\partial z} \underset{\sim}{\overline{w}}\,\overline{u} + \frac{1}{\rho_o} \underset{\sim}{\overline{u}} . \nabla_H \overline{p}) \, dV \\ &= -\rho_o \oint_\Sigma [\underset{\sim}{\overline{u}} . \underset{\sim}{\overline{u}}\,\underset{\sim}{\overline{u}} . \underset{\sim}{n} + (\overline{u}\,\overline{uw} + \overline{v}\,\overline{vw}) n_z + \frac{1}{\rho_o} \overline{p}\, \underset{\sim}{\overline{u}} . \underset{\sim}{n}] \, dS \\ &\quad + \rho_o \int_V (\underset{\sim}{\overline{u}}\,\underset{\sim}{\overline{u}} . \frac{\partial}{\partial x} \underset{\sim}{\overline{u}} + \underset{\sim}{\overline{v}}\,\underset{\sim}{\overline{u}} . \frac{\partial}{\partial y} \underset{\sim}{\overline{u}} + \underset{\sim}{\overline{w}}\,\underset{\sim}{\overline{u}} . \frac{\partial}{\partial z} \underset{\sim}{\overline{u}} + \frac{1}{\rho_o} \overline{p}\, \nabla_H . \underset{\sim}{\overline{u}}) \, dV, \end{aligned} \tag{51}$$

where Σ is the closed surface bounding the system, $\underset{\sim}{n}$ and n_z are respectively the horizontal and vertical components of the unit outward normal vector to Σ. The first term is the input of mean kinetic energy through the boundaries of the system, while the second term represents the exchange of kinetic energy between mean flow and turbulent motions, due to shear and divergence effects. In agreement, with the basic assumptions, vertical fluxes along the boundaries and vertical shear effect are the dominant process, and equation (51) reduces to:

$$\frac{d}{dt} MKE = -\rho_o \oint_\Sigma (\overline{u}\,\overline{uw} + \overline{v}\,\overline{vw}) n_z dS + \rho_o \int_V (\overline{uw} \frac{\partial \overline{u}}{\partial z} + \overline{vw} \frac{\partial \overline{v}}{\partial z}) dV. \tag{52}$$

The exchange term may be rewritten by using (13), (22), and (47):

$$-\rho_o \int_V (\overline{uw}\,\frac{\partial \overline{u}}{\partial z} + \overline{vw}\,\frac{\partial \overline{v}}{\partial z})dV = 2\rho_o m \int_V (u_{rms}\frac{\partial u_{rms}}{\partial z} + v_{rms}\frac{\partial v_{rms}}{\partial z})w_{rms}\,dV$$

$$= \rho_o m \int_V w_{rms}\frac{\partial}{\partial z}(u_{rms}^2 + v_{rms}^2)dV. \qquad (53)$$

b) Potential Energy Budget:

The time rate of change of the potential energy is directly obtained from the heat equation (26):

$$\frac{d}{dt}PE = \alpha g\rho_o \int_V z\left(\frac{\partial}{\partial x}\overline{uT} + \frac{\partial}{\partial y}\overline{vT} + \frac{\partial}{\partial z}\overline{wT}\right)dV$$

$$= \alpha g\rho_o \oint_\Sigma (z\,\overline{\underset{\sim}{u}T}.\underset{\sim}{n} + z\,\overline{wT}.n_z)dS - \alpha g\rho_o \int_V \overline{wT}\,dV. \qquad (54)$$

The first term represents the input of potential energy by means of imposed convective heat flux through boundaries. The last term is the exchange between potential and kinetic energy by convection. It can be rewritten as follows, with use of (13), (22), and (48):

$$\alpha g\rho_o \int_V \overline{wT}\,dV = \alpha g\rho_o \int_V w_{rms}T_{rms}dV$$

$$= \int_V (3\rho_o m\, w_{rms}^2\frac{\partial w_{rms}}{\partial z} + w_{rms}\frac{\partial p_{rms}}{\partial z})\,dV. \qquad (55)$$

c) Turbulent Kinetic Energy Budget:

The sources of turbulent kinetic energy are (i) the exchange with kinetic energy in the mean flow, (ii) the exchange with poten-

tial energy, and (iii) the input at the boundaries. This last contribution is primarily due to vertical fluxes:

$$- \oint_{\Sigma} \{\frac{1}{2} \rho_o \overline{w[(u-\bar{u})^2+(v-\bar{v})^2+(w-\bar{w})^2]} + \overline{w[p-\bar{p}]} \} n_z dS,$$

which can be rewritten in terms of rms fluctuations by using (13), (22), and (44):

$$- \oint_{\Sigma} [\rho_o m\, w_{rms}(u_{rms}^2 + v_{rms}^2 + w_{rms}^2) + w_{rms} p_{rms}] n_z dS. \qquad (56)$$

The sum S of the three sources of turbulent kinetic energy is given by (53), (55), and (56):

$$S = \int_V \rho_o m\, w_{rms} \frac{\partial}{\partial z}(u_{rms}^2 + v_{rms}^2) dV + \int_V (3\rho_o m\, w_{rms}^2 \frac{\partial w_{rms}}{\partial z} + w_{rms} \frac{\partial p_{rms}}{\partial z}) dV$$

$$- \oint_{\Sigma} [\rho_o m\, w_{rms}(u_{rms}^2 + v_{rms}^2 + w_{rms}^2) + w_{rms} p_{rms}] n_z dS.$$

Integrations by parts lead to the cancellation of the boundary terms. It results that:

$$S = - \int_V [\rho_o m(u_{rms}^2 + v_{rms}^2) + p_{rms}] \frac{\partial w_{rms}}{\partial z} dV. \qquad (57)$$

Since the total energy in the system is conserved, the time rate of change of turbulent kinetic energy ought to be equal to S. However, in the present study, the preliminary remark, which states that vertical advection is the dominant contribution to the

substantial derivative, is equivalent to neglecting local time rate of change of turbulent fluctuations compared with the vertical transport, input, and conversion rates. Moreover, evaluation of the orders of magnitude for laboratory experiments and geophysical situations shows that the time rate of change of turbulent kinetic energy is at least one order of magnitude less than each individual term in S (Denman, 1973; Willis and Deardorff, 1974; Niiler, 1975; Lenschow *et al.*, 1980). Therefore, in agreement with both observations and previous assumptions, the sum of the three contributions to the turbulent kinetic energy has to be negligible compared to each individual term, i.e., S = 0 at that level of approximation. This conclusion states in other words, that turbulence adapts itself quasi-instantaneously to local variations. Equation (56) for S=0 is immediately satisfied if

$$p_{rms} = - \rho_o m(u^2_{rms} + v^2_{rms}). \qquad (58)$$

This constitutes the last equation closing the model. The final energy diagram for the system is sketched on figure 2.

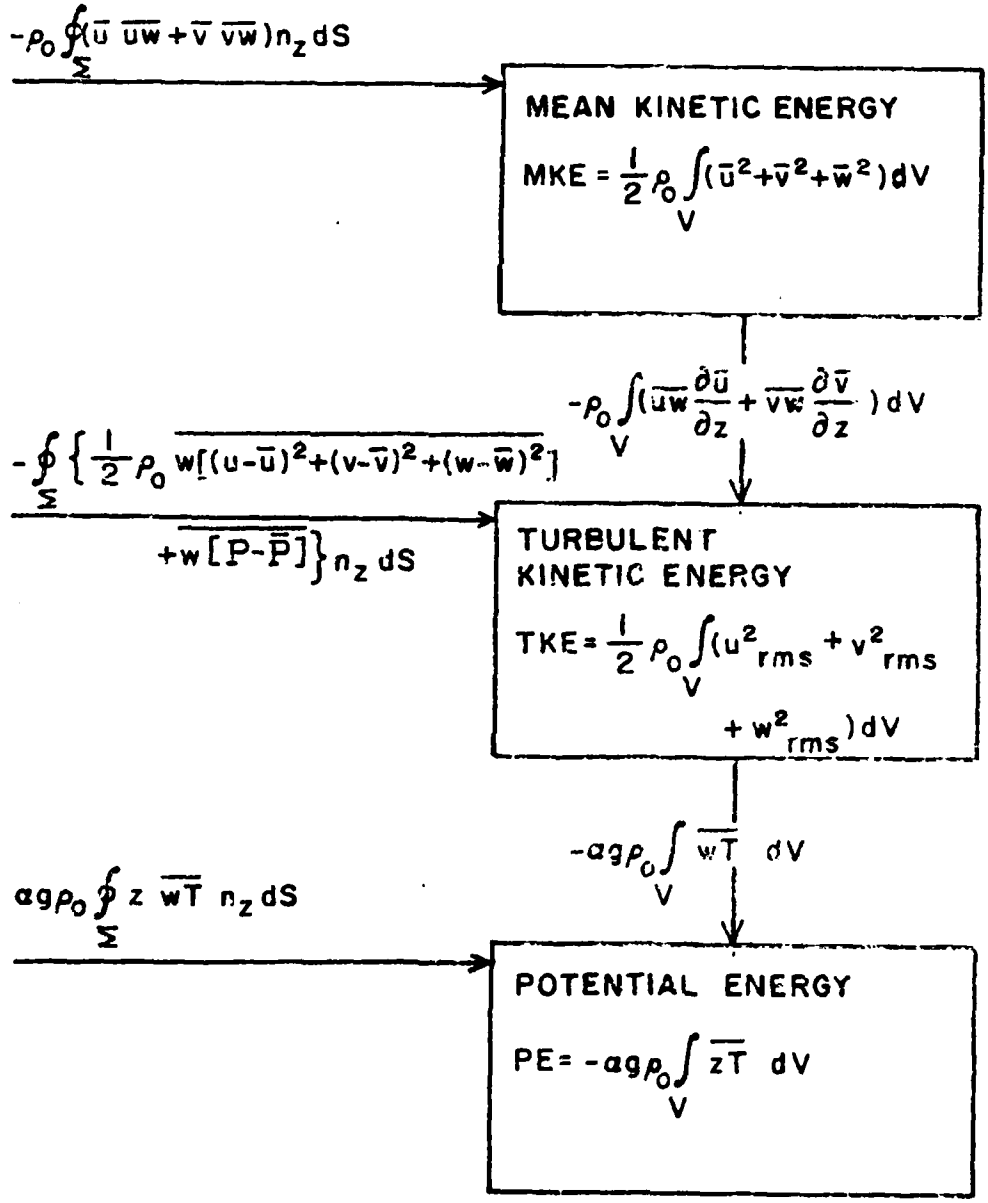

Figure 2. Sketch of energy exchanges between mean kinetic energy, turbulent kinetic energy, and potential energy.

8. SUMMARY AND CONCLUSIONS

Convection is envisioned as the relative motions and interactions of a two-fluid system. Considering only geophysical applications, the Boussinesq approximation is made. Although molecular processes are necessary to diffuse heat and momentum within the thermals and anti-thermals, molecular diffusion is modelled through the parametrization of heat and momentum exchanges between thermals and anti-thermals and does not explicitly appear in the governing equations. The model requires a closure hypothesis. The existence of a stable saturation equilibrium between the two interacting fluids permits an assumption of a constant value of the ratio of areas occupied by these two fluids.

The governing equations may be advantageously rewritten in terms of mean and rms variables. In the particular case of no horizontal variations, the one-dimensional unsteady model may be summarized as follows:

Continuity equations:

$$\overline{w} = 0 \tag{59}$$

$$E = [f(1-f)]^{\frac{1}{2}} \frac{\partial w_{rms}}{\partial z} \tag{60}$$

Heat equations:

$$\frac{\partial \overline{T}}{\partial t} = - \frac{\partial}{\partial z}(w_{rms} T_{rms}) \tag{61}$$

$$\frac{\partial}{\partial z}(\overline{T} + m\, T_{rms}) = 0 \tag{62}$$

Horizontal momentum equations:

$$\frac{\partial \overline{u}}{\partial t} - f_o \overline{v} = - \frac{\partial}{\partial z}(u_{rms} v_{rms}) \tag{63}$$

$$\frac{\partial \overline{v}}{\partial t} + f_o \overline{u} = - \frac{\partial}{\partial z}(v_{rms} w_{rms}) \tag{64}$$

$$\frac{\partial}{\partial z}(\overline{u} + 2m\, u_{rms}) = 0 \tag{65}$$

$$\frac{\partial}{\partial z}(\overline{v} + 2m\, v_{rms}) = 0 \tag{66}$$

Vertical momentum equations:

$$\frac{\partial \overline{p}}{\partial z} = -\rho_o g[1-\alpha(\overline{T}-T_o)] - \rho_o \frac{\partial}{\partial z} w_{rms}^2 \qquad (67)$$

$$3m\, w_{rms} \frac{\partial w_{rms}}{\partial z} = \alpha g\, T_{rms} - \frac{1}{\rho_o} \frac{\partial p_{rms}}{\partial z} \qquad (68)$$

Pressure fluctuation: $$p_{rms} = -\rho_o m(u_{rms}^2 + v_{rms}^2). \qquad (69)$$

In the above set of equations, f and m are two constants, related by (44). Equations (60) and (67) give E and $\overline{p}$ once the solution is found; they may thus be separated from the others. Equations (62), (65), and (66) may be directly integrated; the rms pressure fluctuation may be eliminated in (68) by use of (69). The problem thus reduces to four non-linear first-order coupled differential equations [(61), (63), (64), and (68)]. Examples of applications are presented in subsequent papers.

APPENDIX A

Mathematical treatment of the Preliminary Remark

If a represents any physical quantity, the preliminary remark states:

$$\frac{\partial}{\partial t}(fa') + \frac{\partial}{\partial x}(fu'a') + \frac{\partial}{\partial y}(fv'a') \ll \frac{\partial}{\partial z}(fw'a') , \qquad (A1)$$

$$\frac{\partial}{\partial t}[(1-f)a''] + \frac{\partial}{\partial x}[(1-f)u''a''] + \frac{\partial}{\partial y}[(1-f)v''a''] \ll \frac{\partial}{\partial z}[(1-f)w''a''], \qquad (A2)$$

i.e., the vertical acceleration is the dominant part of the substantial time derivative. The orders of magnitude of the various terms can be quantified by introducing the scale for each variable: T, for the time scale of evolution of the whole system, L, for the horizontal length scale of lateral non-homogeneities in the system, V, for the horizontal-velocity components, H, for the convection-layer thickness, and W, for the vertical velocity of thermals and anti-thermals. The preliminary remark is then equivalent to stating:

$$\frac{1}{T} \ll \frac{W}{H} \quad \text{and} \quad \frac{V}{L} \ll \frac{W}{H} ,$$

or

$$\frac{H}{W} \ll T \quad \text{and} \quad \frac{L}{V} ,$$

i.e., the time taken by the thermals to cross the convective layer is much less than (i) the time scale of evolution of the whole system and (ii) the advective time scale of lateral non-homogeneities.

Mathematically, one may define a dimensionless number, ε, to measure the ratio of these time scales:

$$\varepsilon = \max \left(\frac{H/W}{T} , \frac{H/W}{L/V} \right) . \qquad (A3)$$

The preliminary remark therefore holds as long as:

$$\varepsilon << 1 . \qquad (A4)$$

If the terms of the order of ε and smaller are neglected, the mathematical treatment of the equations leads to the equations proposed in chapter two. It is shown below that all the equations are valid at the order of ε or better.

The continuity equations (19) and (20) may be rewritten as:

$$\frac{\partial}{\partial z} (fw') = E + O (\varepsilon \frac{W}{H}) , \qquad (A5)$$

and

$$\frac{\partial}{\partial z} [(1-f)w''] = -E + O (\varepsilon \frac{W}{H}) , \qquad (A6)$$

the sum of which is:

$$\frac{\partial \bar{w}}{\partial z} = O (\varepsilon \frac{W}{H}) .$$

Since, for most of geophysical situations $\bar{w}$ can be assumed to be zero somewhere (along a boundary, for example), $\bar{w}$ is of order εW and thus is much smaller than w' and w". An integration with respect to z yields:

$$\bar{w} = fw' + (1-f)w'' = O(\varepsilon W) , \qquad (A7)$$

i.e., equation (22) is valid at the order of ε.

Equations (24) and (25) may be rewritten as:

$$\frac{\partial}{\partial z} (fw'T') = \tfrac{1}{2}E (T'+T'') + O (\varepsilon \frac{w\theta}{H}) , \qquad (A8)$$

$$\frac{\partial}{\partial z} [(1-f)w''T'] = -\tfrac{1}{2}E (T'+T'') + O (\varepsilon \frac{w\theta}{H}) , \qquad (A9)$$

where θ is a measure of a temperature difference across the convective layer. Subtracting from (A8) and (A9) the continuity equations (A5) and (A6) pre-multiplied by T' and T", respectively, one obtains:

$$fw' \frac{\partial T'}{\partial z} = \tfrac{1}{2}E\,(T''-T') + O\left(\varepsilon \frac{w\theta}{H}\right) ,$$

$$(1-f)w'' \frac{\partial T''}{\partial z} = \tfrac{1}{2}E\,(T''-T') + O\left(\varepsilon \frac{w\theta}{H}\right) .$$

By virtue of (A7), the difference of these last two equations is:

$$fw' \frac{\partial}{\partial z}(T'+T'') = O\left(\varepsilon \frac{w\theta}{H}\right) ,$$

or

$$\frac{\partial}{\partial z}(T'+T'') = O\left(\varepsilon \frac{\theta}{H}\right) ,$$

i.e., equation (30) is valid at the order of ε.

The same treatment can be carried out in a straightforward manner, and it is concluded that equations (38), (42) and (43) are valid at the order of ε. On the other hand, the governing equations for the mean variables, $\bar{T}$, $\bar{u}$ and $\bar{v}$, are not based on the preliminary remark and are exact equations.

As an example, the application of the theory of chapter two to the deepening of the wind-mixed layer (Chapter three) is governed by the following scales:

$H = 10$ m, $L = \infty$, $T = 10^{4}$s, $W = 10^{-2}ms^{-1}$, $V = 10^{-1}ms^{-1}$,

in which case, ε is of the order of 10^{-1}. Likewise, the application of the theory to oceanic penetrative convection under surface cooling (Chapter four) and to wind-induced oceanic frontogenesis (Chapter five) are based on values of ε of the order of 10^{-4} and 5×10^{-4}, respectively. The theory, as developed in chapter two is thus directly applicable to upper-ocean dynamics.

APPENDIX B

A more general parameterization of the exchanges between thermals and anti-thermals

Exchanges of heat and momentum between thernals and anti-thermals are assumed to take place exclusively through a volume exchange, thus excluding transfer by diffusion or collision. Exchange terms can then be written as the product of E, the volume exchange between thermals and anti-thermals, by the quantity which is being transferred. Since momentum exchanges are analogous to a heat exchange, only the parameterization of the heat exchange is discussed in this appendix. The conclusions will hold for momentum exchanges.

Assuming that the transfer of heat between thermals and anti-thermals is a net transfer of volume, E per unit time and total volume, at a temperature T_{ex}, the heat conservation equations take the form:

$$\frac{\partial}{\partial t}(fT') + \frac{\partial}{\partial x}(fu'T') + \frac{\partial}{\partial y}(fv'T') + \frac{\partial}{\partial z}(fw'T') = E\,T_{ex}\,, \quad \text{(B1)}$$

$$\frac{\partial}{\partial t}[(1-f)T''] + \frac{\partial}{\partial x}[(1-f)u''T''] + \frac{\partial}{\partial y}[(1-f)v''T''] + \frac{\partial}{\partial z}[(1-f)w''T''] = -E\,T_{ex} \quad \text{(B2)}$$

The exchange temperature, T_{ex}, must be a function of T', T'' and possibly f, and has to meet the following requirements:

(i) T_{ex} ranges between T' and T'', (B3)

(ii) $T_{ex} = \bar{T}$, if $T' = T'' = \bar{T}$, (B4)

(iii) $T_{ex}(T', T'', f) = T_{ex}(T'', T', 1-f)$. (B5)

The second requirement states that if thermals and anti-thermals are at the same temperature, the exchange takes place at that temperature, while the third requirement directly follows from the Invariance Principle.

Using the continuity equations and the Preliminary Remark, and performing the same algebraic transformations as in chapter two, one obtains the following equations:

$$fw' \frac{\partial T'}{\partial z} = E (T_{ex} - T') , \tag{B6}$$

$$(1-f)w'' \frac{\partial T''}{\partial z} = E (T'' - T_{ex}) , \tag{B7}$$

which are generalized forms of (28) and (29). The elimination of the vertical velocities from (B6) and (B7) by use of (22) yields:

$$(T''-T_{ex}) \frac{\partial T'}{\partial z} + (T_{ex} - T') \frac{\partial T''}{\partial z} = 0, \tag{B8}$$

which is the generalization of equation (30).

No further information can be drawn from this equation without a parametrization of the exchange temperature, T_{ex}. Since T_{ex} has the dimension of a temperature, a linear function of T' and T" is well-suited:

$$T_{ex} = a(f)\, T' + b(f)\, T'', \tag{B9}$$

where the dimensionless coefficients, a and b, are functions of f in general. The three requirements lead to impose:

$$\text{(i) } 0 \leq a,\ b \leq 1, \tag{B10}$$

$$\text{(ii) } a + b = 1 , \tag{B11}$$

$$\text{(iii) } a(1-f) = b(f) . \tag{B12}$$

In this case, equation (B8) reduces to:

$$a \frac{\partial T'}{\partial z} + b \frac{\partial T''}{\partial z} = 0 , \tag{B13}$$

for the derivation of which (B11) has been used. The coefficients a and b are functions of f only, and it is assumed later that f is constant throughout the system. Therefore, (B13) becomes:

$$\frac{\partial}{\partial z} T_{ex} = \frac{\partial}{\partial z} (aT' + bT'') = 0 \ . \qquad \text{(B14)}$$

This equation is a more general form of equation (30). Since it is linear in T' and T", the same analysis as in chapter two and the subsequent chapters can be carried out. The mathematical formulation remains unchanged; only the dependence of the coefficient m upon f has changed to:

$$m = \frac{a(f) - f}{\sqrt{f(1-f)}} \ . \qquad \text{(B15)}$$

The particular case chosen in chapter two corresponds to $a = b = \frac{1}{2}$ and is the only choice which leads to conserving the total kinetic energy of the flow, i.e.,

$$\frac{f}{2} (u'^2+v'^2+w'^2) + \frac{1-f}{2} (u''^2+v''^2+w''^2) \ .$$

As defined previously, parametrizations of exchanges between thermals and anti-thermals are not based on any coefficient of molecular diffusivity. However, molecular processes are required to homogenize thermals and anti-thermals and are effective as exchanges take place. Therefore, in all precision, molecular diffusion is not neglected but modelled.

CHAPTER THREE

DEEPENING OF THE WIND-MIXED LAYER: A MODEL OF THE VERTICAL STRUCTURE

1. INTRODUCTION

Much of the work on upper ocean mixing is limited to one-dimensional models. These can be useful because bulk temperatures and salinities tend to vary more along a vertical distance of a hundred meters than along a horizontal distance of a thousand kilometers. This holds true over many parts of the world's oceans, except near fronts, because vertical exchange processes between the air and the sea, as well as vertical mixing within the water column, are likely to affect local conditions much more rapidly and effectively than horizontal advection and horizontal mixing (Niiler and Kraus, 1977).

Time-dependent one-dimensional models often assume vertical homogeneity in the mixed layer, and are therefore bulk models. They were reviewed extensively by Niiler and Kraus (1977) and Zilitinkevich, et al., (1979). The four unknowns in these models are the mixed-layer temperature $\bar{T}$, horizontal velocity components $\bar{u}$, $\bar{v}$, and thickness h. These variables are functions of time only and are governed by the overall budgets of heat, horizontal momentum and turbulent kinetic energy. This last budget takes the form:

$$\frac{d}{dt} TKE = F_s + E - \frac{d}{dt} PE - D - F_h \ , \qquad (1)$$

expressing that the time rate of change of the turbulent kinetic energy (TKE) is the sum of a surface flux F_s from the atmosphere through surface-wave breaking and the rate of production E by the

shear of the mean flow minus the rate of increase of potential energy PE, the rate of dissipation D by friction within the mixed layer, and the flux F_h of energy lost by internal gravity waves through the underlying stable layers.

It is reasonable to state that the turbulent kinetic energy responds quasi-instantaneously to time variations and thus to neglect its time rate of change (Denman, 1973; Niiler, 1975; Chapter two). On the other hand, the downward flux by internal gravity waves is often neglected since no acceptable parametrization has yet been proposed. The TKE-budget (1) therefore reduces to:

$$\frac{dPE}{dt} \approx F_s + E - D \ , \qquad (2)$$

which leads to two main classes of models: (i) *Turbulent erosion models* (TEM) for which the increase in potential energy by mixing is exclusively due to the surface flux F_s minus internal dissipation, and (ii) the *dynamic instability models* (DIM) for which the increase in potential energy is entirely due to production of turbulence by the mean-flow shear. The comparison and synthesis of these two models are discussed by Niiler (1975), de Szoeke and Rhines (1976) and Price, et al., (1978).

More recently, various turbulence closure models have been applied to the mixed-layer deepening problem in order to study the vertical structure across the layer (Mellor and Durbin, 1975; Warn-Varnas and Piacsek, 1979; Klein, 1980; Kundu, 1980a). They all show that the assumption of vertical homogeneity is excellent for temperature when the mixed layer is deep enough so that the thermocline is well-defined, but not adequate for

horizontal velocity components for sub-inertial time scales when an Ekman-spiral structure is present

In a parallel way, laboratory simulations of mixed-layer deepening were conducted, either without mean shear (oscillating-grid experiments by Turner and Kraus, 1967; Linden, 1975) or with mean shear (Kato and Phillips, 1969; Moore and Long, 1971; Kantha, Phillips and Azad, 1977).

Finally, theoretical and laboratory results have been compared with observations (Turner, 1969; Denman and Miyake, 1973; Halpern, 1974; Kullenberg, 1977; Price, Mooers and Van Leer, 1978; Dillon and Powell, 1979). The main conclusions resulting from the data are: (i) TEM and DIM both lead to qualitative agreement, (ii) good quantitative agreement is obtained for a well-adjusted dissipation term, and (iii) comparisons of the various terms in (2) favor a TEM when the mixed layer is well developed (15 m or more).

2. THE MODEL

The model presented here is a new turbulent erosion model (TEM). It focuses on the vertical structure of the variables throughout the mixed layer and thermocline. The aim is to predict by simple analytical calculations the thermocline thickness and profiles of temperature, velocity, Reynolds stresses and heat flux. The model is based on a new parametrization of mixing and convection (Chapter two). It can be applied to the most general case of

mixed-layer deepening under variable wind stress and/or variable surface heat flux.

The model envisions mixing as the relative motion of two interacting fluids of different properties. Parcels of fluid rising through the convective layer are given near the surface extra momentum by the wind stress, and their temperature is altered by the surface heat flux. These elements are pushed back into the convective layer by turbulence with new properties. Because they sink in a slightly stratified fluid, they accelerate or decelerate. Ultimately, they will become buoyant and decelerate. As they sink, they also progressively lose their horizontal-momentum excess and heat content by interactions with the upward return flow. As they reach the bottom, they have a null vertical velocity and lose their ability to carry heat and momentum. The active sinking elements are called *thermals*, and the rising elements, *anti-thermals*, by analogy. The model describes the individual dynamics of thermals and anti-thermals, and their exchanges; mean properties and relative differences are then deduced. This permits direct computation of mean profiles and vertical fluxes of momentum and heat.

For better comparison with previous models and laboratory experiments, the present study is limited to the case of no surface heat flux. This wind-mixed layer deepening case is depicted on Figure 3. At the surface, non-buoyant thermals are produced by wind action. As they penetrate the *mixed layer*, they acquire positive buoyancy due to a slight stable stratification

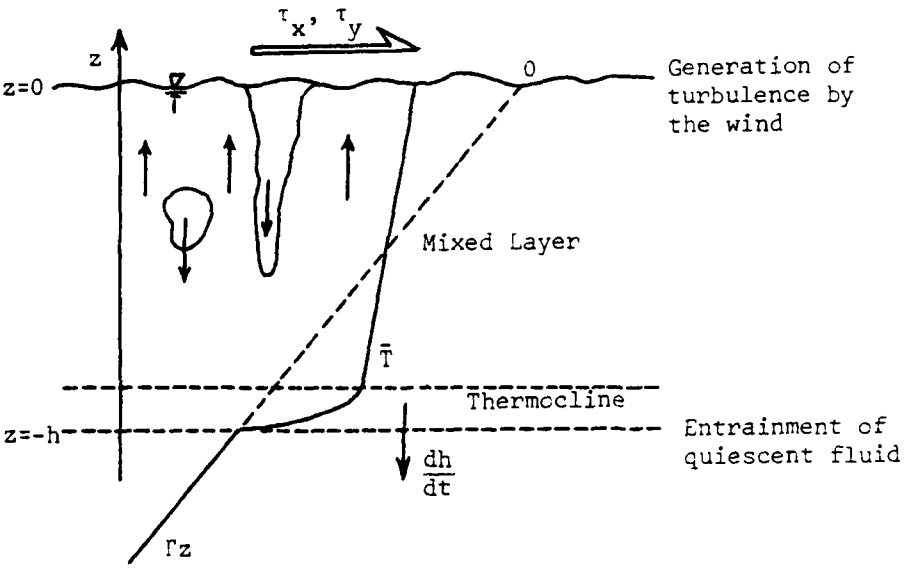

Figure 3. Schematic model of the wind-mixed layer.

existing in that layer, and decelerate. At the bottom of the mixed layer, their vertical velocity is somewhat reduced. As the temperature profile begins to curve at the entrance of the thermocline, the thermals' buoyancy increases sharply, and their vertical velocity decreases rapidly. Since the newly-entrained fluid is subjected there to the largest temperature variations, the vertical heat flux $\overline{wT}$ (negative) is large at the bottom of the mixed layer. A decreasing velocity therefore implies larger temperature contrasts and increasing buoyancy forces, which in turn decelerate thermals even more. The process is cumulative, and gives rise to the formation of a thin layer of rapid variations, the *thermocline*, which lies between the mixed layer and the quiescent stable fluid.

Throughout the mixed layer and thermocline, a saturation equilibrium between thermals and anti-thermals can be assumed (Chapter two). This leads to assigning a constant value to f, the fraction of area occupied by thermals. However, continuity of physical properties at the bottom of the thermocline requires f to vanish at that level. This may be accomplished by assuming the existence of an *entrainment layer* within which f decreases monotonically from its constant value in the mixed layer and thermocline to zero. Calculations carried out in Appendix C show tnat this layer is in fact so thin that it does not play any active role in the deepening process and may be neglected. It is therefore assumed here that f is constant throughout the water column.

3. GOVERNING EQUATIONS

Thermals and anti-thermals are characterized by different velocities, temperatures, densities and pressures. Primed and double-primed quantities refer to thermals and anti-thermals, respectively. If f represents the fraction of area occupied by thermals at any level, the fraction of area available to anti-thermals is (1-f), so that mean properties are defined by:

Mean Temperature $$\bar{T} = fT' + (1-f)T'' , \tag{3}$$

Mean velocity components $$\bar{u} = fu' + (1-f)u'' , \tag{4}$$

$$\bar{v} = fv' + (1-f)v'' , \tag{5}$$

$$\bar{w} = fw' + (1-f)w'' , \tag{6}$$

Mean density $$\bar{\rho} = f\rho' + (1-f)\rho'' , \tag{7}$$

Mean pressure $$p = fp' + (1-f)p'' . \tag{8}$$

Moreover, root-mean-square (rms) fluctuations are defined by:

$$a_{rms} = \sqrt{f(1-f)}\,(a'-a'') = \pm\overline{(a-\bar{a})^2}^{\,\frac{1}{2}}, \tag{9}$$

where a stands for any physical quantity such as temperature, velocity, density or pressure. Rms fluctuations are thus proportional to the difference between thermals and anti-thermals quantities. They may be positive or negative. The vertical convective heat flux can be expressed as:

$$\begin{aligned} \overline{wT} &= fw'T' + (1-f)w''T'' \\ &= \bar{w}\bar{T} + w_{rms}T_{rms} , \end{aligned} \tag{10}$$

and all the other fluxes such as the Reynolds stresses can be written in similar forms:

$$-\overline{uw} = -\bar{u}\,\bar{w} - u_{rms}w_{rms}\,, \tag{11}$$

$$-\overline{vw} = -\bar{v}\,\bar{w} - v_{rms}w_{rms}\,, \tag{12}$$

$$-\overline{ww} = -\bar{w}^2 - w_{rms}^2\,. \tag{13}$$

With these definitions, the one-dimensional convection (no horizontal variations) can be described by the following equations (Chapter two):

Continuity equation:
$$\bar{w} = 0 \tag{14}$$

Heat equations:
$$\frac{\partial \bar{T}}{\partial t} = -\frac{\partial}{\partial z}(w_{rms}T_{rms}) \tag{15}$$

$$\frac{\partial}{\partial z}(\bar{T} + mT_{rms}) = 0 \tag{16}$$

Horizontal momentum equations:
$$\frac{\partial \bar{u}}{\partial t} - f_o\bar{v} = -\frac{\partial}{\partial z}(u_{rms}w_{rms}) \tag{17}$$

$$\frac{\partial \bar{v}}{\partial t} + f_o\bar{u} = -\frac{\partial}{\partial z}(v_{rms}w_{rms}) \tag{18}$$

$$\frac{\partial}{\partial z}(\bar{u} + 2mu_{rms}) = 0 \tag{19}$$

$$\frac{\partial}{\partial z}(\bar{v} + 2mv_{rms}) = 0 \tag{20}$$

Vertical momentum Equations:
$$\frac{1}{\rho_o}\frac{\partial \bar{p}}{\partial z} = -\,g[1-\alpha(\bar{T}-T_o)] - \frac{\partial}{\partial z}w_{rms}^2 \tag{21}$$

$$3mw_{rms}\frac{\partial w_{rms}}{\partial z} = \alpha g T_{rms} - \frac{1}{\rho_o}\frac{\partial p_{rms}}{\partial z} \tag{22}$$

Pressure fluctuation:
$$p_{rms} = -\rho_o m(u_{rms}^2 + v_{rms}^2), \tag{23}$$

where f_o is the Coriolis parameter, ρ_o the reference density at T_o, α the coefficient of thermal expansion, and m a coefficient dependent upon f, defined by

$$m = \frac{1-2f}{\sqrt{f(1-f)}} \quad , \tag{24}$$

and is related to the turbulent kinetic energy input at the surface (Chapter two). Figure 4 exhibits a plot of m versus f.

Eliminating the equations for $\bar{w}$ and $\bar{p}$, (14) and (21), and replacing p_{rms} by its expression (23), the system reduces to seven non-linear first-order coupled differential equations.

4. BOUNDARY CONDITIONS

At the surface, z =0, the Reynolds stresses ought to match the wind stress components:

$$-\overline{uw} = -u_{rms} w_{rms} = \frac{\tau_x}{\rho_o} \quad , \tag{25}$$

$$-\overline{vw} = -v_{rms} w_{rms} = \frac{\tau_y}{\rho_o} \quad , \tag{26}$$

while the vertical convective heat flux is set equal to zero:

$$\overline{wT} = w_{rms} T_{rms} = 0 \quad , \tag{27}$$

since the effect of a surface heat flux is not studied here. Finally, isotropic turbulence is assumed in the wave zone just beneath the surface:

$$w_{rms}^2 = u_{rms}^2 + v_{rms}^2 \quad , \tag{28}$$

expressing that the turbulent vertical velocity equals the turbulent horizontal velocity.

The wind-stress amplitude defines a friction velocity characteristic of the turbulence near the surface:

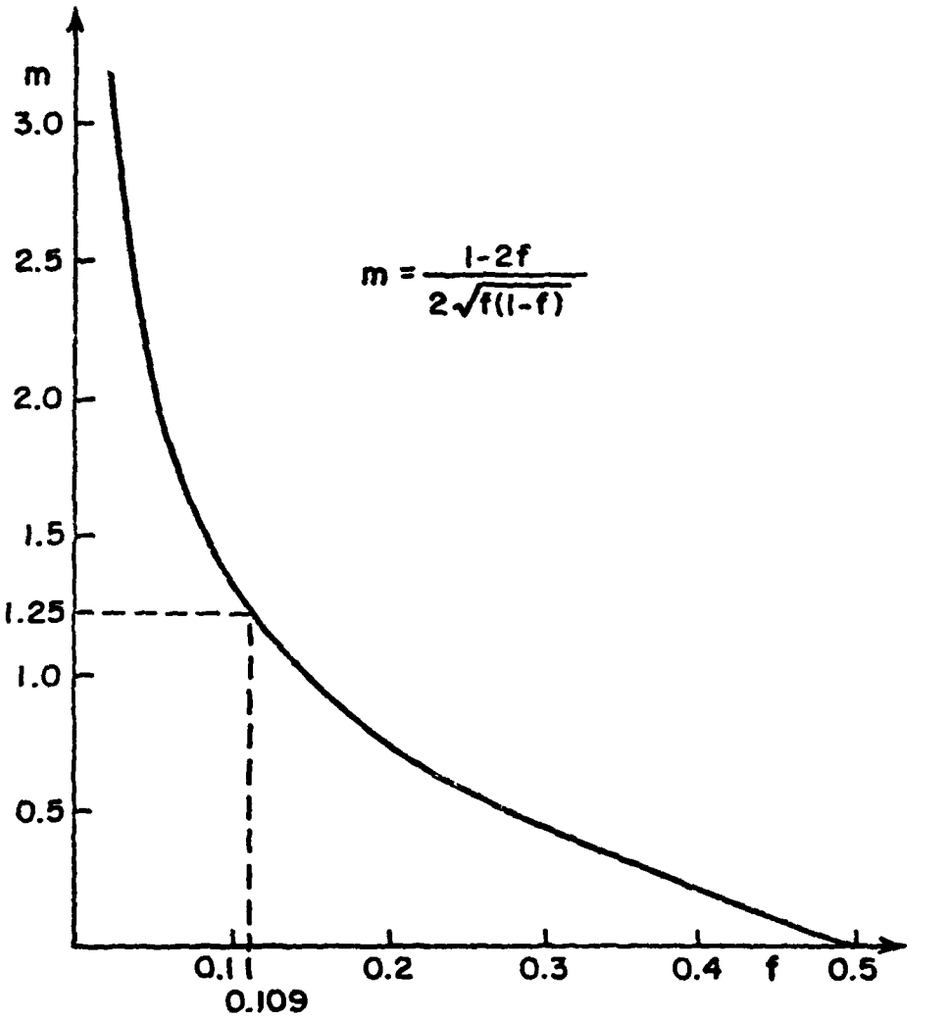

Figure 4. Plot of m versus f, the fraction of area occupied by thermals.

$$u_* = [(\tau_x/\rho_o)^2 + (\tau_y/\rho_o)^2]^{\frac{1}{4}} . \qquad (29)$$

In terms of this friction velocity, the surface boundary conditions (25), (26), (27) and (28) become:

$$u_{rms} = \tau_x/(\rho_o u_*) , \qquad (30)$$

$$v_{rms} = \tau_y/(\rho_o u_*) ,$$

$$w_{rms} = -u_* , \qquad (31)$$

$$T_{rms} = 0 ,$$

where w_{rms} is chosen to be negative because thermals sink ($w'<0<w''$).

At the bottom, $z = -h(t)$, mean quantities match the characteristics of the underlying motionless layer:

$$\bar{u} = 0. ,$$

$$\bar{v} = 0 , \qquad (32)$$

$$\bar{T} = -\Gamma h ,$$

where $\Gamma = d\bar{T}/dz$ is the constant temperature gradient in the stably stratified fluid below the mixed layer (See Figure 3). By definition, the bottom of the thermocline at $z = -h(t)$ is the level beyond which thermals do not penetrate. The thermals' vertical velocity therefore vanishes at that level:

$$w' = 0 . \qquad (33)$$

Strictly, w' ought to be equal to $-dh/dt$, the rate of entrainment at which the bottom of the thermocline deepens. However, the thermals' sinking velocity through the water column is much greater than the rate of deepening of the thermocline, and boundary condition (33) is a valid approximation.

The set of equations requires seven boundary conditions

whereas eight are presently prescribed. The extra condition is precisely the one which will yield a prognostic equation for the mixed-layer depth h(t). The system is thus closed and self-consistent.

5. THE HYPOTHESIS OF A TURBULENT EROSION MODEL (TEM)

For the present boundary conditions, the turbulent kinetic energy input at the surface by the wind is:

$$\begin{aligned} F_s &= -\frac{1}{2}\overline{(w-\bar{w})[(u-\bar{u})^2 + (v-\bar{v})^2 + (w-\bar{w})^2]} - \frac{1}{\rho_o}\overline{(w-\bar{w})(p-\bar{p})} \\ &= -m w_{rms}(u_{rms}^2 + v_{rms}^2 + w_{rms}^2) - \frac{1}{\rho_o} w_{rms} p_{rms} \\ &= m u_*^3 \ , \end{aligned} \tag{34}$$

at z = 0. Thus the coefficient m as defined by (24) is equivalent to the parameter m_o as defined by Niiler (1975).

In the case of no dissipation, the turbulent kinetic energy budget (2) is given by Niiler (1975), de Szoeke and Rhines (1976), Niiler (1977):

$$\frac{1}{4}N^2 h^2 \dot{h} = m u_*^3 + \frac{1}{2}(\bar{\bar{u}}^2 + \bar{\bar{v}}^2)\dot{h} \ , \tag{35}$$

where $\dot{h} = dh/dt$ is the rate of deepening, and the double bar represents a vertical average of mean quantities across the mixed layer. A turbulent erosion model (TEM) balances, in (35), the left-hand side with the first term on the right-hand side, arguing that deepening is caused by erosive action of turbulence propagating from the surface down to the thermocline. A dynamic instability model (DIM), on the other side, balances, in (35), the left-hand

side with the second term on the right-hand side, arguing that deepening results from a shear instability across the thermocline. The computations of de Szoeke and Rhines (1976) show that the DIM holds for times of the order of the inertial period $\frac{2\pi}{f_o}$. At later times, the mass flow in the mixed layer is limited to the Ekman transport, the velocity components $\bar{u}$ and $\bar{v}$ decrease as h^{-1}, and a TEM applies.

Because this study is directed toward long time scales, assumptions will be made to reduce the model to a TEM, and thus decouple the mixed-layer deepening from the mean horizontal flow. The pressure term in equation (22) represents the mechanism of production of turbulent kinetic energy from the mean flow shear (Chapter two). The reduction of the model to a TEM is thus accomplished mathematically by neglecting the pressure term in (22). The final model thus reduces to the following set of equations:

$$\frac{\partial \bar{T}}{\partial t} = -\frac{\partial}{\partial z}(w_{rms}T_{rms}) \tag{36}$$

$$\frac{\partial}{\partial z}(\bar{T}+mT_{rms}) = 0 \tag{37}$$

$$\frac{\partial \bar{u}}{\partial t} - f_o\bar{v} = -\frac{\partial}{\partial z}(u_{rms}w_{rms}) \tag{38}$$

$$\frac{\partial \bar{v}}{\partial t} + f_o\bar{u} = -\frac{\partial}{\partial z}(v_{rms}w_{rms}) \tag{39}$$

$$\frac{\partial}{\partial z}(\bar{u} + 2mu_{rms}) = 0 \tag{40}$$

$$\frac{\partial}{\partial z}(\bar{v} + 2mv_{rms}) = 0 \tag{41}$$

$$3mw_{rms}\frac{\partial w_{rms}}{\partial z} = \alpha g T_{rms} \ , \tag{42}$$

with the boundary conditions at z = 0:

$$T_{rms} = 0 \tag{43}$$

$$u_{rms} = \tau_x/(\rho_o u_*) \tag{44}$$

$$v_{rms} = \tau_y/(\rho_o u_*) \tag{45}$$

$$w_{rms} = -u_* \tag{46}$$

and at z = -h:

$$\bar{T} = -\Gamma h \tag{47}$$

$$\bar{u} = 0 \tag{48}$$

$$\bar{v} = 0 \tag{49}$$

$$w_{rms} = 0. \tag{50}$$

6. CHANGE OF VARIABLE AND FUNCTIONS

Since the mixed layer is constantly deepening it is advantageous to use the similarity variable $\xi = -z/h(t)$ which varies from zero at the surface to one at the bottom of the thermocline.

On the other hand, one may immediately integrate equations (37), (40) and (41) with respect to z and define:

$$\bar{u} = U(t) - 2m\tilde{u}(t,\xi)$$
$$u_{rms} = \tilde{u}(t,\xi) , \tag{51}$$

$$\bar{v} = V(t) - 2m\tilde{v}(t,\xi)$$
$$v_{rms} = \tilde{v}(t,\xi), \tag{52}$$

$$\bar{T} = -\Gamma T(t) - m\,\Gamma\tilde{T}(t,\xi)$$
$$T_{rms} = \Gamma\tilde{T}(t,\xi) , \tag{53}$$

where tilded quantities are ξ and t-dependent and represent rms quantities. The non-tilded quantities U, V and T are constants of intregration and depend upon time only. They will have to be determined by the boundary conditions. Note that due to the presence of the factor Γ, the new temperature variables T(t) and $\tilde{T}(t, \xi)$ have the dimension of a length. The rms vertical velocity may be redefined as:

$$w_{rms} = -\tilde{w}(t, \xi) , \tag{54}$$

in order to work with a positive variable.

With these changes of variable and functions, the remaining governing equations (36), (38), (39), and (42) become:

$$-\dot{\tilde{T}} - m\frac{\partial \tilde{T}}{\partial t} + m\frac{\dot{h}}{h}\xi\frac{\partial \tilde{T}}{\partial \xi} = -\frac{1}{h}\frac{\partial}{\partial \xi}(\tilde{w}\tilde{T}) , \tag{55}$$

$$\dot{U} - 2m\frac{\partial \tilde{u}}{\partial t} + 2m\frac{\dot{h}}{h}\xi\frac{\partial \tilde{u}}{\partial \xi} - f_o V + 2mf_o\tilde{v} = -\frac{1}{h}\frac{\partial}{\partial \xi}(\tilde{u}\tilde{w}) , \tag{56}$$

$$\dot{V} - 2m\frac{\partial \tilde{v}}{\partial t} + 2m\frac{\dot{h}}{h}\xi\frac{\partial \tilde{v}}{\partial \xi} + f_o U - 2mf_o\tilde{u} = -\frac{1}{h}\frac{\partial}{\partial \xi}(\tilde{v}\tilde{w}) , \tag{57}$$

$$3m\tilde{w}\frac{\partial \tilde{w}}{\partial \xi} = -N^2 h\tilde{T}, \tag{58}$$

where $N^2 = \alpha g\Gamma$ is the square of the Brunt-Väisälä frequency in the underlying stratum, and where a dot represents a time derivative. The boundary conditions become:

$$\tilde{T}(0) = 0, \ \tilde{u}(0) = \tau_x/(\rho_o u_*), \ \tilde{v}(0) = \tau_y/(\rho_o u_*), \ \tilde{w}(0) = u_* , \tag{59}$$

and

$$\tilde{T}(1) = (h-T)/m, \ \tilde{u}(1) = U/2m, \ \tilde{v}(1) = V/2m, \ \tilde{w}(1) = 0 \tag{60}$$

This constitutes a set of four coupled first-order non-linear differential equations which require four boundary conditions.

However, they contain four unknown time-dependent functions: T(t), U(t), V(t) and h(t), for which four additional conditions are required. The system consists of eight boundary conditions, precisely what is required.

7. GLOBAL HEAT BUDGET

The heat budget of the whole system yields the temperature T(t) as a function of the mixed-layer depth h(t). Although the result of this section will be recovered after having solved the equations, it is useful to anticipate that result in order to define the Richardson numbers of the next section.

The global heat budget of the mixed layer and thermocline, integrated over time, expresses that the temperature difference from the initial value integrated over the water column is equal to the time integration of the net surface heat flux, which is zero in the present case:

$$\int_{-h}^{0} (\bar{T}-\Gamma z)dz = 0.$$

Using expression (53) for $\bar{T}$ and the vertical momentum equation (58) to eliminate $\tilde{T}$, one obtains:

$$\int_{0}^{1} (-\Gamma T + \frac{3m^2\Gamma}{N^2 h} \tilde{w}\frac{\partial \tilde{w}}{\partial \xi} + \Gamma h\xi)hd\xi = 0 \ ,$$

and, with the use of boundary conditions (59) and (60), the integral yields:

$$T(t) = \frac{h}{2}(1-3m^2\frac{u_*^2}{N^2h^2}) \ . \qquad (61)$$

For oceanic values corresponding to time scales greater than the inertial period, i.e.,

$N \sim 10^{-2} s^{-1}$, $u_* \sim 10^{-2} ms^{-1}$, $h \gtrsim 20$ m, m of the order one,

it is easily seen that the second term in the parentheses in (61) is of order of 10^{-2}. Therefore, because the mixed layer is deep enough ($h >> \frac{u_*}{N}$), the heat budget reduces at the leading order to:

$$T = \frac{h}{2} . \tag{62}$$

This approximate result could have been easily anticipated. Indeed, assuming a well-developed mixed layer of perfectly homogeneous temperature and bounded by a zero-thickness thermocline (see Figure 5.), the global heat budget requires the equality of areas A and B, and therefore $T = h/2$. Because the mean temperature profile $\bar{T}$ is not exactly z-independent, the correction $\tilde{T}$, due to a slight gradient through the mixed layer and to a non-zero thermocline thickness, leads to a value of T which is somewhat reduced, as expressed by (61).

The total buoyancy in the mixed layer is:

$$B = g\frac{\Delta\rho}{\rho_o}h ,$$

where $\Delta\rho$ is the density jump across the thermocline, and ρ_o the reference density. Since $\Delta\rho = \rho_o \alpha \Delta T$, $\Delta T = -\Gamma h/2 + \Gamma h = -\Gamma h/2$, by virtue of (62) (see also Figure 5.), and $N^2 = \alpha g \Gamma$, the total buoyancy may be rewritten as:

$$B = \frac{N^2 h^2}{2} . \tag{63}$$

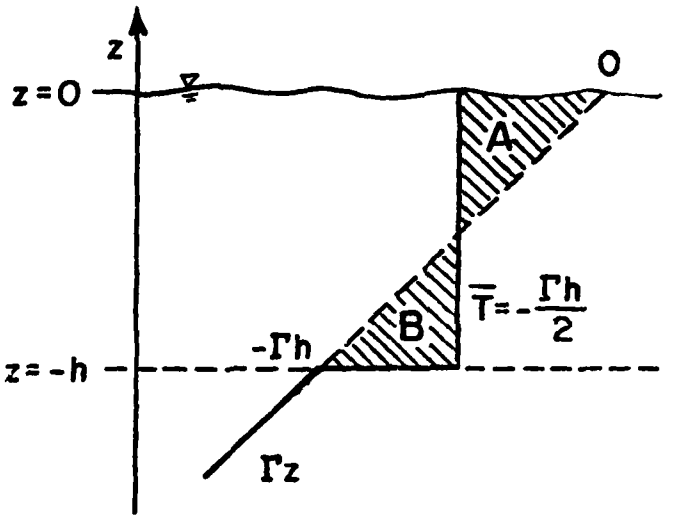

Figure 5. Limiting case of a perfectly homogeneous mixed layer bounded below by a zero-thickness thermocline. The global heat budget requires: Area A = Area B.

8. RICHARDSON NUMBERS

The mixed-layer deepening under the action of a surface wind stress is successfully characterized by the values of two Richardson numbers, ratios of the total buoyancy in the mixed layer to the square of a velocity. The *Frictional Richardson number* is the ratio of B as defined by (63) to the square of the friction velocity u_* as defined by (29), based on the wind-stress amplitude:

$$Ri = \frac{N^2h^2}{2u_*^2} \quad . \tag{64}$$

This is the Richardson number used by Turner and Kraus (1967), Kato and Phillips (1969), Kim (1976), Kullenberg (1977), and Price, Mooers and Van Leer (1978). The *Overall Richardson number* is the ratio of B to the square of the mean horizontal velocity in the mixed layer, here approximated by U^2+V^2 as introduced by (51) and (52):

$$R_v = \frac{N^2h^2}{2(U^2+V^2)} \cdot \tag{65}$$

R_v is the Richardson number used by Pollard, Rhines and Thompson (1973), Garwood (1977), Dillon and Powell (1979), Price (1979) and Kundu (1980a).

Both numbers Ri and R_v are time-dependent through h, U and V, and increase as the mixed layer deepens. They characterize at anytime the state of the system. The frictional number, Ri, is the dominant number in TEM's, for turbulence induced by vertical shear across the thermocline is neglected compared to the surface input. Because the present model is a TEM, the frictional

Richardson number, Ri, will play an essential role. It increases from zero, when the wind starts to blow, to values much larger than unity, when the mixed layer is well-developed ($Ri \sim 10^2$ for orders of magnitude listed in the previous section).

Mathematically, it will be assumed here that the mixed-layer + thermocline system may be treated as an interior + boundary-layer problem. It will be shown *a posteriori* that this simplification holds when

$$Ri >> 1,$$

i.e., when the mixed layer is well-developed.

Another important dimensionless number is the rate of entrainment

$$E = \frac{\dot{h}}{u_*} , \tag{66}$$

the ratio of the deepening rate to the friction velocity, as defined by Kato and Phillips (1969). The friction velocity is characteristic of the vertical downward velocity of thermals. It is anticipated to be large compared to the rate of deepening of the thermocline because thermals take a short time to sink from the surface down to the thermocline compared to the time scale of evolution of the whole system. The entrainment parameter is thus expected to be very small compared to one.

Dimensional analysis leads to the solution of the mixed-layer deepening:

$$E = F(Ri) \tag{67}$$

and $$\frac{U}{u_*} = G_1(Ri), \frac{V}{u_*} = G_2(Ri), \frac{T}{h} = G_3(Ri),$$

where the four functions, F, G_1, G_2 and G_3 result from the solution of the equations.

9. SOLUTION

a) Hypotheses of a quasi-homogeneous mixed layer:

It is well known from observations and laboratory experiments that when the mixed layer is well-developed, it is quasi-homogeneous and bounded below by a thin layer of large gradients, called the thermocline. This behavior may be anticipated a priori and a boundary-layer treatment is therefore the appropriate method of solution. The system is divided into two regions, the interior region where the horizontal velocity and temperature are almost constant with depth

$$\tilde{u} << U,\ \tilde{v} << V,\ \tilde{T} << T\ ,$$
$$\frac{\partial}{\partial \xi} = O(1), \tag{68}$$

and the thermocline, where vertical gradients are anticipated to be very large:

$$\tilde{u} \sim U,\ \tilde{v} \sim V,\ \tilde{T} \sim T,$$
$$\frac{\partial}{\partial \xi} >> O(1). \tag{69}$$

These assumptions will be verified a posteriori, and it will be shown that they are correct provided that Ri is much greater than

b) Solution in the mixed layer

Assuming a quasi-homogeneous mixed layer, equations (55) to (58) reduce to:

$$-\dot{\tilde{T}} = -\frac{1}{h}\frac{\partial}{\partial\xi}(\tilde{w}\tilde{T}) \quad , \tag{70}$$

$$\dot{U} - f_o V = -\frac{1}{h}\frac{\partial}{\partial\xi}(\tilde{u}\tilde{w}) \quad , \tag{71}$$

$$\dot{V} + f_o U = -\frac{1}{h}\frac{\partial}{\partial\xi}(\tilde{v}\tilde{w}) \quad , \tag{72}$$

$$3m\tilde{w}\frac{\partial\tilde{w}}{\partial\xi} = -N^2 h\tilde{T} \quad . \tag{73}$$

The left-hand sides of the first three equations are independent of ξ. Integrations with respect to ξ and use of surface boundary conditions (59) yield:

$$\tilde{T} = \frac{h\dot{\tilde{T}}\xi}{\tilde{w}} \quad , \tag{74}$$

$$\tilde{u} = \frac{\tau_x/\rho_o - h(\dot{U}-f_o V)\xi}{\tilde{w}} \quad , \tag{75}$$

$$\tilde{v} = \frac{\tau_y/\rho_o - h(\dot{V}+f_o U)\xi}{\tilde{w}} \quad . \tag{76}$$

Replacing $\tilde{T}$ by (74) in equation (73) yields a single equation for $\tilde{w}$ whose solution is:

$$\tilde{w}^3 = u_*^3 - \frac{N^2 h^2 \dot{\tilde{T}}}{2m}\xi^2 \quad , \tag{77}$$

after the surface boundary condition (59) has been used.

c) Solution in the thermocline:

The dominant terms in the governing equations are now those which include derivatives with respect to ξ. Moreover, since this boundary layer lies near $\xi = 1$, ξ may be replaced by one where it appears. Equations (55) to (58) now reduce to:

$$m\frac{\bar{h}}{h}\frac{\partial\tilde{T}}{\partial\xi} = -\frac{1}{h}\frac{\partial}{\partial\xi}(\tilde{w}\tilde{T}) \quad , \tag{78}$$

$$2m\frac{\bar{h}}{h}\frac{\partial\tilde{u}}{\partial\xi} = -\frac{1}{h}\frac{\partial}{\partial\xi}(\tilde{u}\tilde{w}) \quad , \tag{79}$$

$$2m\frac{\bar{h}}{h}\frac{\partial\tilde{v}}{\partial\xi} = -\frac{1}{h}\frac{\partial}{\partial\xi}(\tilde{v}\tilde{w}) \quad , \tag{80}$$

$$3m\tilde{w}\frac{\partial\tilde{w}}{\partial\xi} = -N^2h\tilde{T} \quad . \tag{81}$$

These last equations may be easily integrated with respect to ξ. The constants of integration are determined by using the bottom boundary conditions (60):

$$\tilde{T} = \frac{(h-T)\bar{h}}{\tilde{w}+m\bar{h}} \quad , \tag{82}$$

$$\tilde{u} = \frac{\bar{h}U}{\tilde{w}+2m\bar{h}} \quad , \tag{83}$$

$$\tilde{v} = \frac{\bar{h}V}{\tilde{w}+2m\bar{h}} \quad , \tag{84}$$

where $\tilde{w}$ is implicitly given by the cubic polynominal:

$$\tilde{w}^3 + \tfrac{3}{2}m\bar{h}\tilde{w}^2 = \frac{N^2h(h-T)\bar{h}}{m}(1-\xi) \quad . \tag{85}$$

10. MATCHING OF SOLUTIONS

The two sets of solutions were obtained independently for the mixed layer and thermocline by using surface and bottom boundary conditions, respectively. However, they ought to be the asymptotic forms of a unique set of solutions valid throughout the whole water column. This requires imposing matching conditions. As a result,

four prognostic equations for the time-dependent functions T, U, V and h will be obtained.

Mathematically, matching conditions are obtained by writing that, for each variable $\tilde{T}$, $\tilde{u}$, $\tilde{v}$ and $\tilde{w}$, the mixed layer solution for ξ approaching unity is equal to the thermocline solution for $\tilde{w}$ much greater than $\dot{h}$. The resulting relations are:

$$\frac{h\dot{\tilde{T}}}{\tilde{w}} = \frac{(h-T)\dot{h}}{\tilde{w}} \quad ,$$

$$\frac{\tau_x/\rho_o - h(\dot{U}-f_oV)}{\tilde{w}} = \frac{\dot{h}U}{\tilde{w}} \quad ,$$

$$\frac{\tau_y/\rho_o - h(\dot{V}+f_oU)}{\tilde{w}} = \frac{\dot{h}V}{\tilde{w}} \quad ,$$

$$u_*^3 - \frac{N^2h^2\dot{\tilde{T}}}{2m} + \frac{N^2h^2\dot{\tilde{T}}}{m}(1-\xi) = \frac{N^2h(h-T)\dot{h}}{m}(1-\xi) \, .$$

The above equations can be rewritten as:

$$(hT)^{\cdot} = h\dot{h} \quad , \tag{86}$$

$$(hU)^{\cdot} - f_o(hV) = \frac{\tau_x}{\rho_o} \quad . \tag{87}$$

$$(hV)^{\cdot} + f_o(hU) = \frac{\tau_y}{\rho_o} \quad , \tag{88}$$

$$N^2h^2\dot{\tilde{T}} = 2mu_*^3 \quad . \tag{89}$$

Equation (86) can be integrated over time in order to obtain T in terms of h:

$$T = \frac{h}{2}\left[1 + \frac{\text{constant}}{h^2}\right] \quad . \tag{90}$$

The constant of integration cannot be determined by the initial conditions, since the boundary-layer technique breaks down at the incipient deepening, when the mixed layer and thermocline are not well-defined. But, equation (90) is identical to the global heat budget (61), which is an exact result for all times. The constant of integration is therefore $-3m^2u_*^2/N^2$ and,

$$T = \frac{h}{2}\left(1 - \frac{3m^2}{2Ri}\right) \quad , \tag{91}$$

which reduces to (62), because Ri is much greater than one.

Equations (87) and (88) are the classical transport equations, whose general solution contains inertial oscillations superimposed on an Ekman drift to the right of the wind stress. For a time-dependent wind stress, the solution is:

$$hU = h_oU_o + \frac{1}{\rho_o}\int_o^t [\tau_x(\tau)\ \mathrm{cosf}_o(t-\tau) + \tau_y(\tau)\ \mathrm{sinf}_o(t-\tau)]d\tau \quad ,$$

$$hV = h_oV_o + \frac{1}{\rho_o}\int_o^t [\tau_y(\tau)\ \mathrm{cosf}_o(t-\tau) - \tau_x(\tau)\ \mathrm{sinf}_o(t-\tau)]d\tau \quad .$$

The last relation (89) combined with (91) is the prognostic equation for the mixed-layer depth, and is discussed in the next section. Finally, the vertical profiles valid throughout the water column are:

$$\tilde{T} = \frac{h\dot{T}\xi}{m\dot{h}+\tilde{w}} \quad , \tag{92}$$

$$\tilde{u} = \frac{\tau_x/\rho_o(1-\xi) + \dot{h}U\xi}{\tilde{w} + 2m\dot{h}} \quad , \tag{93}$$

$$\tilde{v} = \frac{\tau_y/\rho_o(1-\xi) + \dot{h}V\xi}{\tilde{w} + 2m\dot{h}} \quad , \tag{94}$$

where $\tilde{w}$ is implicitly given by:

$$\tilde{w}^3 + \tfrac{3}{2}mh\dot{\tilde{w}}^2 = u_*^3(1-\xi^2) \ . \qquad (95)$$

It is evident from the structure of this final solution (92) to (95) that similarity solutions do not exist. None of the variables can be expressed as single products of time dependent and ξ-dependent functions. The approach of Kundu (1980b) is therefore not justified.

11. MIXED-LAYER DEEPENING

Equations (91) and (89) form a coupled set of equations for T and h. Eliminating T, a prognostic equation for h is obtained:

$$(N^2h^2 + 3m^2u_*^2)\dot{h} = 4mu_*^3 \ , \qquad (96)$$

which reduces to

$$N^2h^2\dot{h} = 4mu_*^3 \ , \qquad (97)$$

since it was assumed that Ri>>1. This last equation is the turbulent kinetic energy budget for a TEM without dissipation, expressing that the time rate of change of potential energy equals the turbulent kinetic energy input by wind at the surface. If the wind-stress amplitude is constant with time, the mixed-layer depth increases in time as $t^{\frac{1}{3}}$.

In a dimensionless form, (96) and (97) become:

$$E = \frac{2m}{\frac{3m^2}{2}+Ri} \ , \qquad (98)$$

and

$$E = \frac{2m}{Ri} \ , \qquad (99)$$

respectively, where E and Ri are defined by (66) and (64). The dependence of the entrainment rate on the inverse of the frictional Richardson number has long been observed in the laboratory (Kato and Phillips, 1969) as well as in oceans and lakes (Kullenberg, 1977; Price, et al., 1978; Dillon and Powell, 1979).

Various values of m are proposed by authors while more can be computed from data in the literature. A summary is shown in Table 1. From the table, one concludes that all the values of m agree rather well, approximately one or slightly larger. Values of f, the fraction of area occupied by thermals, were computed by (24) and are found of order of 10%. Thermals are thus rather small disturbances among a return flow which occupies most of the available surface. This result agrees with numerical calculations (Piacsek, 1968) and laboratory observations (Turner, 1973), which all show that thermals or plumes are narrow and occupy a small fraction of the total area of any level. For a system where the roles played by thermals and anti-thermals are perfectly symmetric, one can argue that the value of f ought to be 50%. However, in the present situation, thermals are locally generated very near the surface while anti-thermals are progressively formed in the water column as they rise, and an excess of momentum is input locally at the surface, while it is progressively consumed for an evenly-distributed momentum increase of the water column. These asymmetries explain why thermals are narrow and anti-thermals diffuse and thus why f differs markedly from 50%.

The correction in the denominator of (98) is reminiscent of

TABLE 1

Year	Author(s)	Data	R_i	m	f
1969	Kato and Phillips	Laboratory	15-400	1.25	0.11
1973	Denman and Miyake	Station Papa	150	1.0	0.15
1974	Halpern	Northeast Pacific	80	2.8	0.03
1977	Kullenberg	Coastal waters - Lakes	$10-10^4$	1.1	0.13
1978	Price et al.	West Florida cont. shelf	300	0.9	0.17
1979	Dillon and Powell	Lake Tahoe, CA-NV	30	0.90-1.6	0.08-0.17

Table 1. Values of the coefficient m found in the literature or computed from published data. The values of the frictional Richardson number for which the data were taken and the values of f computed from (24) are also given.

Of the one proposed by Kim (1976):

$$E = \frac{2m}{(c_m/u_*)^2+Ri} \quad ,$$

where $\frac{1}{2}c_m^2$ is the average turbulent kinetic energy across the mixed layer. For m = 1.25, Kim proposes $(c_m/u_*)^2 = 9$, while (98) yields $\frac{3m^2}{2} = 2.34$. The corrections are thus of the same order of magnitude.

The results of this section permit justification of the assumptions which were stated before solving the equations. One has to show that the approximations

$$\tilde{T}<<T, \ \tilde{u}<<U, \ \tilde{v}<<V$$

hold in the mixed layer as long as Ri>>1. In the mixed layer, $\tilde{w}$ is of order of u_*, its surface value, which is much larger than $\mathring{h}$ according to (99). From (92), (93) and (94), one obtains:

$$\frac{\tilde{T}}{T} \sim \frac{\tilde{u}}{U} \sim \frac{\tilde{v}}{V} \sim \frac{\mathring{h}}{u_*} \sim Ri^{-1} << 1 \ ,$$

which validates the method of solution chosen for this problem.

12. THICKNESS OF THE THERMOCLINE

Due to non-linearities, the boundary-layer method applied here differs from classical applications to linear systems, and caution must be exercised when one evaluates the boundary-layer thickness. At first, one could think that the thermocline is the region where $\tilde{w}$ is of order $\mathring{h}$, so that corrections in the denominators of (92) to (94) become important. This argument leads to a dimensionless thermocline thickness of order Ri^{-3}, which is

much too small. There is a thicker layer where boundary corrections start to appear in the solution. Indeed, in the temperature equation (55),

$$\underset{(a)}{-\dot{\tilde{T}}} \; \underset{(b)}{-\; m\frac{\partial \tilde{T}}{\partial t}} \; + \; \underset{(c)}{m\frac{\dot{h}}{h}\xi\frac{\partial \tilde{T}}{\partial \xi}} \; = \; \underset{(d)}{-\frac{1}{h}\frac{\partial}{\partial \xi}(\tilde{w}\tilde{T})} \; ,$$

The right-hand side, term (d), balances term (a) in the mixed layer, while it balances term (c) in the thermocline. The top of the thermocline is thus the level where term (c) begins to take over term (a). Boundary corrections therefore start to appear where these two terms compete, i.e., where

$$\dot{T} \sim \frac{\dot{h}}{h}\xi\frac{\tilde{T}}{\delta\xi} \; ,$$

where $\delta\xi$ is the dimensionless thermocline thickness. Because the boundary layer is a thin region, ξ is almost one, and, according to (89) and (92), T is of order of $\frac{hu_*}{Ri\tilde{w}}$, so that:

$$\delta\xi \sim \frac{u_*}{Ri\tilde{w}} \qquad (100)$$

The balance of the vertical-momentum equation (58) combined with (89) requires:

$$\frac{\tilde{w}^2}{\delta\xi} \sim \frac{u_*^3}{\tilde{w}} \; . \qquad (101)$$

Combination of (100) with (101) finally yields:

$$\delta\xi \sim Ri^{-\frac{3}{4}} \; , \qquad (102)$$

$$\tilde{w} \sim u_* Ri^{-\frac{1}{4}} \; . \qquad (103)$$

Therefore the dimensionless thickness of the thermocline is $Ri^{-\frac{3}{4}}$ rather than Ri^{-3}.

In a study of turbulence and entrainment within the interfacial zone bounding a mixed layer, Long (1978) concludes that turbulent

patches have a dimension $hRi^{-\frac{3}{4}}$, and that the rms vertical velocity in the mixed layer near the interface is of order $u_{*}Ri^{-\frac{1}{4}}$. The agreement between the two approaches is perfect, and supports the modelling by two interacting fluids as a theory of convective turbulence.

The actual dimensional thickness of the thermocline is:

$$h\delta\xi = \left(\frac{u_{*}}{N}\right)^{\frac{3}{2}} h^{-\frac{1}{2}} , \qquad (104)$$

and decreases as the mixed layer deepens. This interface shallowing was observed in laboratory experiments (Kato and Phillips, 1969) and in numerical experiments (Kundu, 1980a).

13. VERTICAL PROFILES

Solutions (92) to (95) govern the vertical variations of rms fluctuations throughout the mixed layer and thermocline. They can be used in (51) to (54) to yield the profiles of mean quantities they can also be combined to form vertical fluxes.

Figures 6 to 13 are plots of vertical profiles of physical quantities of interest. The wind stress is taken in the x-direction:

$$\tau_x/\rho_o = u_{*}^2 ,$$

$$\tau_y/\rho_o = 0 ,$$

and mean currents at 45° to its right:

$$U = -V = ku_{*} .$$

The values assigned to the various parameters are:

$$Ri = 100,\ m = 1.25\ (f = 0.11),\ k = 7.$$

Figure 6 is a plot of the turbulent vertical velocity, which is proportional to the thermals' vertical velocity. Thermals leave the surface with the friction velocity imposed by the surface stress. As they sink, they become slightly buoyant and decelerate. Their velocity vanishes precisely at the bottom of the thermocline.

Figure 7 shows the mean temperature profile. The temperature is almost homogeneous in the mixed layer and equal to $-\Gamma h/2$, as required by heat conservation. There is however a slight stable gradient of order Ri^{-1}, so that thermals progressively become buoyant and decelerate as they sink through the mixed layer. The thermocline is well-defined, and its thickness corresponds to (102). Figure 8 shows the development of the mixed layer and the shallowing of the thermocline as time goes on.

Figure 9 shows the vertical profiles of horizontal velocity components, $\bar{u}$ and $\bar{v}$. The mixed layer is quasi-homogeneous as required by the assumptions made in order to solve analytically the governing equations. This excludes Ekman veering with depth, and separates the flow into a depth-independent inertial oscillation and a quasi-steady shearing flow that carries the turbulent stresses downward through the mixed layer. This is similar to the results of Kundu (1980a) for time scales greater than the inertial period, when his model becomes a TEM. The velocity $\bar{u}$ in the direction of

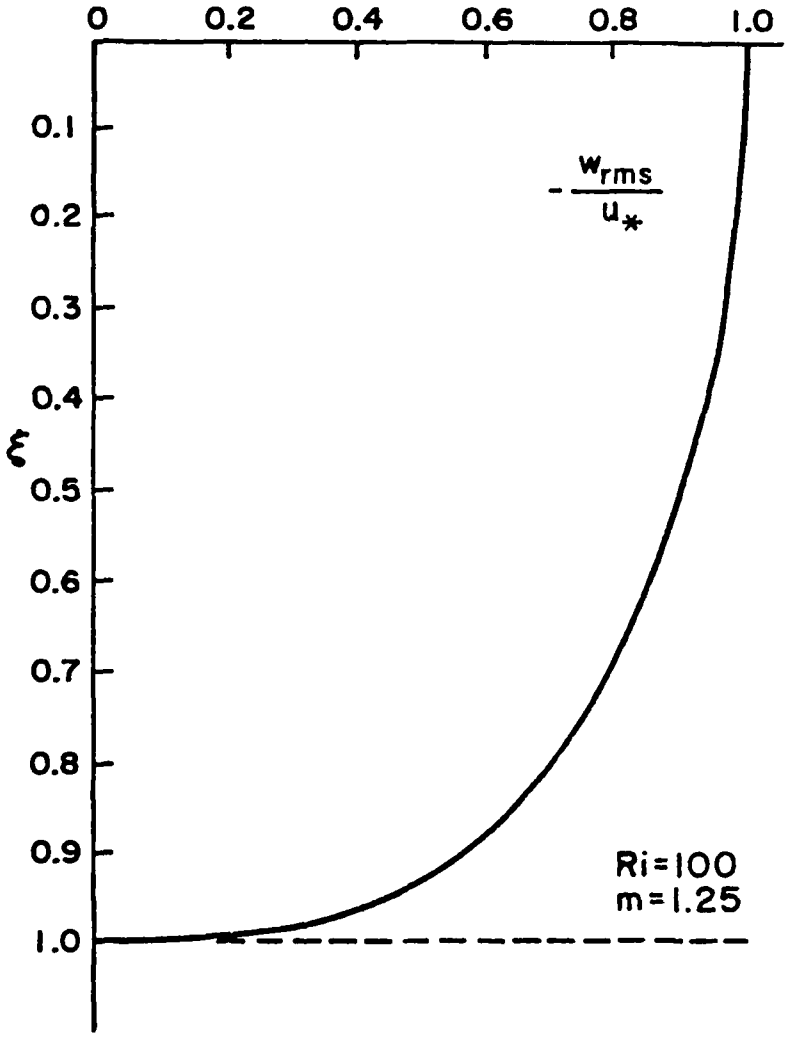

Figure 6. Profile of turbulent vertical velocity, scaled by the friction velocity.

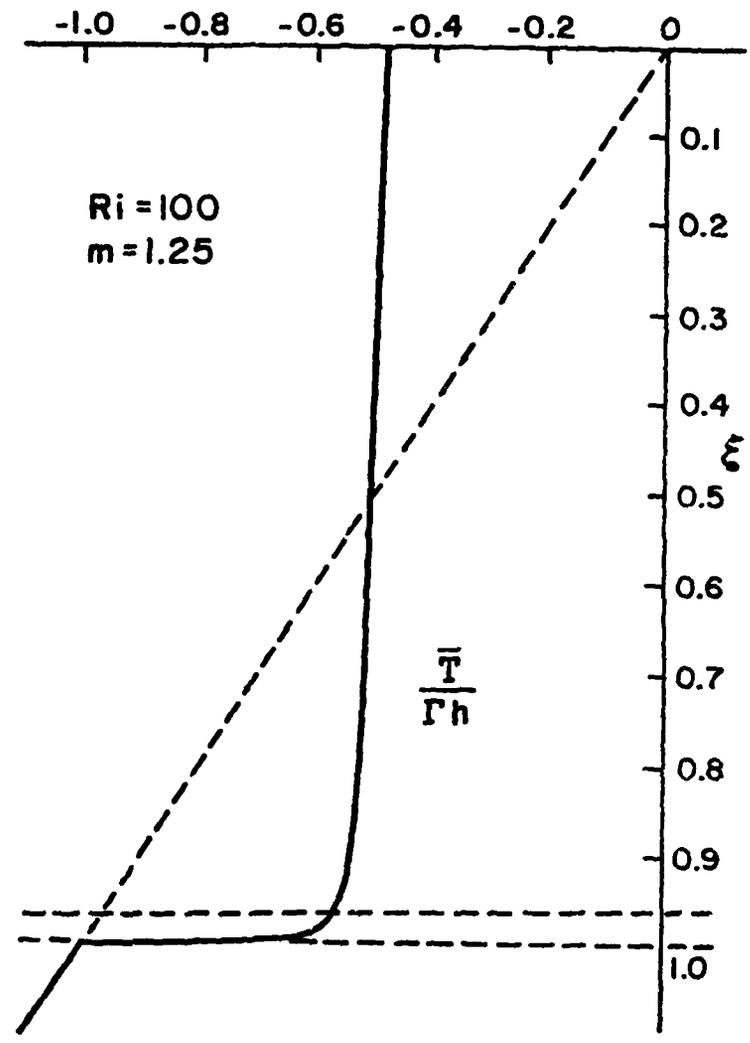

Figure 7. Mean temperature profile.

AD-A093 101 FLORIDA STATE UNIV TALLAHASSEE MESOSCALE AIR-SEA INT--ETC F/G 8/3
MIXING, CONVECTION, AND ADVECTION IN THE UPPER OCEAN.(U)
NOV 80 B CUSHMAN-ROISIN N00014-75-C-0201
UNCLASSIFIED 171 NL

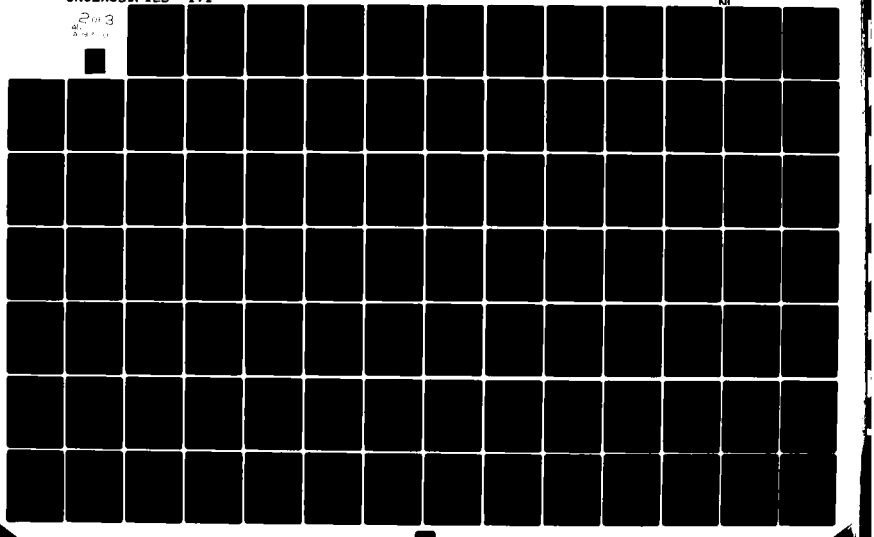

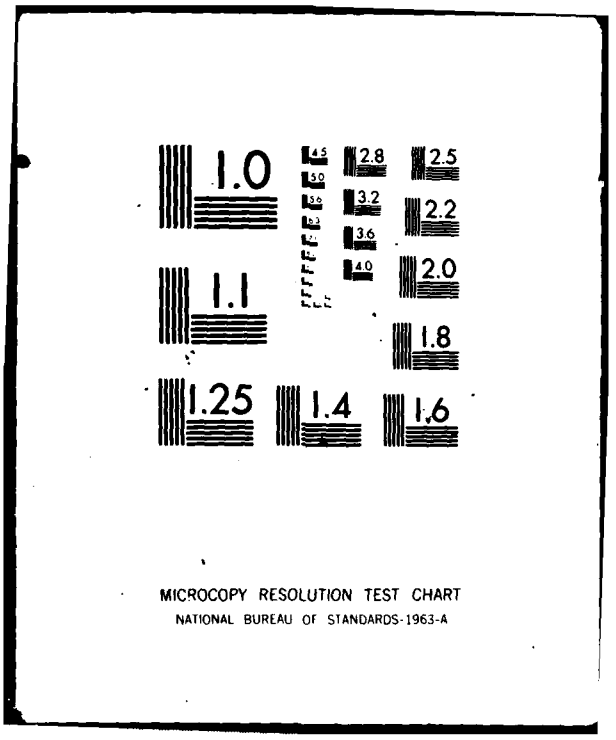
1.0
1.1
1.25
1.4
1.6
1.8
2.0
2.2
2.5
2.8
3.2
3.6
4.0
4.5
5.0
5.6
6.3
7.1
8.0
9.0
10.0
11.0
12.5
14.0
16.0
18.0
20.0
22.0
25.0
28.0
32.0
36.0
40.0
45.0
50.0
56.0
63.0
71.0
80.0
90.0
100.0
MICROCOPY RESOLUTION TEST CHART
NATIONAL BUREAU OF STANDARDS-1963-A

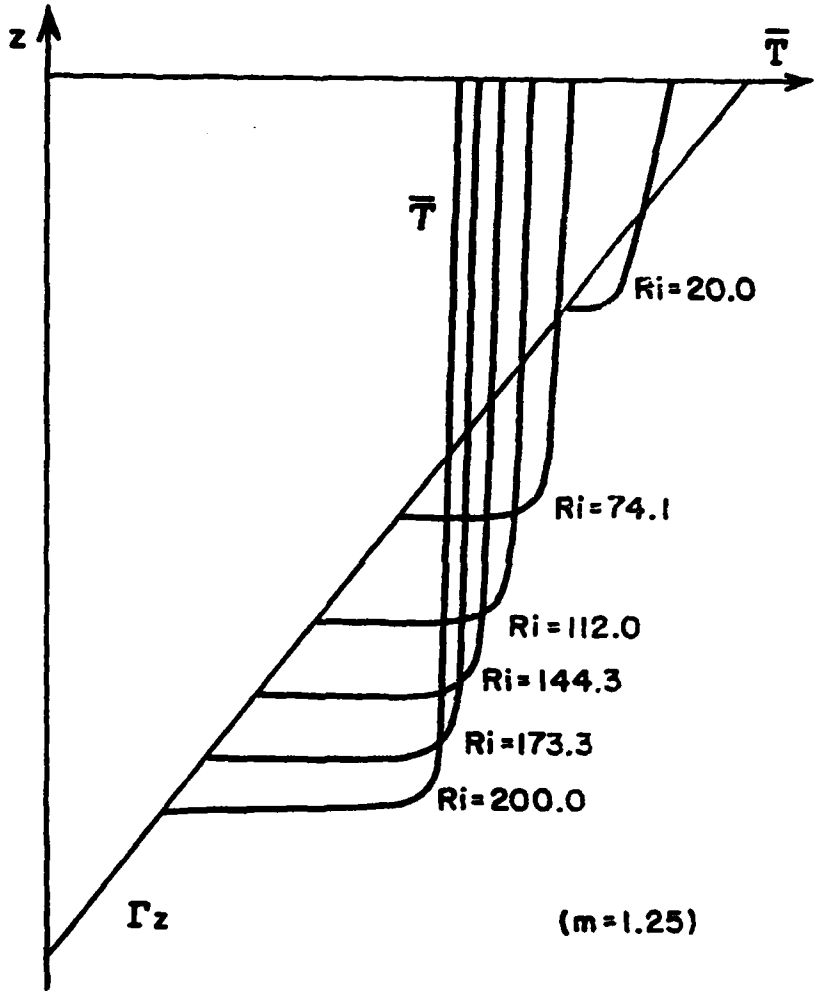

Figure 8. Development of the mixed layer. Constant time intervals separate mean temperature profiles.

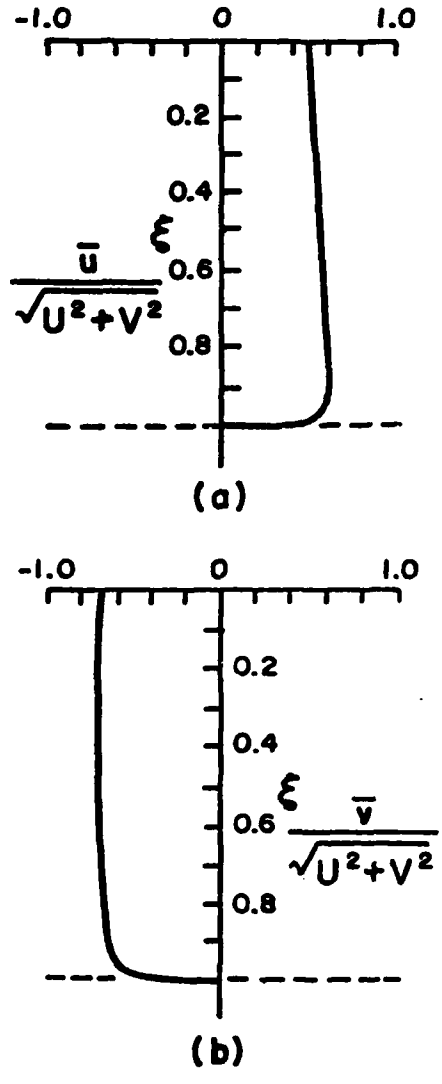

Figure 9. Profiles of mean horizontal velocity components, scaled by $\sqrt{U^2+V^2}$; $\bar{u}$ is in the direction of the imposed wind stress.

the surface stress increases slightly with depth. The reason is the following: as thermals sink, they progressively exchange with anti-thermals the extra momentum they have received near the surface. This reduces the turbulent fluctuations, and increases the mean value accordingly. The $\bar{v}$-profile does not exhibit such behavior since there is no extra-momentum in the y-direction given at the surface. In the thermocline, both profiles curve sharply and vanish so as to match the bottom boundary conditions.

Figures 10a and b show the vertical profiles of the Reynolds stresses, $-\overline{uw}$ and $-\overline{vw}$, scaled by the surface stress. Both stresses vary linearly through the mixed layer, from the imposed value at the surface, to a residual value at the top of the thermocline. These residual values are $\mathring{h}U$ and $\mathring{h}V$, and are precisely the jump conditions imposed by authors of bulk models (Niiler, 1975, for example). The stresses decrease rapidly through the thermocline to zero so as to meet bottom boundary conditions.

From mean profiles and stresses, one can compute eddy viscosities defined by:

$$\nu_u = \frac{-\overline{uw}}{\frac{\partial \bar{u}}{\partial z}} \quad \text{and} \quad \nu_v = \frac{-\overline{vw}}{\frac{\partial \bar{v}}{\partial z}} \ .$$

Figures 11a and b show the results. The eddy viscosity in the x-direction is negative in the mixed layer due to the increase of $\bar{u}$ with depth. The negative values are correlated with a transfer of momentum from turbulent motions to mean current. The turbulence generated at the surface by the wind is progressively

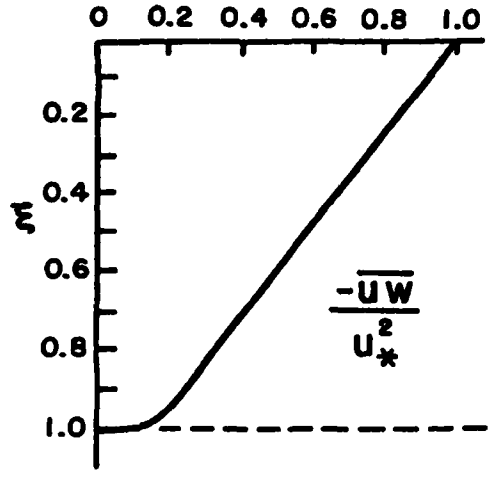

(a)

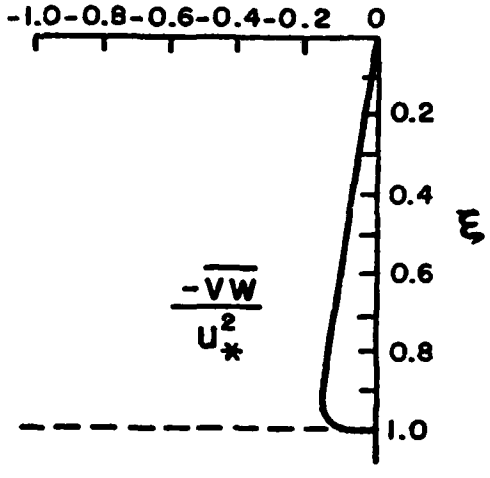

(b)

Figures 10a and b. Profiles of the Reynolds stresses $-\overline{uw}$ and $-\overline{vw}$, scaled by the surface stress u_*^2 in the x-direction.

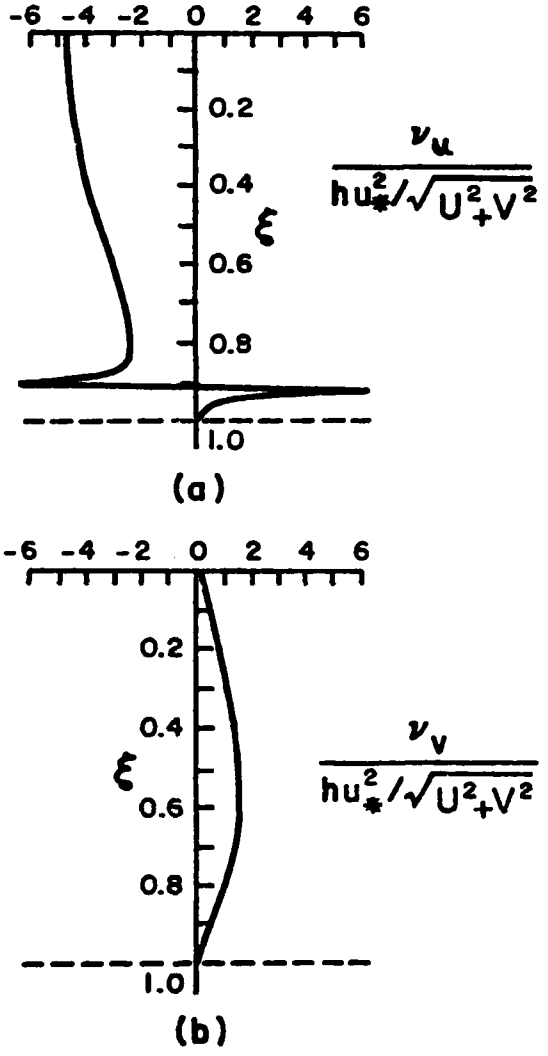

Figures 11a and b. Profiles of the eddy viscosities ν_u and ν_v (cfr. text), scaled by $hu_*^2/\sqrt{U^2+V^2}$.

structured to increase the mean current. In the y-direction, no turbulence is supplied at the surface, and fluctuations increase downward due to differences between sinking thermals and rising anti-thermals. At the level where $\bar{u}$ is maximum, a little above the thermocline, ν_u is unbounded, as a result of its definition. Below that level, in the thermocline, the strong shear of the mean flow generates turbulence, and eddy viscosities are both positive. They vanish at the bottom of the thermocline, where stresses vanish, and shear is maximum. It is worth noting that ν_u is quasi-constant near the surface, and that ν_v increases linearly from the surface like

$$\nu_v \sim \frac{u_*}{2m} |z| ,$$

in agreement with the classical theory of turbulence. The corresponding Von Kármán constant is

$$\kappa = \frac{1}{2m} = 0.40 ,$$

for m = 1.25. This result is encouraging. There is therefore a link between the parameter m and the Von Kármán constant. The laboratory value obtained for m is in perfect agreement with laboratory measurements of turbulent flow.

Figure 12 shows the profile of the vertical convective heat flux. Mixing brings cold water from below, cools the surface layers and heats the fluid recently entrained in the convective process. There is therefore downward transfer of heat. This is the reason why the heat flux is negative everywhere. The constant gradient through the mixed layer corresponds to a homogeneous

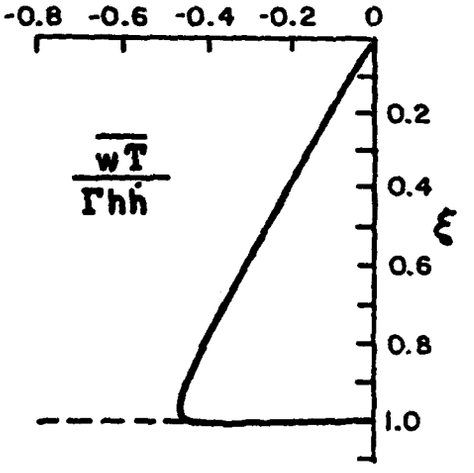

Figure 12. Profile of the vertical convective heat flux $\overline{wT}$, scaled by $\Gamma h \dot{h}$.

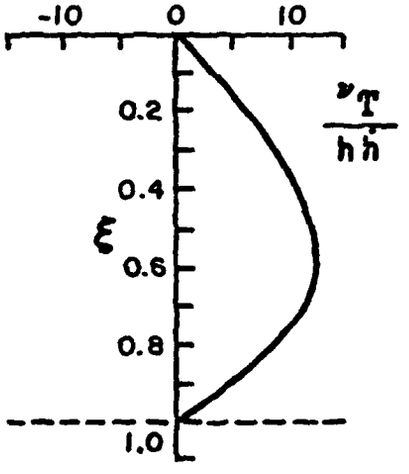

Figure 13. Profile of the eddy heat diffusivity ν_T (cfr. text), scaled by $h\dot{h}$.

cooling of the fluid, as stated by the heat equation (15). The maximum negative value at the top of the thermocline is close to $-\frac{1}{2}\Gamma h\dot{h}$, which is the jump condition across the thermocline, used in bulk models (Kraus and Turner, 1967, for example).

Figure 13 shows the profile of the eddy heat diffusivity defined by

$$\nu_T = \frac{-\overline{wT}}{\overline{\frac{\partial T}{\partial z}}} \quad .$$

It is positive everywhere, and has a profile similar to ν_v .

14. MONIN-OBUKOV LENGTH

The Monin-Obukov length is a measure of turbulence in convection. It is generally defined as (Turner, 1973; Zilitinkevich, et al., 1979):

$$\ell = \frac{u_*^3}{\kappa \overline{B}}$$

where u_* is the friction velocity characteristic of the turbulence, κ the Von Kármán constant, and $\overline{B}$ the vertical buoyancy flux.

In the present case, the vertical buoyancy flux is noted

$$\overline{B} = \alpha g |\overline{wT}| \quad ,$$

which is zero at the surface and at the bottom of the thermocline. It is maximum near the top of the thermocline. The value of that maximum is obtained (at the leading order in Ri^{-1}) as the limit of the mixed-layer buoyancy flux as ξ tends to one:

$$\overline{B} = \lim_{\xi \to 1} \alpha g |\overline{wT}| = N^2 h\dot{T} \quad ,$$

by using (10), (14) and (74). Using this value in the definition of ℓ, one obtains:

$$\ell = \frac{2u_*^3}{\kappa N^2 h\tilde{h}} = \frac{1}{2\kappa m} h ,$$

by virtue of (89). The Monin-Obukov length is therefore proportional to h. The coefficient of proportionality $(2\kappa m)^{-1}$ equals unity for $\kappa = 0.40$ and $m = 1.25$. This result has a physical reason: the wind-mixed layer is a convective system generated by surface turbulence; therefore, turbulence and convection have equal importance, and the Monin-Obukov length has to be proportional to and of order of the depth of the layer i.e., h.

Inversely, this physical argument could have been used independently, by writing *a priori* $\ell = h$ (Zilitinkevich, et al., 1979). The model would therefore conclude that $(2\kappa m)^{-1}$ equals one, or

$$m = 1.25,$$

for $\kappa = 0.40$. The value of m can therefore be inferred from the theory, and be compared to observations and laboratory experiments (see Table 1). The agreement is excellent.

When a buoyancy flux (cooling or heating) is imposed at the surface, convection or re-stratification may dominate turbulence. In such a case, the Monin-Obukov length is expected to be smaller or larger than h, and the resulting values of m are expected to be greater or smaller than 1.25.

15. CONCLUSIONS

A new model of convection and mixing was applied to the study of mixed-layer deepening under the action of wind stress. It is based on a modelling by two interacting fluids. Emphasis was not on the energetics, but rather on the dynamics of mixing. Turbulence production by mean shear near the thermocline was neglected in order to simplify the vertical-momentum equation. The model is thus a turbulent erosion model, for which the potential-energy increase required for deepening is provided by turbulence input at the surface.

A simple analytical solution was found in the case where the mixed layer is well-mixed and separated from the underlying quiescent fluid by a sharp thermocline. The results are valid if the frictional Richardson number is much greater than unity, the condition for a sharp thermocline to exist. Expressions for the thermocline thickness and turbulence scale near the thermocline are in very good agreement with previous results of turbulence theory.

Vertical profiles were then plotted. The turbulent vertical velocity decreases monotonically from a maximum value at the surface down to zero at the bottom of the thermocline, without showing any sudden variations in the thermocline. The temperature profile is composed of a quasi-constant value through the mixed layer and of a rapid variation in the thermocline. Velocity

profiles show the separation of the flow into a depth-independent inertial oscillation and a quasi-steady shearing flow that carries the turbulent stresses downward through the mixed layer. In the thermocline, the profiles curve sharply in order to match the zero mean velocity in the underlying stable fluid. Reynolds stresses and vertical convective heat flux vary linearly through the mixed layer from their respective imposed surface values to residual values required for entraining new fluid in the mixing process. In the thermocline, they rapidly decrease to zero. Resulting eddy diffusivities of heat and momentum were computed and plotted. The eddy viscosity of the flow in the direction of the wind stress is negative near the surface, implying that a part of the turbulent energy supplied at the surface goes to the mean flow. In the direction perpendicular to the surface stress, the eddy viscosity varies like the eddy heat diffusivity, vanishing at the surface and at the bottom of the thermocline, and reaching a maximum somewhere at mid-depth. Finally, an argument based on the proportionality between the Monin-Obukov length and the mixed-layer depth led to relate the parameter m, ratio of the turbulent kinetic energy input to the cube of the friction velocity, to the Von Kármán constant. The value was found to be equal to the one proposed by Kato and Phillips (1969) and in good agreement with field observations.

APPENDIX C

The entrainment layer

The results presented in the previous section [equations (92) to (95)] were based on the assumption of a constant fraction of area occupied by thermals throughout the mixed layer and thermocline. This, however, leads to some inconsistencies. At the bottom of the thermocline (z=-h), the anti-thermals' variables are given by:

$$T'' = -\frac{1-f}{1-2f}\,\Gamma h\ ,$$

$$u'' = -\frac{f}{1-2f}\,U\ , \qquad \text{(C1)}$$

$$v'' = -\frac{f}{1-2f}\,V\ .$$

At that level, however, anti-thermals are constituted of newly entrained fluid, and the expected values are

$$T'' = -\Gamma h,\ u'' = v'' = 0\ . \qquad \text{(C2)}$$

The values (C1) reduce to (C2) if f = 0.

Therefore, these inconsistencies can be removed by including a new boundary layer below the thermocline, here named the *entrainment layer*. The role of this layer is to allow f to decrease from its constant value in the mixed layer and thermocline, through this entrainment layer, down to zero in the quiescent fluid underneath it.

The purpose of this appendix is to show that, based on scaling arguments, this entrainment layer is in fact very thin and, thus, cannot have any effect on the dynamics of the whole system.

In a thin layer of large gradients, the mean-temperature equation reduces to (78), implying that the scale for the vertical-velocity fluctuation, w_{rms}, is $\dot{h}$. Physically, this scaling expresses that, in that region, thermals sink at a velocity comparable to the rate of deepening.

Assuming that heat transfers between thermals and anti-thermals are controlled by molecular diffusion in the entrainment layer, one can write

$$\frac{\dot{h}}{d} \Delta T = \frac{\nu \Delta T}{d^2} \tag{C3}$$

where d is the thickness of the layer, ΔT, the scale for the temperature difference between thermals and anti-thermals, and ν, the molecular heat diffusivity ($\nu = 1.4 \times 10^{-7} m^2 s^{-1}$, for water at 15°C). From the above equation it appears that the layer thickness is:

$$d = \frac{\nu}{\dot{h}} \tag{C4}$$

For typical oceanic values, $\dot{h}$ is of the order of $10^{-4} ms^{-1}$ and, therefore, d is of the order of the millimeter.

In conclusion, the entrainment layer, where thermals are converted to anti-thermals by molecular diffusion, is a very thin layer and is not capable of controlling the evolution of the overall mixing processes.

CHAPTER FOUR

PENETRATIVE CONVECTION DUE TO SURFACE COOLING

1. INTRODUCTION

In early fall, the upper ocean usually has a continuous, moderately stable density distribution, bounded at its top by a thin daily wind-mixed layer. Past mid-fall and during winter, a net cooling of the ocean surface sets in. Instability and natural convection occur. Cold elements produced near the surface become unstable and sink through the water column, eroding the stratification built up during the previous summer. Contrary to the diurnal thermocline formation, this erosion is accomplished at a slow but continuous rate throughout the winter period. A mixed layer is formed, penetrating the stable stratified fluid below and entraining new fluid in the convective process. The lower boundary is marked by a density change that, on a macroscopic scale, is almost discontinuous. As deepening proceeds, this density jump, called the seasonal thermocline, becomes deeper and stronger. The maximum depth of the wintertime erosion marks the permanent thermocline.

Wind stirring plays an important role at the start, but rapidly convection dominates the process. Thermal instability itself supplies the kinetic energy required for stirring and deepening. In the present modelling, therefore, the wind effect is ignored. The system is highly convective, and molecular diffusion of heat is not important.

The problem has long antecedence in studies of the atmospheric boundary layer. Indeed, convection above a heated ground

exhibits the same features of upper-ocean mixing due to surface cooling (Scorer, 1978). The models of Yamada and Mellor (1975), and Zeman and Lumley (1976), based on second-order closure hypotheses, realistically predict the structure of buoyancy-driven mixed layers. Comparisons with laboratory experiments (Willis and Deardorff, 1974; Heidt, 1977) and observations (Telford and Warner, 1964; Warner and Telford, 1967; Lenschow, 1970) support these theories.

The present study shows that simple analytical calculations as opposed to sophisticate turbulence numerical models, can describe the general features of a convective layer. The philosophy resembles the one of Manton (1975) in a study of penetrative convection in a stratified fluid due to a field of thermals. The present work, however, describes the dynamics and turbulent characteristics of convection in more detail.

Although the results presented here focus on convection in the upper ocean forced by surface cooling, they apply directly to convection in the lower atmosphere above a heated ground.

2. THE MODEL

The model is based on a new parametrization of mixing and convection (Chapter two). It can be applied to the most general case of mixed-layer deepening under variable wind stress and/or variable surface heat flux. The present work is a direct application to upper ocean convection due to surface cooling.

The model envisions convection as the relative motion of two interacting fluids of different properties. The active sinking elements are called *thermals*, and the rising return flow, *anti-thermals*, by analogy. The model describes the individual dynamics of thermals and anti-thermals, and their interactions. Mean properties and relative differences then result from the solution. This permits direct computation of mean profiles and vertical fluxes of momentum and heat.

Throughout the mixed layer and thermocline, a saturation equilibrium between thermals and anti-thermals can be assumed (Manton, 1975; Chapter two). This leads to assigning a constant value to f, the fraction of area occupied by thermals. This hypothesis closes the set of equations without introducing any empirical coefficient of entrainment by thermals.

Parcels of fluid rising through the convective layer are given, near the surface, negative buoyancy by the outward surface heat flux (see Figure 14). These elements, the thermals, become heavier than their environment, and sink back into the convective layer. They accelerate and gradually mix with the upward return flow until they reach the neutral level, where they are no longer buoyant. Because of their non-zero velocity and their inertia, they overshoot that equilibrium level, become buoyant, and progressively decelerate. As the mean temperature profile begins to curve at the bottom of the mixed layer, the elements' buoyancy increases sharply, and their vertical velocity decreases rapidly. Since the newly-entrained fluid is subjected there to

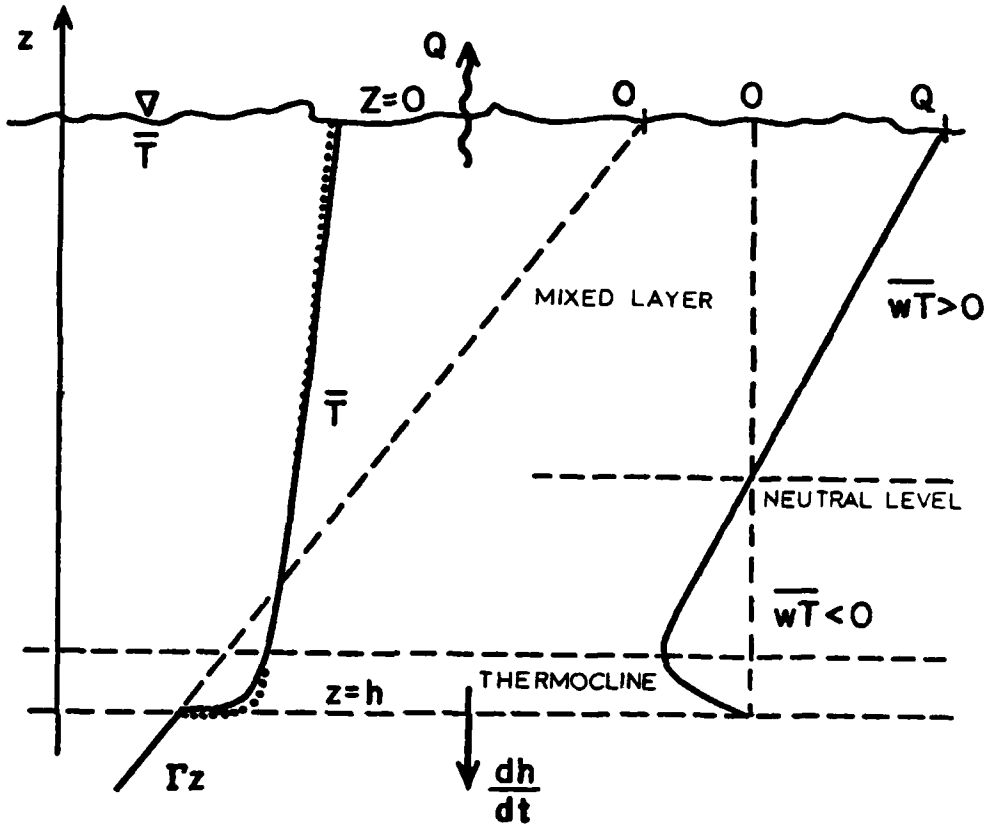

Figure 14. Sketch of penetrative convection in the upper ocean due to surface cooling by an imposed heat flux Q. In the mixed layer, the mean temperature $\bar{T}$ is almost constant, while the convective heat flux $\overline{wT}$ decreases with depth. In the thermocline, $\bar{T}$ varies sharply, while $\overline{wT}$ increases rapidly. The neutral level is the level where thermals and anti-thermals have the same temperature. The dotted curve is the mean temperature profile at a later time, showing the cooling in the mixed layer and the heating in the thermocline.

the largest temperature changes, the vertical convective heat flux $\overline{wT}$ (downward) is large. A decreasing vertical velocity therefore implies larger temperature contrasts and increasing buoyancy, which in turn decelerate the sinking elements even more. The process is cumulative, and gives rise to the formation of a thin layer of rapid variations, the *thermocline*, which lies under the *mixed layer* and above the *quiescent stably-stratified fluid.*

Above the neutral level, thermals transport a lack of heat downward. The heat flux is thus positive (upward) in that region. It decreases with depth as the temperature difference between sinking and rising fluids is progressively reduced by mixing. Below the neutral level, the sinking elements are buoyant and carry an excess of heat downward. The heat flux there is negative (downward). At the bottom of the thermocline, thermals stop, and the heat flux vanishes again. The heat-flux profile therefore behaves as shown on Figure 14, with a negative minimum value near the bottom of the mixed layer. The level at which the minimum value of $\overline{wT}$ is reached can be thought of as being the top of the thermocline.

The heat-conservation equation is

$$\frac{\partial \bar{T}}{\partial t} = -\frac{\partial}{\partial z} \overline{wT} \ , \qquad (1)$$

and implies that, in the mixed layer, the mean temperature $\bar{T}$ decreases, while in the thermocline, it increases with time. After a short while, the temperature profile will behave like the dotted curve in Figure 14. The water temperature therefore

does not change at the top of the thermocline. Of course, that level deepens with time, allowing every layer of fluid to be somewhat heated before being cooled. This heating process in a system forced by cooling only is explained by the ability of convection to generate its own kinetic energy for mixing.

3. GOVERNING EQUATIONS

Thermals and anti-thermals have different properties, here noted by primed and double-primed quantities, respectively. If f represents the fraction of area occupied by thermals at any level, the fraction available to anti-thermals is (1-f), so that one may define

the mean vertical velocity $\bar{w} = fw' + (1-f)w''$, (2)

the mean temperature $\bar{T} = fT' + (1-f)T''$, (3)

the vertical convective heat flux $\overline{wT} = fw'T' + (1-f)w''T''$. (4)

Root-mean-square (rms) fluctuations can also be defined (Chapter two):

$$w_{rms} = \sqrt{f(1-f)}\,(w'-w'') , \quad (5)$$

$$T_{rms} = \sqrt{f(1-f)}\,(T'-T'') . \quad (6)$$

Note that, according to these definitions, rms fluctuations can be positive or negative.

In the absence of lateral variations (one-dimensional model), continuity requires $\bar{w}$ to be constant with depth (Chapter two). Since there is no overall upwelling nor downwelling in the system, $\bar{w}$ vanishes everywhere. As a consequence, the vertical convective

heat flux, as defined by (4), may be rewritten in terms of rms fluctuations only:

$$\overline{wT} = w_{rms}\, T_{rms} \quad . \tag{7}$$

With these definitions, and in the absence of horizontal velocity, the one-dimensional model of convection (Chapter two) can be summarized as follows:

Heat equations:

$$\frac{\partial \bar{T}}{\partial t} = -\frac{\partial}{\partial z}\left(w_{rms}\, T_{rms}\right) \quad , \tag{8}$$

$$\frac{\partial}{\partial z}\left(\bar{T} + m T_{rms}\right) = 0 \quad , \tag{9}$$

Vertical momentum equation:

$$3mw_{rms}\frac{\partial w_{rms}}{\partial z} = \alpha g T_{rms} + \delta, \tag{10}$$

where m is a coefficient depending on f only, defined by:

$$m = \frac{1-2f}{2\sqrt{f(1-f)}} \quad . \tag{11}$$

The first equation expresses that the time rate of change of the mean temperature is due to the divergence of the convective heat flux. The second equation relates mean and rms temperatures in a simple linear way, and is a direct result of the assumption that turbulent motions respond quasi-instantaneously to local variations in the system (Chapter two). The third equation expresses that thermals' inertia is balanced by the buoyancy force and a friction force, δ. The friction force was not included in the model of chapter two, but is introduced here because of its importance in deep convection processes. The Monin-Obukov similarity theory (Wyngaard, Coté, and Izumi, 1971), theoretical studies (Lenschow, 1974), laboratory experiments (Willis and Deardorff, 1974), as

well as atmospheric boundary layer observations (Lenschow, *et al.*, 1980), suggest that the rate of dissipation of kinetic energy is constant with depth, but decreases rapidly toward zero near the interface. This implies that δ behaves like $|w_{rms}|^{-1}$, except in the thermocline where it has to remain bounded. On the other hand, global turbulence arguments suggest that the total dissipation is proportional to the cube of turbulent velocity scale. A parametrization of the friction force which satisfies all these requirements is:

$$\delta = \frac{mD}{\kappa h} \frac{w_*^3}{|w_{rms}| + m\dot{h}} \quad ,$$

where D is a dimensionless parameter, and w_* the scale of the turbulent vertical velocity, which will be defined in the next section. The small term $m\dot{h}$ in the denominator is introduced to yield a friction force bounded everywhere; its form is chosen for further convenience in the mathematical formulation of the solution. The vertical length scale is chosen to be κh, the Von Kármán constant times the convective layer depth.

The problem consists of three non-linear first-order coupled differential equations. It requires thus three boundary conditions. At the surface, z = 0, the convective heat flux equals the imposed surface flux, and a friction velocity prescribes the rms vertical velocity:

$$w_{rms}\, T_{rms} = Q \quad , \tag{12}$$

$$w_{rms} = -u_* \quad . \tag{13}$$

The surface flux Q is the kinematic heat flux (heat flux divided

by $\rho_o C_p$), and is positive in a cooling situation (upward flux). The rms vertical velocity is negative since thermals sink while anti-thermals rise ($w'<0<w''$).

At the bottom of the thermocline, $z = -h(t)$, the mean temperature ought to match the temperature of the underlying stratum:

$$\bar{T} = -\Gamma h \ , \tag{14}$$

where Γ is the initial temperature gradient of the water (see Figure 14).

In the formulation of the problem, the mixed-layer depth, $h(t)$, is still unknown. An extra boundary condition has thus to be imposed in order to close the problem. This condition is precisely the definition of the base of the thermocline, i.e., the level beyond which thermals do not penetrate:

$$w' = 0 \ ,$$

which implies:

$$w_{rms} = 0 \ . \tag{15}$$

4. CHANGE OF VARIABLE AND FUNCTIONS

Since the mixed layer is constantly deepening, it is advantageous to use the similarity variable $\xi = -z/h$ which varies from zero at the surface to one at the bottom of the thermocline.

On the other hand, one may immediately integrate equation (9) with respect to z, and define:

$$\bar{T} = -\Gamma T(t) - m\Gamma\tilde{T}(t,\xi) \ , \tag{16}$$

$$T_{rms} = \Gamma\tilde{T}(t,\xi) \ , \tag{17}$$

where T is a function of time only, and $\tilde{T}$ is a function of both time and ξ. Note that, due to the presence of the factor Γ, the new temperatures T and $\tilde{T}$ have the dimension of a length. The rms vertical velocity may be redefined:

$$w_{rms} = -\tilde{w}(t,\xi) \ , \tag{18}$$

in order to work with a positive variable.

With these changes of variable and functions, the governing equations (8) and (10) become:

$$-\dot{T} - m\frac{\partial \tilde{T}}{\partial t} + m\frac{\dot{h}}{h}\xi\frac{\partial \tilde{T}}{\partial \xi} = -\frac{1}{h}\frac{\partial}{\partial \xi}(\tilde{w}\tilde{T}) \ , \tag{19}$$

$$3\tilde{w}\frac{\partial \tilde{w}}{\partial \xi} = -\frac{N^2 h}{m}\tilde{T} - \frac{D}{\kappa}\frac{w_*^3}{\tilde{w}+m\dot{h}} \tag{20}$$

where $N^2 = \alpha g \Gamma$ is the square of the Brunt-Väisälä frequency in the underlying stratum, and where a dot represents a time derivative. The boundary conditions become:

$$\tilde{T}(0) = -\frac{Q}{\Gamma u_*} \ , \quad \tilde{w}(0) = u_* \ , \tag{21}$$

and

$$\tilde{T}(1) = \frac{h-T}{m} \ , \quad \tilde{w}(1) = 0 \ . \tag{22}$$

This constitutes a set of two coupled non-linear first-order differential equations which require two boundary conditions. However, they contain two time-dependent unknowns: T(t) and h(t), for which two additional conditions are prescribed. The system is thus closed and self-consistent.

5. SCALES AND THE RICHARDSON NUMBER

The characteristic parameters of penetrative convection due

to surface cooling are the buoyancy flux at the surface $\mathcal{B} = \alpha g Q$, the mixed-layer depth h, the Brunt-Väisälä frequency in the underlying stable fluid $N = (\alpha g \Gamma)^{\frac{1}{2}}$, and the friction velocity u_* (computed from the surface wind stress). The comparison of wind-induced turbulence to convective motion is expressed by the Monin-Obukov length:

$$\ell = \frac{u_*^3}{\kappa \mathcal{B}} . \tag{23}$$

For very convective situations ($h >> \ell$), when wind-stirring becomes a negligible part of the kinetic-energy release from potential energy, the turbulence structure in the mixed layer no longer depends on u_* (Kaimal, *et al.*, 1976). The characteristic velocity becomes the convective vertical-velocity scale:

$$w_* = (\kappa \mathcal{B} h)^{\frac{1}{3}} = (\kappa \alpha g h Q)^{\frac{1}{3}} . \tag{24}$$

According to the assumption that wind-stirring plays a secondary role in the deepening process, w_* is the correct scale in the mixed layer if:

$$w_*^3 >> u_*^3 , \tag{25}$$

by virtue of (23) and (24).

The total buoyancy in the mixed layer is

$$B = g \frac{\Delta \rho}{\rho_o} h ,$$

where $\Delta \rho$ is the density jump across the thermocline, and ρ_o the reference density. Since $\Delta \rho = \rho_o \alpha \Delta T$, where ΔT is the temperature jump across the thermocline, the total buoyancy may be rewritten as:

$$B = \alpha g h \, \Delta T. \tag{26}$$

The Richardson number is defined as the ratio of the total mixed-layer buoyancy, B, to the square of the characteristic vertical velocity, w_*,

$$Ri = \frac{\alpha g h \Delta T}{(\kappa \alpha g h Q)^{\frac{2}{3}}} \quad . \tag{27}$$

As the mixed layer deepens, the temperature jump across the thermocline increases (Willis and Deardorff, 1974; Heidt, 1977). The Richardson number therefore increases with time. It is well known, too, from observations and laboratory experiments that when the mixed layer is deep enough, it is quasi-homogeneous and bounded below by a thin layer of large gradients. It will be shown here *a posteriori* that this situation corresponds to:

$$Ri >> 1 \quad . \tag{28}$$

For penetrative convection in the upper ocean due to winter cooling, typical values are

$Q \sim 3\times10^{-4}{}^{o}Cms^{-1}$, $\Gamma \sim 0.1{}^{o}Cm^{-1}$, $\kappa = 0.40$, $u_* \sim 10^{-2}ms^{-1}$, $\Delta T \sim 1{}^{o}C$, $h \sim 100$ m

which corresponds to:

$B \sim 3\times10^{-7}m^2s^{-3}$, $N \sim 10^{-2}s^{-1}$, $\ell \sim 10$ m, $w_* \sim 2.3\ 10^{-2}ms^{-1}$, $Ri \sim 190$.

It is therefore seen that, for the purpose of this work, the inequalities $h/\ell >> 1$ and $Ri >> 1$ are met. The latter permits use of a boundary-layer technique to solve the equations, while the former will simplify the discussion of mixed-layer deepening, as shown later.

6. SOLUTION

Mathematically, it is assumed here that the mixed-layer and thermocline system may be treated as an interior and boundary-layer problem. The solution found here will therefore apply if Ri is much greater than one.

The system is thus divided into two regions, the interior region, where the temperature is quasi-constant with depth, i.e.,

$$\frac{\partial}{\partial \xi} = O(1) \ , \ \tilde{T} << T \ , \tag{29}$$

and the thermocline, where vertical gradients are anticipated to be very large:

$$\frac{\partial}{\partial \xi} >> 1 \ , \ \tilde{T} \sim T \ . \tag{30}$$

These assumptions will be verified *a posteriori*, and it will be shown that they are correct provided that (28) is met.

a) Solution in the mixed layer:

Assuming a quasi-homogeneous mixed layer, equations (19) and (20) become:

$$-\dot{T} = -\frac{1}{h}\frac{\partial}{\partial \xi}(\tilde{w}\tilde{T}) \ , \tag{31}$$

$$3\tilde{w}\frac{\partial \tilde{w}}{\partial \xi} = -\frac{N^2 h}{m}\tilde{T} - \frac{Dw_*^3}{\kappa \tilde{w}} \tag{32}$$

The left-hand side of (31) is independent of ξ, and an integration can be performed. Use of surface boundary conditions (21) gives:

$$\tilde{T} = \frac{-\frac{Q}{\Gamma} + h\dot{T}\xi}{\tilde{w}} \quad . \tag{33}$$

Replacing $\tilde{T}$ by this expression into (32) yields a single differential equation for $\tilde{w}$:

$$3\tilde{w}^2\frac{\partial\tilde{w}}{\partial\xi} = \frac{w_*^3}{m\kappa} - \frac{N^2h^2\dot{T}}{m}\xi - \frac{D}{\kappa}w_*^3$$

whose solution is:

$$\tilde{w}^3 = u_*^3 + \frac{1-mD}{\kappa m}w_*^3\xi - \frac{N^2h^2\dot{T}}{2m}\xi^2 \quad , \tag{34}$$

after the surface boundary condition (21) has been used.

b) Solution in the thermocline:

The dominant terms in the equations are now those which include derivatives with respect to ξ. However, since this boundary layer lies near $\xi = 1$, ξ may be replaced by one where it appears. Equations (19) and (20) now reduce to:

$$m\frac{\dot{h}}{h}\frac{\partial\tilde{T}}{\partial\xi} = -\frac{1}{h}\frac{\partial}{\partial\xi}(\tilde{w}\tilde{T}) \quad , \tag{35}$$

$$3\tilde{w}\frac{\partial\tilde{w}}{\partial\xi} = -\frac{N^2h}{m}\tilde{T} - \frac{Dw_*^3}{\kappa(\tilde{w}+m\dot{h})} \quad . \tag{36}$$

These last equations can be easily integrated with respect to ξ. The constants of integration are determined by using the bottom boundary conditions (22). The implicit solution is:

$$\tilde{T} = \frac{(h-T)\dot{h}}{\tilde{w}+m\dot{h}} \quad , \tag{37}$$

$$\tilde{w}^3 + \tfrac{3}{2}mh\tilde{w}^2 = \left(\frac{N^2h(h-T)\dot{h}}{m} + \frac{D}{\kappa}w_*^3\right)(1-\xi) \quad . \tag{38}$$

c) Matching of solutions:

The two sets of solutions were obtained independently for the mixed layer and thermocline by using surface and bottom boundary conditions, respectively. However, they ought to be the asymptotic forms of a unique set of solutions valid throughout the whole water column. This requires imposing matching conditions. As a result, two prognostic equations for the time-dependent functions T and h will be obtained.

Mathematically, matching conditions are obtained by writing that, for each variable $\tilde{T}$ and $\tilde{w}$, the mixed-layer solution for ξ approaching unity is identical to the thermocline solution for $\tilde{w}$ much greater than $\dot{h}$. The resulting relations are:

$$\frac{-\frac{Q}{\Gamma} + h\dot{T}}{\tilde{w}} = \frac{(h-T)\dot{h}}{\tilde{w}} ,$$

$$u_*^3 + \frac{1-mD}{\kappa m} w_*^3 - \frac{N^2h^2\dot{T}}{2m} - \left(\frac{1-mD}{\kappa m} w_*^3 - \frac{N^2h^2\dot{T}}{m}\right)(1-\xi) = \left(\frac{N^2h(h-T)\dot{h}}{m} + \frac{D}{\kappa} w_*^3\right)(1-\xi) .$$

They can be rewritten as:

$$(hT)^{\cdot} = h\dot{h} + \frac{Q}{\Gamma} , \tag{39}$$

$$\left(\frac{w_*^3}{\kappa} - \frac{N^2h^2\dot{T}}{2}\right) + mu_*^3 = \frac{mD}{\kappa} w_*^3 . \tag{40}$$

Equation (39) is the global heat budget of the system. Indeed, the overall heat budget expresses that the temperature difference from the initial value, $\Gamma z - \bar{T}$, integrated over the water column is equal to the time integration of the net surface

heat flux, Q:

$$\int_{-h}^{o} (\Gamma z - \bar{T}) dz = \int_{o}^{t} Q dt \ . \tag{41}$$

Using expression (16) for $\bar{T}$ and the vertical momentum equation (20) to eliminate $\tilde{T}$, one obtains:

$$hT - \frac{m^2}{N^2} \int_{o}^{1} (3\tilde{w} \frac{\partial \tilde{w}}{\partial \xi} + \frac{D}{\kappa} \frac{w_*^3}{\tilde{w}+m\tilde{h}}) d\xi = \frac{h^2}{2} + \int_{o}^{t} \frac{Q}{\Gamma} dt \ . \tag{42}$$

The integral is estimated to be of order w_*^2. The second term of the left-hand side is thus found to be of the order of $\frac{\alpha g h \Delta T}{Ri}$. Estimating ΔT to be comparable to $\bar{T}$ (somewhat smaller according to laboratory experiments), this term is estimated to be not greater than $\frac{hT}{Ri}$, which is much smaller than the first term for Ri>>1, as assumed previously. The global heat budget thus reduces to:

$$hT = \frac{h^2}{2} + \int_{o}^{t} \frac{Q}{\Gamma} dt \ , \tag{43}$$

whose time derivative is precisely (39).

Equation (40) is the turbulent kinetic energy budget of the system. It expresses that the turbulent kinetic energy is in quasi-equilibrium at all times (Chapter two), so that the sum of the release of potential energy and the surface input equals the rate of dissipation in the water column. Indeed, the release of potential energy is:

$$\begin{aligned} -\frac{1}{\rho_o} \frac{dPE}{dt} &= \alpha g \int_{-h}^{0} \overline{w\tilde{T}} \, dz, \\ &= -N^2 h \int_{o}^{1} \left(-\frac{Q}{\Gamma} + h\dot{T}\xi \right) d\xi \ , \\ &= \frac{w_*^3}{\kappa} - \frac{N^2 h^2 \dot{T}}{2} \ , \end{aligned} \tag{44}$$

according to (7), (17), (18), (24), and (33); the surface input is

$$-\tfrac{1}{2}\,\overline{w(w-\bar{w})^2}\Big|_{z=o} = -mw_{rms}^3(z=o) \ , \qquad = mu_*^3 \ , \tag{45}$$

according to (13).

Combined with (39), equation (40) yields the prognostic equation for the mixed-layer depth. Due to its importance and its consequences, that equation is derived in the next section.

The vertical profiles of $\tilde{T}$ and $\tilde{w}$ valid throughout the water column are, after matching:

$$\tilde{T} = \frac{-\frac{Q}{\rho} + h\dot{T}\xi}{\tilde{w}+m\dot{h}\xi} \ , \tag{46}$$

$$\tilde{w}^3 + \tfrac{3}{2}m\dot{h}\tilde{w}^2 = u_*^3(1-\xi^2) + \frac{1-mD}{\kappa m} w_*^3\,\xi(1-\xi) \ . \tag{47}$$

Since the friction velocity u_* cannot exceed the convective velocity scale, equations (45) shows that w_* is, indeed, the appropriate vertical-velocity scale, as assumed previously. It is worth noting that the solution is implicit in $\tilde{w}$, but vertical profiles can be plotted without real difficulties.

7. MIXED-LAYER DEEPENING

Equations (39) and (40) form a coupled set of equations for T and h. Eliminating T yields a prognostic equation for h, which can then be solved if the time variations of Q and u_* are known. Such a substitution is possible. However, it is advantageous to consider T as a function of h. Eliminating then

the variable t between (39) and (40) yields:

$$2(1-mD)(1+\frac{m}{1-mD}\frac{\ell}{h})(h\frac{dT}{dH} + T-h) = h\frac{dT}{dh} . \qquad (48)$$

Although an exact solution can be found, an approximate solution is obtained without great difficulty, based on the inequality

$$\ell << h .$$

The method of regular perturbation yields:

$$T = \varepsilon h[1-\frac{\kappa m}{2(1-mD)^2}\frac{\ell}{h}] \qquad (49)$$

where the coefficient ε is defined by:

$$\varepsilon = \frac{2(1-mD)}{3-4mD} . \qquad (50)$$

The constant of integration was chosen such that T remains bounded for h = 0. At the leading order ($\ell/h = 0$), (49) reduces to:

$$T = \varepsilon h . \qquad (51)$$

The mean temperature in the mixed layer is thus proportional to the depth of convection. This has been shown to be the case in laboratory experiments (Heidt, 1977). The coefficient of proportionality, noted ε by Heidt, is given by (50).

Now eliminating T in (39) by use of (49) leads to the prognostic equation for the mixed-layer depth:

$$(1-\frac{\kappa m}{1-mD}\frac{\ell}{h})h\dot{h} = (3-4mD)\frac{Q}{\Gamma} . \qquad (52)$$

For a given surface heat flux, Q, and friction velocity, u_*, known as functions of time, this equation can be integrated by quadrature. If Q is steady, and if the mixed-layer is deep enough ($h >> \ell$), the depth of the layer increases as $t^{\frac{1}{2}}$. This

rate of growth was found by most of the bulk models and laboratory experiments (Betts, 1973, and Heidt, 1977, for example).

From the previous relationships, one may compute the temperature jump across the thermocline, the heat flux at the base of the mixed layer, and the Richardson number. The temperature jump across the thermocline is:

$$\Delta T = -\Gamma T + \Gamma h \ ,$$

$$= \frac{1-2mD}{3-4mD} \Gamma h \left(1+\frac{\kappa m}{(1-mD)(1-2mD)} \frac{\ell}{h}\right) \ , \qquad (53)$$

according to (49). The temperature jump increases with time as h. The heat flux at the base of the mixed layer is the limit for ξ approaching one of the mixed-layer flux $\overline{wT} = -\Gamma\overline{wT}$ derived from (33):

$$\overline{wT}\Big|_{-h} = Q - h\dot{T} \ ,$$

$$= -Q\left[1-2mD+2\kappa m\frac{\ell}{h}\right] \ , \qquad (54)$$

according to (49) and (52). That heat flux is negative (downward), and thus opposite to the surface flux (upward). This results from the previous description of thermals' dynamics. Thermals are buoyant in the bottom of the mixed layer, below the neutral level. They thus carry an excess of heat downward. The heat flux is therefore negative (downward) and opposite to the surface flux. The same situation commonly occurs in the atmosphere. The atmospheric convective boundary layer, which forms above a heated ground (upward heat flux), is capped by an inversion, at the base of which a downward heat flux is observed. This phenomenon was first reported by Ball (1960), and since

then has been reported in many observational surveys.

The heat flux at the base of the mixed layer is proportional to the surface flux, Q. The coefficient of proportionality, noted A by various authors, is:

$$A = 1 - 2mD + 2\, m \frac{\ell}{h} \quad . \tag{55}$$

The Richardson number, defined by (27), can be computed from (53). At the first order in $\frac{\ell}{h}$, it takes the form:

$$Ri = \frac{1-2mD}{3-4mD} \left[\frac{\Gamma N h^2}{\kappa Q}\right]^{2/3} \left[1 + \frac{\kappa m}{(1-mD)(1-2mD)} \frac{\ell}{h}\right] \tag{56}$$

and increases with time as $h^{4/3}$. The rate of deepening, $\dot{h}$, decreases with time as $Ri^{-3/4}$, according to (52) and (56).

The Richardson number can be used to write the prognostic equation for the mixed-layer depth in a non-dimensional form. If the rate of entrainment, E, is defined by the ratio of rate of deepening, $\dot{h}$, over the characteristic velocity scale, w_*, a simple algebraic relationship between Ri and E can be obtained:

$$E = \frac{A}{\kappa Ri} \quad . \tag{57}$$

The rate of entrainment is therefore inversely proportional to the Richardson number. Since Ri is much greater than one, E is small, and $\dot{h}$ is much less that w_*. Thermals thus sink much faster than the mixed layer deepens.

8. COMPARISON WITH OBSERVATIONS AND PREVIOUS MODELS

Various values of the coefficients A and ε were proposed

in the literature. These two parameters are not independent. Indeed, eliminating mD between (50) and (55), one obtains, at the leading order:

$$A = \frac{1-\varepsilon}{2\varepsilon-1} \quad . \tag{58}$$

Table 2 presents an extended version of a table of values of the parameters A and ε compiled by Heidt (1977). Values proposed in the literature are based on atmospheric observations, laboratory experiments, and various models of penetrative convection, applied to the atmosphere and ocean. From this table it appears that (i) no values were proposed in the literature as a result of oceanic observations, (ii) models without dissipation yield invariable values ($A = 1$, $\varepsilon = \frac{2}{3}$), (iii) highly dissipative experiments or models yield extreme values ($A \simeq 0$, $\varepsilon \simeq 1$), and (iv) atmospheric observations, numerical models, and laboratory experiments are in satisfactory agreement ($A = 0.12\text{-}0.25$, $\varepsilon = 0.83\text{-}0.90$). The scattering of the values can be explained as follows. By this model, A and ε are related to the parameter m (see Figure 15), which in turn depends upon f, the fraction of area occupied by thermals. The value of f strongly depends upon the surface unstable layer where thermals are generated, and there is no reason to believe that laboratory experiments and a heated ground generate thermals in the same conditions.

Simple non-dissipative models underestimate the value of ε, while laboratory experiments, where molecular viscosity acts as

TABLE 2

YEAR	AUTHOR(S)	SOURCE	A	ε
1960	Ball	Atmospheric bulk model, without dissipation	1	0.67
1967	Kraus and Turner	Oceanic bulk model, in case of no dissipation	1	0.67
1968	Lilly	Atmospheric bulk model - without dissipation - for minimum entrainment	1 0	0.67 1
1968	Lenschow and Johnson	Airplane measurements	0.25	0.83
1969	Deardorff, *et al.*	Laboratory experiments, strong molecular viscosity effect	0.02	0.98
1973	Betts	Atmospheric bulk model, with dissipation; empirical coefficient from observations in the Tropics	0.25	0.83
1973	Carson	Observations of the atmospheric boundary layer	0 - 0.5	0.75 - 1
1973	Lenschow	Observations of the atmospheric boundary layer over the Great Lakes	0.08	0.93
1973	Pollard, *et al.*	Oceanic bulk model, without dissipation	1	0.67
1973	Tennekes	Atmospheric bulk model, with dissipation; empirical coefficient from studies of convection	0.2	0.86
1974	Deardorff	Second-order turbulence numerical model .	0.14 - 0.21	0.85 - 0.89
1974	Lenschow	Bulk model, empirical coefficients from aircraft measurements over a lake	0.15	0.86
1974	Willis and Deardorff	Laboratory experiments	0.10	0.91
1975	Manton	Simple model of convection, with strong dissipation	0	1
1976	Gill and Turner	Oceanic bulk model, coefficient of penetrative convection estimated from atmospheric observations	0.15	0.88
1976	Zeman and Lumley	Second-order turbulence numerical model	0.10 - 0.15	0.88 - 0.91
1977	Heidt	Laboratory experiments	0.12 - 0.24	0.84 - 0.90
1979	Poisin	Model of oceanic convection due to a field of thermals, no dissipation	1	0.67
1980	Cushman-Roisin	Present analytical model, with dissipation (function of f)	0 - 1	0.67 - 1

Table 2. Summary of values for the parameters A and ε proposed in the literature. The parameter A is a measure of the heat flux at the base of the mixed layer, and ε is the coefficient of proportionality between T and h.

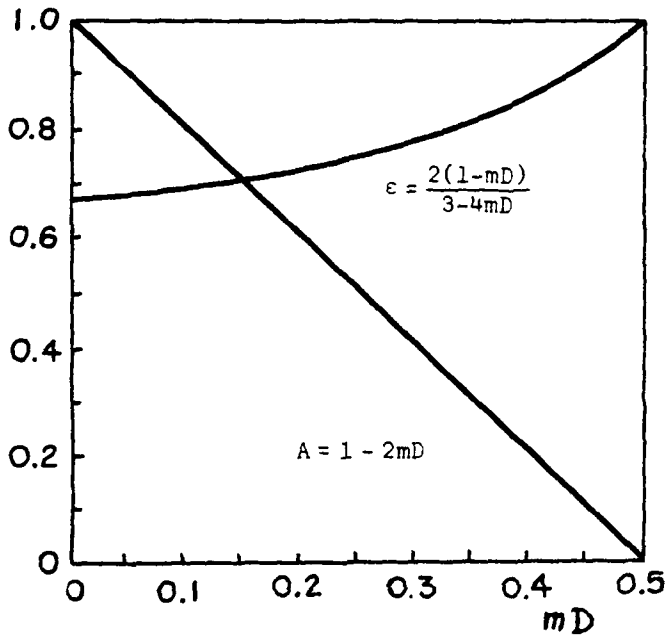

Figure 15. Plots of the coefficients ε and A defined by (50) and (58); ε is the ratio $\overline{T}/(-\Gamma h)$, and A is the ratio $-(\overline{wT})_{-h}/Q$.

a strong dissipative mechanism, overestimate ε. The reason is found in the discussion of the turbulent kinetic energy budget. The excess of the potential energy in the mixed layer over the potential energy of the initial state is, at the leading order:

$$\frac{1}{\rho_o} PE = -\alpha g \int_{-h}^{o} (\bar{T}-\Gamma z) z dz$$

$$= -\frac{3\varepsilon-2}{6} N^2 h^3 .$$

Its time rate of change is:

$$\frac{1}{\rho_o} \frac{dPE}{dt} = -\alpha g \int_{-h}^{o} \overline{wT} dz$$

$$= -\frac{3\varepsilon-2}{2} N^2 h^2 \dot{h} \quad .$$

For ε greater than $2/3$, the time rate of change is negative, expressing that release of potential energy occurs. The kinetic energy so produced feeds convective motions and is finally dissipated. A model without dissipation, therefore, does not allow a net global potential-energy release, and yields $\varepsilon = 2/3$, establishing a minimum value for ε. This value is recovered in the present model if the friction coefficient, D, is set equal to zero in (50). Increasing dissipation requires increasing release of potential energy for convective motions and, therefore, an increasing value of ε. Values of ε greater than unity cannot occur, for, in such a case, the temperature difference across the thermocline would be destabilizing (mixed-layer temperature lower than underlying stable fluid temperature). In laboratory experiments for which molecular viscosity plays a dominant role,

the value to ε is close to unity.

Second-order closure turbulence numerical models lead to decreasing values of ε as the mixed layer develops. Indeed, at the early stage, dissipation is dominant, and ε is close to one; but as time goes on, dissipation has less importance and ε decreases slightly. The present analytical study is based on the assumption of a well-developed mixed layer ($Ri \gg 1$), the value to be assigned to ε in the present model is thus to be compared with the lowest values of the numerical models (0.84-0.85).

9. THICKNESS OF THE THERMOCLINE

Due to non-linearities, the boundary-layer method applied here differs from classical applications to linear systems, and caution has to be taken in the evaluation of the boundary-layer thickness. At first, one could think that the thermocline is the region where $\tilde{w}$ is of order $\dot{h}$, so that the correction in the denominator of (46) becomes important. This argument leads to a dimensionless thermocline of order Ri^{-3}, much too small. There is a thicker layer where boundary corrections start to appear in the solution. Indeed, in the temperature equation (19):

$$-\dot{\tilde{T}} - m\frac{\partial \tilde{T}}{\partial t} + m\frac{\dot{h}}{h}\xi\frac{\partial T}{\partial \xi} = -\frac{\partial}{\partial z}(\tilde{w}\tilde{T}) \ , \qquad (59)$$

the term on the right-hand side balances the first term in the mixed layer, and the third term in the thermocline. The top of the thermocline was defined as the level where the convective

heat flux reaches its maximum negative value, i.e., where the right-hand side of (59) vanishes. Equation (59) thus requires a balance between the first and third terms at that level:

$$T \sim \frac{\dot{h}}{h} \xi \frac{\tilde{T}}{\delta \xi} ,$$

where $\delta\xi$ is the dimensionless thermocline thickness. Because the boundary layer is anticipated to be a thin region, ξ is almost one, and according to (46) and (49), $\tilde{T}$ and $\dot{T}$ are of the order of $\frac{Q}{\Gamma \tilde{w}}$ and $\dot{h}$, respectively, so that:

$$\delta\xi \sim \frac{Q}{\Gamma h \tilde{w}} . \tag{60}$$

On the other hand, the balance of the vertical-momentum equation (20) requires:

$$\frac{\tilde{w}^2}{\delta \xi} \sim N^2 h \frac{Q}{\Gamma \tilde{w}} . \tag{61}$$

Combination of (60) and (61) and use of (24) and (56) yield:

$$\delta\xi \sim Ri^{-3/4} , \tag{62}$$

and

$$\tilde{w} \sim w_{*} Ri^{-1/4} \tag{63}$$

Therefore, the dimensionless thickness of the thermocline is $Ri^{-3/4}$ rather than Ri^{-3}.

In a study of turbulence and entrainment within the interfacial zone bounding a mixed layer, Long (1978) concludes that turbulent patches have a dimension of $hRi^{-3/4}$, and that the rms vertical velocity in the mixed layer near the interface is of order of $w_{*}Ri^{-1/4}$. The agreement between the approaches is perfect and supports modelling by two interacting fluids as a theory of

convective turbulence.

With dimensions, the actual thickness of the thermocline is:

$$h\delta\xi \sim \left(\frac{Q}{\Gamma N}\right)^{\frac{1}{2}} \tag{64}$$

and does not depend upon h. If Q is steady, the mixed layer deepens with time, but is bounded below by a thermocline of constant thickness. For typical oceanic values ($Q \sim 3\times10^{-4}$°Cms^{-1}, $\Gamma \sim 0.1$°Cm^{-1}, $N \sim 10^{-2}$s^{-1}), the thermocline thickness is found to be of the order of 50 cm.

The boundary-layer method required that (i) $\tilde{T}$ is negligible compared to T in the mixed layer, and (ii) the thermocline thickness is small compared to the mixed-layer depth. In the mixed layer, $\tilde{T}$ is of the order $\frac{Q}{\Gamma w_*}$, while T is of the order of h, i.e.,

$$\frac{\tilde{T}}{T} \sim \frac{Q}{\Gamma h w_*} \sim \left(\frac{\kappa Q}{\Gamma N h^2}\right)^{2/3} \sim Ri^{-1} \quad ,$$

according to (24) and (56). On the other hand, the ratio of the thermocline thickness to the mixed-layer depth is $\delta\xi$, and is of the order of $Ri^{-3/4}$. It is therefore concluded that the boundary-layer method is applicable to the present problem provided that Ri is much greater than unity, as anticipated.

10. COMPARISON WITH SIMILARITY THEORY

The solution presented and discussed in the previous paragraphs is not a similarity solution, for the ratio thermocline

thickness to mixed-layer depth is not constant with time. However, it is shown here that the asymptotic behavior near the surface takes a similarity form, and is formally identical to the solution obtained by Wyngaard, Coté and Izumi (1971). The theory presented by these authors is an extension of the Monin-Obukov similarity theory to free convection regime under very unstable conditions ($\ell << h$). Its validity is confirmed by atmospheric observations (Wyngaard, *et al.*, 1971).

Near the surface, the characteristic dimensionless variable is:

$$\eta = -\frac{z}{\ell} = \frac{h}{\ell}\,\xi \ , \tag{65}$$

where ℓ is the Monin-Obukov length defined by (23). For η of order one, turbulence and convection compete, and the Monin-Obukov similarity theory applies. For η much greater than one (but still less than h/ℓ), free convection takes over surface-generated turbulence, and the theory degenerates in simple $\frac{1}{3}$ power laws, as shown by Wyngaard, *et al.*

Near the surface ($\xi << 1$), the solution of the present model takes the form:

$$\tilde{T} \simeq -\frac{Q}{\Gamma \tilde{w}} \ , \tag{66}$$

$$\tilde{w}^3 \simeq u_*^3 + \frac{1-mD}{\kappa m} w_*^3\,\xi \ , \tag{67}$$

according to (46) and (47). In terms of the variable η, (66) and (67) become:

$$\tilde{T} \simeq -\frac{Q}{\Gamma u_*} \left(1 + \frac{1-mD}{\kappa m}\eta\right)^{-\frac{1}{3}} \ , \tag{68}$$

$$\tilde{w} = u_* \left(1 + \frac{1-mD}{\kappa m}\eta\right)^{1/3} . \tag{69}$$

From these expressions for the rms fluctuations of temperature and vertical velocity, second- and third-order correlations can be computed. For example:

$$\overline{w^2}^{1/2} = u_* \left(1 + \frac{1-mD}{\kappa m}\eta\right)^{1/3} , \tag{70}$$

$$\overline{w^2(T-\bar{T})} = -2mu_* Q \left(1 + \frac{1-mD}{\kappa m}\eta\right)^{1/3} . \tag{71}$$

Figures 16a and b are plots of vertical profiles of expressions (70) and (71), for which Wyngaard, Coté and Izumi (1971) had observations from the atmospheric boundary layer. The agreement between theory and data is best for:

$$\frac{1-mD}{\kappa m} = 5 ,$$

and

$$2m = 0.64 .$$

These values correspond to a fraction of area occupied by thermals of 35% (f = 0.348, m = 0.32) and a friction coefficient D = 1.125. From (50) and (58), the values of ε and A are

$$\varepsilon = 0.82 ,$$

$$A = 0.28 .$$

This is the range of values observed in the atmospheric boundary layer for unstable conditions (Lenschow and Johnson, 1968; Carson, 1973). It is worth noting that values of ' and ε obtained here are deduced exclusively from surface conditions. The theory is, therefore, capable of predicting bulk properties of the atmospheric boundary layer or oceanic mixed layer by using only

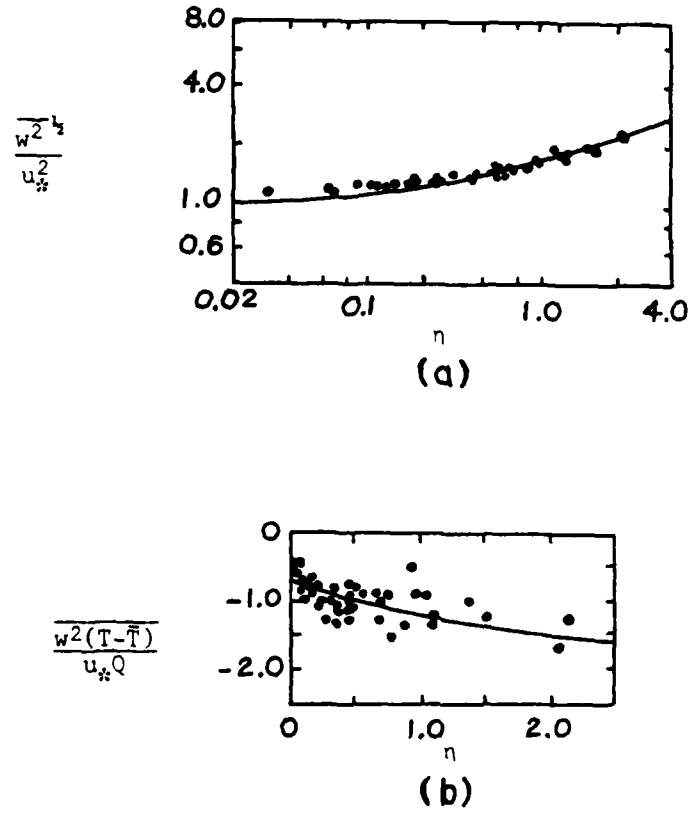

Figure 16. (a) Dimensionless vertical velocity variance and (b) Dimensionless vertical turbulent flux of vertical heat flux near the surface, for (1-mD)/κm=5 and 2m=0.64. Dots correspond to atmospheric observations presented by Wyngaard *et al.* (1971).

surface turbulence conditions.

11. VERTICAL PROFILES

Solutions (46) and (47) govern the vertical variations of rms fluctuations throughout the mixed layer and thermocline. They can be used to compute profiles of mean quantities such as mean temperature, heat flux, turbulent kinetic energy flux and variances.

Figures 17 to 24 are plots of vertical profiles of physical quantities of interest. The values assigned to the parameters are:

$$m = 0.5, \ (f = 0.276),$$

$$D = 0.8$$

$$\frac{\ell}{h} = 0.1 \ ,$$

$$Ri = 20 \ ,$$

and were chosen in order to reproduce the laboratory experiments, run S1, of Willis and Deardorff (1974). The four parameters were computed to match the Richardson number Ri, the rate of entrainment E, the ratio u_*/w_*, and the total rate of dissipation.

Figure 17 is a plot of the turbulent vertical velocity, which is proportional to the thermals' vertical velocity. Thermals leave the surface with the friction velocity u_*. As they sink, they accelerate under gravity. Due to the combined action of friction and a decreasing downward buoyancy force due to mixing with the environment, their velocity reaches a maximum. Below that level, the buoyancy force is still directed downward, but

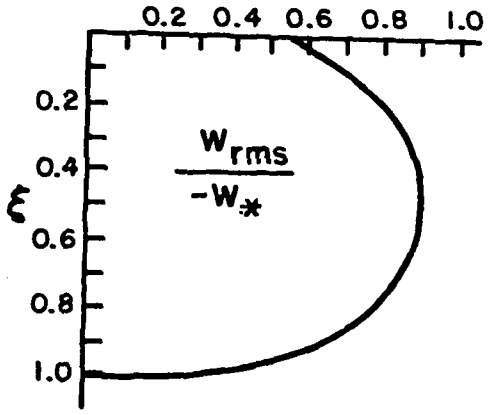

Figure 17. Vertical profile of the rms vertical velocity, scaled by $-w_*$.

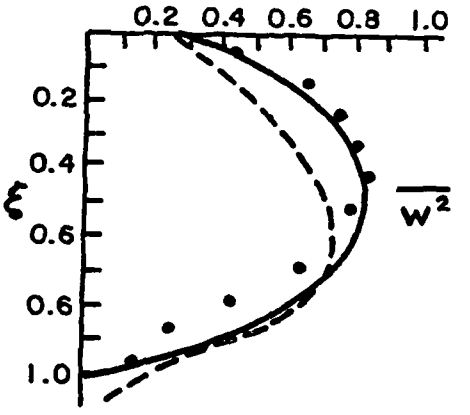

Figure 18. Vertical profiles of the vertical-velocity variance, $\overline{w^2}$, scaled by w_*^2. The solid curve is the solution of the present model. The dashed curve is the numerical solution of Zeman and Lumley (1976). The dots represent the data of Willis and Deardorff (1974), run S1.

friction dominates, and thermals decelerate. Ultimately, they become lighter than their environment. Both friction and an upward buoyancy force bring the thermals' velocity to zero, precisely at the bottom of the thermocline.

Figure 18 is a plot of the vertical-velocity variance, defined by $\overline{w^2}$. It is a measure of the turbulent kinetic energy. Dots reproduce Willis and Deardorff's data for run S1. Figure 19 is a plot of the vertical flux of turbulent kinetic energy. defined by $-\frac{1}{2}\overline{ww^2}$, which is the reduced form of the total turbulent kinetic energy when only the vertical velocity is important. Dots reproduce Willis and Deardorff's data for run S1. The agreement of the theory with laboratory experiments is excellent in both cases. The accuracy of the present simple analytical calculations is comparable to the one of the second-order turbulence numerical model of Zeman and Lumley (1976), whose solutions are shown in dashed lines for comparison.

Figure 20 is a plot of the temperature variance, defined by $\overline{(T-\bar{T})^2}$. It is maximum at surface and decreases with depth as the temperature difference between thermals and anti-thermals is reduced by mixing. The temperature variance vanishes at the neutral level, where thermals and anti-thermals have the same temperature, and increases below that level, where turbulence is generated. Dots reproduce Willis and Deardorff's data for run S1. The agreement is satisfactory. Although none of the observed values is zero near the neutral level (as one may expect in laboratory or in geophysical situations), a

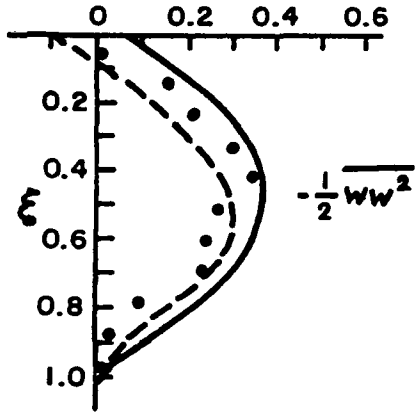

Figure 19. Vertical profiles of the vertical flux of turbulent kinetic energy, $-\frac{1}{2}\overline{ww^2}$, scaled by w_*^3. The solid curve is the solution of the present model. The dashed curve is the numerical solution of Zeman and Lumley (1976). The dots represent the data of Willis and Deardorff (1974), run S1.

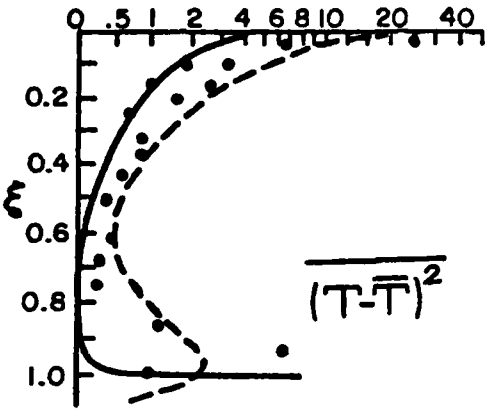

Figure 20. Vertical profiles of the temperature variance, $\overline{(T-\bar{T})^2}$, scaled by $(u_*/Q)^2$. The solid curve is the solution of the present model. The dashed curve is the solution of Zeman and Lumley (1976). The dots represent the data of Willis and Deardorff (1974), run S1.

well-pronounced minimum is present in the bottom half of the mixed layer.

Figure 21 is a plot of the vertical temperature profile through the mixed layer and thermocline. The temperature is almost homogeneous in the mixed layer. The thermocline is well-defined, and its thickness corresponds to (62). Figure 22 shows the profile of the vertical convective heat flux, $\overline{wT}$. Near the surface, it is positive (upward) and matches the imposed flux. It decreases almost linearly with depth, corresponding to a homogeneous cooling of fluid, as stated by the heat equation (1). The level at which the convective heat flux vanishes corresponds to the neutral level beyond which thermals become buoyant. Below that level, the heat flux is negative (downward). The maximum negative value at the top of the thermocline is equal to -AQ, which is the jump condition across the thermocline used in bulk models (Kraus and Turner, 1967, for example). Dots reproduce Willis and Deardorff's data for run S1. The linear decrease through the mixed layer was also observed in the atmospheric boundary layer (Lenschow, 1974).

From the profiles of mean temperature and heat flux, one can compute an eddy diffusivity of heat, defined by:

$$\nu_T = \frac{-\overline{wT}}{\frac{\partial \overline{T}}{\partial z}} .$$

Figure 23 shows the resulting profile of ν_T. The eddy heat diffusivity is negative above the neutral level, where the heat

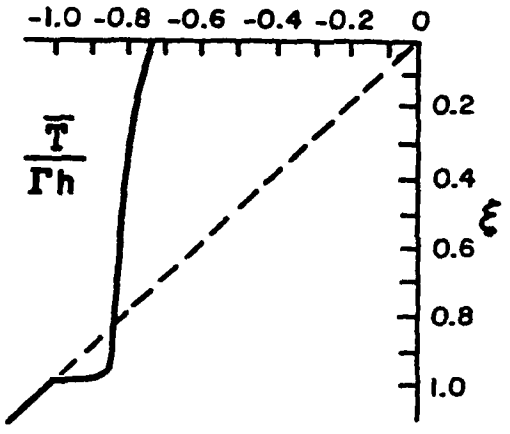

Figure 21. Vertical profile of mean temperature, $\bar{T}$, scaled by Γh.

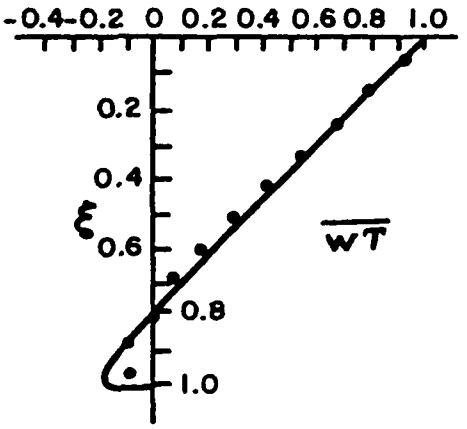

Figure 22. Vertical profile of the vertical convective heat flux $\overline{wT}$, scaled by the surface flux Q. The dots represent the data of Willia and Deardorff (1974), run S1.

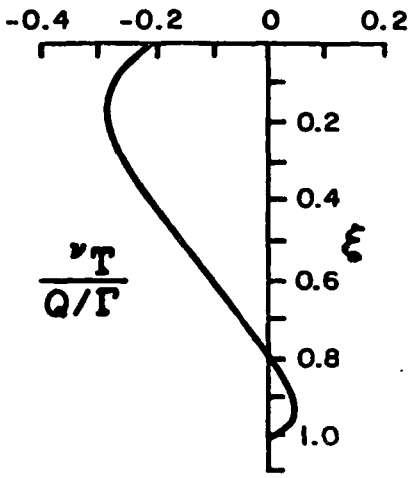

Figure 23. Vertical profile of the eddy heat diffusivity, ν_T, scaled by Q/Γ.

flux is positive. The heat taken out of the fluid near the surface creates thermals, which sink with a heat deficiency. Along the sinking motions, that heat deficiency is progressively reduced by mixing between thermals and anti-thermals. The turbulent temperature fluctuations generated at the surface are thus progressively structured to change the mean temperature. The negative sign of the eddy heat diffusivity expresses that the transfer of energy is from turbulence to mean structure. Below the neutral level, the heat flux is negative, and the eddy heat diffusivity is positive. The transfer is from mean structure to turbulence. The eddy heat diffusivity vanishes again at the bottom of the thermocline where the heat flux vanishes, and the temperature gradient is maximum.

Figure 24 shows the terms of the turbulent kinetic energy budget, obtained from the vertical momentum equation (10):

$$0 = -3m\, w_{rms}^2 \frac{\partial w_{rms}}{\partial z} + \alpha g\, w_{rms} T_{rms} - \frac{mD}{\kappa} w_*^3 \frac{w_{rms}}{|w_{rms}| + mh} \quad .$$

Advection, release of potential energy, and dissipation balance exactly to yield a zero time rate of change of turbulent kinetic energy. The release of potential energy is proportional to the heat flux; release occurs only above the neutral level; below that level, thermals decelerate under the action of the buoyancy force and convert the kinetic energy, which was not dissipated, back to potential energy. The rate of dissipation is quasi-constant with depth and decreases rapidly through the thermocline. This is not surprising since the dissipation term was parametrized

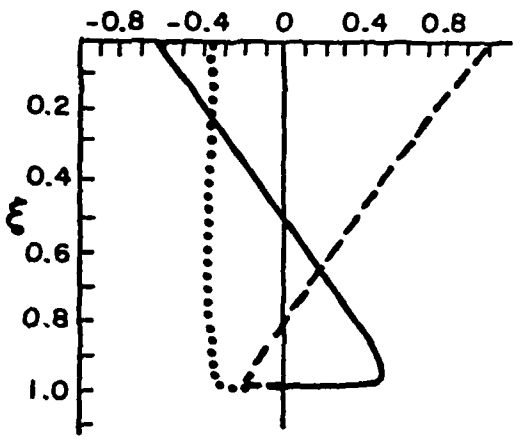

Figure 24. Dimensionless turbulent kinetic energy budget: release of potential energy (dashed line), transport (solid line), and dissipation (dotted line).

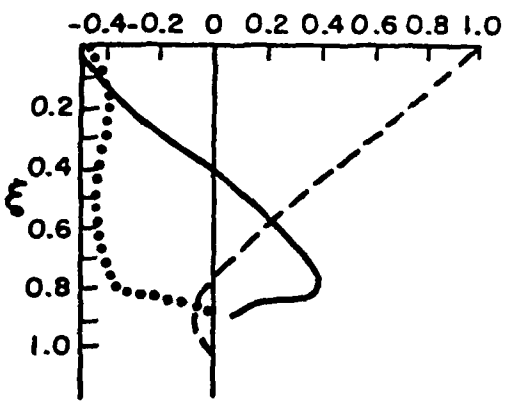

Figure 25. Same as figure 24, but for run S1 of Willis and Deardorff (1974).

for that purpose. Figure 25 reproduces Willis and Deardorff's computations from their data of run S1. The agreement is excellent.

Figure 26 to 28 are plots similar to the previous ones, to be compared with run S2 of Willis and Deardorff (1974). Values of m and D were unchanged since there is no reason to expect that the fraction of area occupied by thermals and the friction coefficient differ from run S1. The ratio ℓ/h and the Richardson number were recalculated to represent the different conditions of the experiment ($\ell/h = 0.1$, $Ri = 45$). Figures 26 to 28 show plots for which data were available for comparison. The other plots do not differ greatly from those related to run S1.

12. CONCLUSIONS

A new model of convection and mixing was applied to the study of penetrative convection in the upper ocean due to surface cooling. It is based on modelling by two interacting fluids. Cold elements produced near the surface become unstable and sink through the water column while continuity of mass forces an upward return flow. The model describes the individual dynamics of these two fluid motions. Mean properties and fluxes up to third-order correlations are then computed. Dissipation is included in order to model realistically the deepening of the mixed layer. The new parametrization of dissipation presented here is dictated by laboratory experiments, atmospheric observations, and turbulence

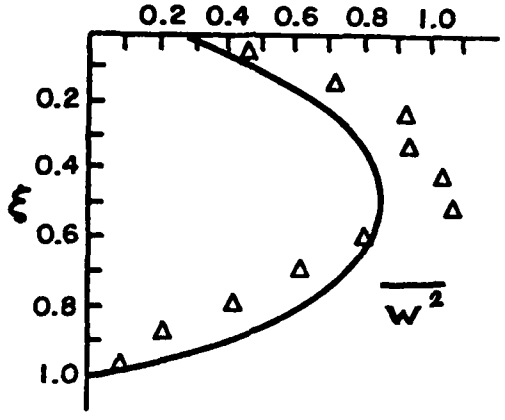

Figure 26. Vertical profile of the vertical-velocity variance, $\overline{w^2}$, scaled by w_*^2, as on figure 18 but for Ri = 45. The triangles represent the data of Willis and Deardorff (1974), run S2.

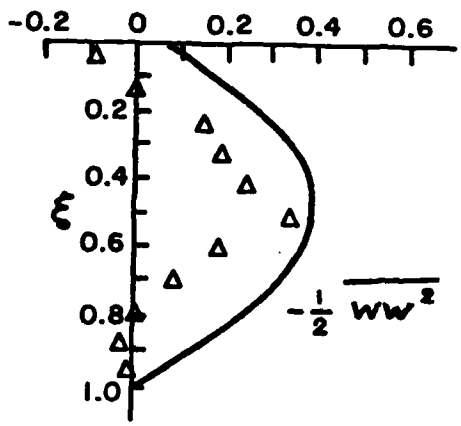

Figure 27. Vertical profile of the vertical flux of turbulent kinetic energy, $-\frac{1}{2}\overline{ww^2}$, scaled by w_*^3, as figure 19, but for Ri = 45. The triangles represent the data of Willis and Deardorff (1974), run S2.

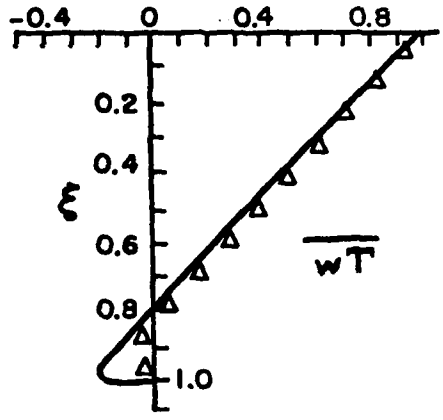

Figure 28. Vertical profile of the vertical convective heat flux, $\overline{wT}$. scaled by the surface flux Q, as on figure 20 but for Ri = 45. The triangles represent the data of Willis and Deardorff (1974), run S2.

arguments.

A simple non-similar analytical solution is found in the case of a well-mixed layer separated from the underlying quiescent fluid by a thin thermocline. The results are valid if the Richardson number is much greater than unity, the condition for the existence of a sharp thermocline. Expressions for the thermocline thickness and turbulence scale near the thermocline are in very good agreement with previous results of turbulence theory. The asymptotic behavior of the solution near the surface has a similarity form as predicted by the similarity theory of Monin and Obukov. Moreover, in the interior of the mixed layer, far away from the surface and the thermocline, the solution degenerates in simple $\frac{1}{3}$-power laws as proposed by Wyngaard, Coté and Izumi (1971).

Bulk properties of the solution were compared with atmospheric observations of the surface boundary layer, laboratory experiments, and previous models (see Table 2). Scattering in the values of the coefficients proposed in the literature implies that no universal values can be assigned to those coefficients. The present model does not assign any specific value; rather, it shows a dependence on the fraction of area occupied by sinking elements. This fraction of area strongly depends upon the surface unstable layer where thermal instability occurs, and is not expected to take the same values in laboratory experiments, in the ocean, or in the atmosphere.

Vertical profiles of vertical-velocity variance and vertical flux of turbulent kinetic energy (Figures 18 and 19, respectively) have a broad maximum near mid-depth, as observed in laboratory experiments. At the surface, they match the imposed turbulence imput by the wind, and, at the bottom of the thermocline, they both vanish without showing any sudden variations in the thermocline. The temperature variance decreases from the surface down to zero at the neutral level, where sinking and rising fluids are at the same temperature. Below that level, it increases again and has a large gradient in the thermocline. As expected, observations do not show a vanishing temperature variance at any level, but a well-pronounced decrease is observed precisely at the neutral level. The temperature profile is composed of a quasi-constant value through the mixed layer and a rapid variation in the thermocline. The vertical convective heat flux varies linearly throughout the mixed layer. It is positive (upward flux) above the neutral level, vanishes at the neutral level, and is negative (downward flux) below it. In the thermocline, the heat flux rapidly decreases from its maximum negative value down to zero. A resulting eddy diffusivity of heat is computed from the mean-temperature gradient and the convective heat flux. The heat diffusivity is found to be negative above the neutral level. This implies that the temperature variance supplied at the surface by the forcing is progressively used to change the mean temperature, as cold

elements move downward. Below the neutral level, the heat diffusivity is positive; in that lower region of the mixed layer and in the thermocline, turbulence is generated by the system itself. As shown in figures 18 to 28, computed profiles and available laboratory data agree remarkably well. Moreover, the accuracy of the simple analytical results presented here is comparable to that of sophisticated turbulence numerical models.

CHAPTER FIVE

EFFECTS OF HORIZONTAL ADVECTION: A CASE OF FRONTOGENESIS

1. INTRODUCTION

The large-scale upper ocean fronts across the central North Pacific are fronts associated with the convergence of Ekman transports (Roden, 1976). In that region, the wind field is dominated by westerlies and the trade winds. This results in eastward stresses and southward Ekman drifts in the north, and in westward stresses and northward Ekman drifts in the south. The region of convergence of these water transports is highly frontogenetical. Continuity of mass requires that the water either downwells (convergence) or escapes laterally in a zonal flow (confluence). According to Roden (1980), the central North Pacific is characterized by these two dynamic features. Observations show two zones of strong surface *convergence* of Ekman transports, one at the southern edge of the westerlies and the other at the northern edge of the easterlies, and a transition zone of *confluence* in between. What mechanism determines whether convergence or confluence occurs, remains however unclear.

Wind stresses generate Ekman transports and, at the same time, vigorously stir the upper layer of the ocean. If there is no advection, wind stirring erodes the stably-stratified fluid underneath and entrains heavier water in the mixed layer; the surface density increases with time as the mixed layer deepens. On the other hand, if there is no mixing, positive buoyancy advection (cold or saline water advection) locally increases the surface density, while negative buoyancy advection (warm or fresh

water advection) locally decreases the surface density. Therefore, wind stirring and wind-driven horizontal advection can add or subtract their respective effects. In the case of an oceanic front generated by the convergence of Ekman transports, positive buoyancy advection generally occurs on the northern side, and negative buoyancy advection on the southern side of the front. Wind mixing thus reinforces advection north of the front, while it opposes advection south of the front. As a result such a front is asymmetric: the horizontal density gradient is stronger on the northern side of the front than it is on the southern side. The asymmetry was observed in the subtropical frontal zone in the central North Pacific (Roden, 1976 and 1980), where fronts exhibit a well-defined southern edge which separates weak density gradients to the south from strong density gradients to the north. The Subarctic Front around 42°N escapes this asymmetry, for temperature and salinity fronts compensate each other, yielding very weak density gradients (non-baroclinic front).

Another source of asymmetry results from the initial horizontal density gradient. Positive buoyancy advection tends to transport heavy water masses over lighter water masses and thus to reduce the density jump at the bottom of the mixed layer. There results an asymmetry in the pycnocline strength between northern and southern sides of the front: the pycnocline is weaker in the north and stronger in the south. Moreover, the resistance to mixed-layer deepening is less where the density

jump across the pycnocline is weaker. As a consequence, the mixed layer is slightly deeper on the northern side. Observations (Roden, 1980) and results presented here both show these asymmetries in the pycnocline strength and mixed-layer depth in both sides of the front.

MacVean and Woods (1980) developed a two-dimensional oceanic frontogenesis model forced by a barotropic horizontal deformation field associated with meso-scale eddies. Turbulent mixing is neglected and Ertel's potential vorticity theorem governs the cross-front velocity. The present approach drastically differ from this study, for the forcing is a surface wind stress capable of generating both drift currents and turbulent mixing. The cross-front flow is the Ekman transport. Moreover, for the scales chosen herein, mixing effects are found to be as important as advective effects.

The present study is aimed at wind-induced frontogenesis with emphasis (i) on the distinction between convergence and confluence in frontal zones, and (ii) on the dual role played by the wind: advection and mixing. An initially quiescent ocean is characterized by linear density gradients in both vertical and meridional directions. (Heavier water is encountered in the deep layers and in the northern region.) The vertical stratification is suppressed near the surface and is replaced by an initially very shallow vertically-homogeneous upper layer. A wind-stress field suddenly takes place and remains constant with time. The

wind stress is positive (westerlies) at the north, and negative (easterlies) at the south. Ekman transports to the right of the wind thus converge toward the middle of the basin, where the wind-stress curl is maximum. The flow pattern is frontogenetical, and a density front is progressively generated by heavy water advection from the north, and light water advection from the south. A wind-mixed layer also deepens on both sides, reinforcing advection in the north and opposing advection in the south. The mixed layer deepens faster away from the front, where the magnitude of the wind stress is larger, and on the northern side where the pycnocline is weaker. The two cases of convergence and confluence are treated separately. In the case of convergence, a downwelling is superimposed on the system. This effect is maximum at the front itself where the wind-stress curl is maximum. In the case of confluence, water flows away laterally along the front, and no downwelling is present. For the sake of simplicity, dissipation is not included, the front strengthens endlessly, and no steady state is reached. The β-effect is neglected, since a frontal zone has, by definition, a small meridional extent.

2. MODEL

The model developed herein is based on modelling of mixing and convection by two interacting fluids (Chapter two). The present work is a generalization of a one-dimensional version of the model applied to the deepening of the wind-mixed layer

(Chapter three), in order to study the effects of lateral advection on mixing.

The model envisions mixing as the relative motion of two interacting fluids of different properties. Parcels of fluid rising through the mixed layer are given, near the surface, extra momentum by the wind stress. These elements are pushed back into the convective layer by turbulence with new properties. Because they sink in a slightly stratified fluid, they are buoyant and decelerate. As they sink, they also progressively lose their excess of horizontal momentum by interactions with the upward return flow. As they reach the bottom of the pycnocline, they have a null vertical velocity and lose their ability to carry heat and momentum. The active sinking elements are called *thermals*, and the rising elements, *anti-thermals*, by analogy. The model describes the individual dynamics of thermals and anti-thermals and their exchanges.

The one-dimensional model developed in chapter three is capable of predicting the vertical structure of mean and fluctuating properties throughout the mixed layer and the pycnocline. Since the level of turbulence responds quasi-instantaneously to temporal and local variations (advective effects are equivalent to temporal variations), turbulent fluxes and vertical-structure properties are given by the one-dimensional model. Therefore, using the results of the one-dimensional model, an advective bulk model is developed and solved. Emphasis is placed on the discussion of mixed-layer depth, mean currents, and horizontal density

gradient, all bulk properties affected by advection, rather than on vertical profiles of turbulence structure which are not affected by lateral advection.

Another generalization is also proposed. Since open ocean frontogenesis depends on both temperature and salinity fields, salinity is included in the formalism. Double-diffusive processes fall out of the scope of the present study, and diffusion is neglected. This simplification permits combination of temperature and salinity in a unique thermodynamic variable, the buoyancy, defined by:

$$b = g(-\alpha T + \beta S), \tag{1}$$

where T is the temperature, S the salinity, α the coefficient of thermal expansion, and β the coefficient of saline contraction. The so-defined buoyancy is dimensional, greater for cold and saline water, and smaller for warm and fresh water. The initial buoyance field is chosen to be:

$$b = b_o + \Gamma_2 y - \Gamma_3 z \ , \quad \text{for } z < -h_o \ ,$$

and

$$b = b_o + \Gamma_2 y + \tfrac{1}{2} \Gamma_3 h_o \ , \ \text{for } -h_o < z \leq 0, \tag{2}$$

where b_o is a reference buoyancy (pure constant), Γ_2 and Γ_3 the horizontal and vertical gradients, respectively, and h_o

the non-zero initial mixed-layer depth. The factor $\frac{1}{2}$ is introduced, in agreement with the one-dimensional model of the wind-mixed layer (Chapter three).

3. GOVERNING EQUATIONS

Thermals and anti-thermals are characterized by different velocities, densities, and pressures. Primed and double-primed quantities refer to thermals and anti-thermals, respectively. If f represents the fraction of area occupied by thermals at any level, the fraction of area available to anti-thermals is (1-f), so that mean properties are defined by:

$$\bar{a} = fa' + (1-f)a'' \ , \tag{3}$$

where a stands for any physical quantity such as velocity components, buoyancy, or pressure (u, v, w, b, or p). Moreover, root-mean-square (rms) fluctuations are defined by:

$$a_{rms} = \sqrt{f(1-f)}\,(a'-a'') = \pm\overline{(a-\bar{a})^2}^{\frac{1}{2}} \ . \tag{4}$$

Rms fluctuations are thus proportional to the difference between thermals and anti-thermals quantities. They may be positive or negative. Second-order turbulence correlations are expressed as:

$$\overline{ac} = fa'c' + (1-f)a''c'' \ , \tag{5}$$

where a and c stand for any physical quantities. Simple calculations using (3) and (4) yield:

$$\overline{ac} = \bar{a}\bar{c} + a_{rms}c_{rms} \quad . \tag{6}$$

Throughout the mixed layer and pycnocline, a saturation equilibrium between thermals and anti-thermals can be assumed (Chapter two). This leads to assigning a constant value to f, the fraction of area occupied by thermals. It has been shown in chapter three that oceanic observations and laboratory experiments suggest a value close to 10%.

With these definitions and the closure hypothesis, the advective model is governed by the following non-linear equations (Chapter two):

Continuity equation:
$$\frac{\partial \bar{u}}{\partial x} + \frac{\partial \bar{v}}{\partial y} + \frac{\partial \bar{w}}{\partial z} = 0 \quad , \tag{7}$$

Buoyancy equations:
$$\frac{\partial}{\partial t}\bar{b} + \frac{\partial}{\partial y}\overline{vb} + \frac{\partial}{\partial z}\overline{wb} = 0 \quad , \tag{8}$$

$$\frac{\partial}{\partial z}(\bar{b}+mb_{rms}) = 0 \quad , \tag{9}$$

Horizontal momentum equations:
$$\frac{\partial}{\partial t}\bar{u} + \frac{\partial}{\partial y}\overline{uv} + \frac{\partial}{\partial z}\overline{uw} - f_o\bar{v} = 0 \quad , \tag{10}$$

$$\frac{\partial}{\partial t}\bar{v} + \frac{\partial}{\partial y}\overline{vv} + \frac{\partial}{\partial z}\overline{vw} + f_o\bar{u} = -\frac{1}{\rho_o}\frac{\partial \bar{p}}{\partial y} \quad , \tag{11}$$

$$\frac{\partial}{\partial z}(\bar{u} + 2m\, u_{rms}) = 0 \quad , \tag{12}$$

$$\frac{\partial}{\partial z}(\bar{v} + 2m\, v_{rms}) = 0 \quad , \tag{13}$$

Vertical momentum equations:
$$\frac{1}{\rho_o}\frac{\partial \bar{p}}{\partial z} = -(1 + \bar{b}) \quad , \tag{14}$$

$$3m\, w_{rms} \frac{\partial}{\partial z} w_{rms} = -b_{rms} \ , \tag{15}$$

where f_o is the Coriolis parameter (positive and constant), ρ_o the reference density, and m is a coefficient dependent upon f only, defined by:

$$m = \frac{1-2f}{2\sqrt{f(1-f)}} \ . \tag{16}$$

Three small terms were neglected: (i) a correction due to vertical advection in the hydrostatic balance (14), (ii) a correction due to a non-zero mean vertical velocity $\bar{w}$ in (15), (iii) the pressure term in (15). These simplifications hold as long as

$$w_{rms}^2 << gh \ , \tag{17}$$

$$\bar{w} << |w_{rms}| \ , \tag{18}$$

$$(\bar{u}^2+\bar{v}^2)\frac{\partial h}{\partial t} << mu_*^3 \ , \tag{19}$$

respectively. The last requirement is equivalent to neglecting the turbulence production in the pycnocline by mean shear compared to the surface turbulence input (Chapter three). This simplification is valid for time scales much larger than the inertial period which is met in the case of frontogenesis.

In the case of frontogenesis, it is reasonable to anticipate that the zonal mean velocity, $\bar{u}$, is geostrophically balanced by a cross-front mean pressure gradient, $\partial\bar{p}/\partial y$, and that the meridional mean velocity, $\bar{v}$, is the depth-independent Ekman flow induced by the zonal wind stress. In the mixed layer, equations (10) and (11) thus reduce to:

$$f_o \bar{v} = \frac{\partial}{\partial z} \overline{uw} \ , \tag{20}$$

and

$$f_o \bar{u} = -\frac{1}{\rho_o} \frac{\partial \bar{p}}{\partial y} \ . \tag{21}$$

Assuming that $\bar{b}$ is depth-independent in the mixed layer, (21) can be solved for $\bar{u}$ in terms of the horizontal buoyancy gradient (so-called thermal-wind relationship):

$$\bar{u} = \frac{1}{f_o} \frac{\partial \bar{b}}{\partial y} (z+h) \ . \tag{22}$$

Since $\bar{u}$ vanishes at the bottom of the mixed layer, the newly-entrained fluid from below is not given zonal momentum in the thermocline. The Reynolds stress $-\overline{uw}$ therefore vanishes at $z = -h$, and equation (20) can be integrated to yield:

$$\bar{v} = -\frac{\tau_x}{\rho_o f_o h} \ , \tag{23}$$

where $\tau_x(y)$ is the local wind stress at the surface, and $h(y,t)$ the local instantaneous mixed-layer depth. North of the front τ_x is positive and $\bar{v}$ is negative; south of the front τ_x is negative and $\bar{v}$ is positive. These two Ekman flows meet at the front (y=0), and continuity requires the water to flow either vertically (convergence), laterally (confluence), or both ways. At the present state of knowledge, it is unclear from observations what mechanism determines whether convergence or confluence occurs. In the present work, the two extreme cases of convergence and confluence are thus studied separately. In nature various combinations of these two cases occur simultaneously, as described by Roden (1980).

In the *case of convergence*, the continuity equation (7) is reduced to $\partial\bar{v}/\partial y + \partial\bar{w}/\partial z = 0$ and yields:

$$\bar{u} = \frac{1}{f_o} \frac{\partial \bar{b}}{\partial y} (z+h) \quad , \quad \bar{w} = \frac{z}{\rho_o f_o} \frac{\partial}{\partial y} \left(\frac{\tau_x}{h}\right) \quad . \tag{24}$$

In the *case of confluence*, $\bar{w}$ at the bottom of the mixed layer is the vertical component of the velocity along the sloping pycnocline ($\bar{w} = -\bar{v}\ \partial h/\partial y$ as $z = -h$), and the full continuity equation (7) has to be used. This yields:

$$\bar{u} = \frac{1}{f_o} \frac{\partial \bar{b}}{\partial y} (z+h) + \frac{x}{\rho_o f_o h} \frac{\partial \tau_x}{\partial y} \quad , \quad \bar{w} = \frac{z\tau_x}{\rho_o f_o} \frac{\partial}{\partial y}\left(\frac{1}{h}\right) \quad . \tag{25}$$

where the origin of the zonal coordinate x is undefined. At the bottom of the mixed layer, the mean vertical velocity $\bar{w}$ is:

$$\begin{aligned} \bar{w} &= -\frac{h}{\rho_o f_o}\frac{\partial}{\partial y}\left(\frac{\tau_x}{h}\right) \qquad \text{(convergence)}, \\ \bar{w} &= -\frac{h\tau_x}{\rho_o f_o}\frac{\partial}{\partial y}\left(\frac{1}{h}\right) \qquad \text{(confluence)} . \end{aligned} \tag{26}$$

The Ekman downwelling in the underlying stratified fluid is given by:

$$\begin{aligned} w_{Ek} &= -\frac{1}{\rho_o f_o}\frac{\partial \tau_x}{\partial y} \qquad \text{(convergence)}, \\ w_{Ek} &= 0 \qquad\qquad\qquad \text{(confluence)} . \end{aligned} \tag{27}$$

The Ekman downwelling is related to the wind-stress curl and is dependent of the mixed-layer depth. It differs from the mean vertical velocity at the bottom of the mixed layer. The difference is the vertical component of the velocity along the sloping pycnocline.

The expression

$$\dot{h} = \frac{\partial h}{\partial t} + \bar{v}\frac{\partial h}{\partial y} + \bar{w} = \frac{\partial h}{\partial t} + w_{Ek} \tag{28}$$

represents the rate of entrainment of fluid from below into the mixing process. It vanishes if the mixed layer deepens solely by Ekman downwelling without entraining new fluid in the mixed layer.

The initial buoyancy field in the underlying stratified fluid is advected downward by the Ekman downwelling velocity given by (27). If the wind forcing is steady, the buoyancy field under the mixed layer at any time is:

$$b_-(y, z, t) = b_o + \Gamma_2 y - \Gamma_3(z - w_{Ek}t) , \qquad (29)$$

where t = 0 corresponds to the initial time when the wind starts to blow.

4. JUMP CONDITIONS ACROSS THE PYCNOCLINE

Due to the presence of large vertical gradients, the terms which dominate the governing equations in the pycnocline differ from those which dominate the equations in the mixed layer. To bring out the dominant terms, the governing equations are advantageously expressed with the similarity vertical coordinate $\xi = -z/h(t)$. Replacing z by ξ, equations (8), (10) and (11) become:

$$\frac{\partial \bar{b}}{\partial t} + \frac{\partial \overline{vb}}{\partial y} - \frac{\xi}{h}\frac{\partial h}{\partial t}\frac{\partial \bar{b}}{\partial \xi} - \frac{\xi}{h}\frac{\partial h}{\partial y}\frac{\partial \overline{vb}}{\partial \xi} - \frac{1}{h}\frac{\partial \overline{wb}}{\partial \xi} = 0 ,$$

$$\frac{\partial \bar{u}}{\partial t} + \frac{\partial \overline{uv}}{\partial y} - \frac{\xi}{h}\frac{\partial h}{\partial t}\frac{\partial \bar{u}}{\partial \xi} - \frac{\xi}{h}\frac{\partial h}{\partial y}\frac{\partial \overline{uv}}{\partial \xi} - \frac{1}{h}\frac{\partial \overline{uw}}{\partial \xi} - f_o\bar{v} = 0 ,$$

$$\frac{\partial \bar{v}}{\partial t} + \frac{\partial \overline{vv}}{\partial y} - \frac{\xi}{h}\frac{\partial h}{\partial t}\frac{\partial \bar{v}}{\partial \xi} - \frac{\xi}{h}\frac{\partial h}{\partial y}\frac{\partial \overline{vv}}{\partial \xi} - \frac{1}{h}\frac{\partial \overline{vw}}{\partial \xi} + f_o\bar{u}$$

$$= -\frac{1}{\rho_o}\frac{\partial \bar{p}}{\partial y} + \frac{1}{\rho_o}\frac{\xi}{h}\frac{\partial h}{\partial y}\frac{\partial \bar{p}}{\partial \xi} .$$

The pycnocline is a very thin layer of large gradients ($\frac{\partial}{\partial \xi} >> 1$ for all quantities except $\partial \bar{p}/\partial \xi$) and is located at the bottom of the mixed layer ($\xi = 1$). Therefore, the above equations can be simplified by retaining only the terms including derivatives with respect to ξ (except $\partial \bar{p}/\partial \xi$) and by replacing ξ by one. Integrations with respect to ξ then yield:

$$\bar{b} \frac{\partial h}{\partial t} + \overline{vb} \frac{\partial h}{\partial y} + \overline{wb} = b_{-}(-h)\left(\frac{\partial h}{\partial t} + w_{Ek}\right) , \tag{30}$$

$$\bar{u} \frac{\partial h}{\partial t} + \overline{uv} \frac{\partial h}{\partial y} + \overline{uw} = 0 \tag{31}$$

$$\bar{v} \frac{\partial h}{\partial t} + \overline{vv} \frac{\partial h}{\partial y} + \overline{vw} = 0 , \tag{32}$$

where the constants of integration were determined by expressing that all the rms fluctuations, $\bar{u}$, and $\bar{v}$ vanish below the pycnocline; $b_{-}(-h)$ is the value of the buoyancy at the top of the underlying stratified fluid:

$$b_{-}(-h) = b_o + \Gamma_2 y + \Gamma_3 (h + w_{Ek} t) , \tag{33}$$

according to (29) for $z = -h$.

In the mixed layer, $\bar{b}$ and $\bar{v}$ are quasi-independent of depth. From (9) and (13), it results that the rms fluctuations b_{rms} and v_{rms} are much smaller than the mean variables $\bar{b}$ and $\bar{v}$ throughout the mixed layer. Relations (30) to (32), which are applicable in the pycnocline, can thus be simplified in the limit near the bottom of the mixed layer. Using (6) and (28), they become:

$$w_{rms}\, b_{rms} = \dot{h}[b_{-}(-h) - \bar{b}] , \tag{34}$$

$$u_{rms}\, w_{rms} = -\dot{h}\bar{u}(-h) , \tag{35}$$

$$v_{rms}\, w_{rms} = -\dot{h}\bar{v} . \tag{36}$$

These equations relate the values of variables at the top and bottom of the pycnocline. They are the classical jump conditions used in one-dimensional bulk models (Kraus and Turner, 1967, and Niiler, 1975, for example). It was, however, necessary to derive them in the context of non-zero lateral variations, for the slope of the pycnocline and the vertical velocity modify the expression of the rate of entrainment $\dot{h}$.

5. SCALING IN THE MIXED LAYER

Since the front sharpens endlessly with time, there is no proper cross-front length scale in this problem. Therefore, the scale, L, of the meridional coordinate, y, is chosen to be the length scale of the wind-stress field. The buoyancy difference across the front is scaled by $B = \Gamma_2 L$, the initial buoyancy difference over the length scale of the wind-stress field. The vertical coordinate, z, and the mixed-layer depth, h, are scaled by $H = B/\Gamma_3$, the initial vertical height corresponding to a buoyancy difference B. The wind stress is scaled by $\rho_o U_*^2$, the order of magnitude of its maximum value away from the frontal zone. In the mixed layer, the along-front mean velocity $\bar{u}$ is scaled by $U = HB/Lf_o$, the cross-front mean velocity $\bar{v}$ by $V = U_*^2/f_o H$, and the vertical velocities $\bar{w}$ and w_{Ek} by $W = U_*^2/f_o L$, as dictated by (22), (23), (26) and (27). The time variable t is scaled by the advective time scale $T = L/V$. Rms fluctuations in the mixed layer are scaled as follows: u_{rms} and w_{rms} by U_* (since $-\overline{uw} = \tau_x/\rho_o$

at the surface), b_{rms} by HB/TU_*, and v_{rms} by HV/TU_*, as suggested by (34) and (36), respectively.

Typical values for scales corresponding to large-scale oceanic frontogenesis in the central North Pacific can be found in Roden (1980). Primary and computed scales are proposed in Table 3. From Table 3, it can be seen that the calculated height scale of the mixed layer ($H \sim 100$ m) corresponds to observed values (Roden, 1980). As anticipated, rms fluctuations b_{rms} and v_{rms} are much smaller than their respective mean values in the mixed layer. The rms vertical velocity w_{rms} is much greater than $\bar{w}$ and $\dot{h}$, since thermals sink from the surface down to the pycnocline in a time relatively short compared to the time of evolution of the whole system. The frontogenesis time scale is of the order of four months, i.e., much larger than a week, which is the response time of a pre-existing oceanic front to atmospheric variations (Roden and Paskausky, 1978). From Table 3, it can also be shown that requirements (17) to (19) are met.

Using unchanged notations for dimensionless variables, equations (8), (10), (11) and (15) become:

$$\frac{\partial \bar{b}}{\partial t} + \bar{v}\frac{\partial \bar{b}}{\partial y} + \bar{w}\frac{\partial \bar{b}}{\partial z} + \left(\frac{H}{TU_*}\right)^2 \frac{\partial}{\partial y}(v_{rms}b_{rms}) + \frac{\partial}{\partial z}(w_{rms}b_{rms}) = 0 , \qquad (37)$$

$$\frac{U}{V}R_o\left(\frac{\partial \bar{u}}{\partial t} + \bar{v}\frac{\partial \bar{u}}{\partial y} + \bar{w}\frac{\partial \bar{u}}{\partial z}\right) + \frac{H}{L}R_o\frac{\partial}{\partial y}(u_{rms}v_{rms}) + \frac{\partial}{\partial z}(u_{rms}w_{rms}) - \bar{v} = 0 , \qquad (38)$$

TABLE 3

Notation	Physical Interpretation	Scale	Source or Relation to others	Order of Magnitude
y	Meridional coordinate	L	Roden, 1980	$5\ 10^{5}$ m
Γ_2	Initial meridional buoyancy gradient	Γ_2	Roden, 1980	$8\ 10^{-9}\ s^{-2}$
$\bar{b}-b_o$	Buoyancy in the mixed layer	B	$B=\Gamma_2 L$	$4\ 10^{-3}\ ms^{-2}$
b_--b_o	Buoyancy in the stratified fluid	B	id.	$4\ 10^{-3}\ ms^{-2}$
Γ_3	Initial vertical buoyancy gradient	Γ_3	Roden, 1980	$4\ 10^{-5}\ s^{-2}$
z,h	Vertical coordinate, mixed-layer depth	H	$H = B/\Gamma_3$	100 m
$u_\star=\left\lvert\frac{\tau_x}{\rho_o}\right\rvert^{\frac{1}{2}}$	Friction velocity	$U_\star$	Roden, 1980	$2\ 10^{-2}\ ms^{-1}$
f_o	Coriolis parameter	f_o	30°N	$10^{-4}\ s^{-1}$
g	Gravitational acceleration	g	-	$10\ ms^{-2}$
$\bar{u}$	Mean long-front velocity	U	$U = HB/Lf_o$	$8\ 10^{-3}\ ms^{-1}$
$\bar{v}$	Mean cross-front velocity	V	$V = U_\star^2/f_o H$	$4\ 10^{-2}\ ms^{-1}$
$\bar{w}$, w_{Ek}	Mean vertical velocities	W	$W = U_\star^2/f_o L$	$8\ 10^{-6}\ ms^{-1}$
t	Time	T	$T = L/V$	10^7 s ∿ 4 months
b_{rms}	Buoyancy fluctuation	-	$HB/TU_\star$	$2\ 10^{-6}\ ms^{-2}$
u_{rms}	Long-front velocity fluctuation	-	$U_\star$	$2\ 10^{-2}\ ms^{-1}$
v_{rms}	Cross-front velocity fluctuation	-	$HV/TU_\star$	$2\ 10^{-5}\ ms^{-1}$
w_{rms}	Vertical-velocity fluctuation	-	$U_\star$	$2\ 10^{-2}\ ms^{-1}$
$\dot{h}$	Rate of entrainment	-	H/T	$10^{-5}\ ms^{-1}$
$\rho_o^{-1}\partial\bar{p}/\partial y$	Cross-front pressure gradient	-	HB/L	$8\ 10^{-7}\ ms^{-2}$
m	Coefficient defined by (16)	m	Chapter three	1

Table 3. Orders of magnitude of physical quantities used for scaling. The values are characteristic of large-scale oceanic frontogenesis in the central North Pacific.

$$\frac{1}{Ri}\left(\frac{\partial \bar{v}}{\partial t} + \bar{v}\frac{\partial \bar{v}}{\partial y} + \bar{w}\frac{\partial \bar{v}}{\partial z}\right) + \frac{1}{Ri}\left(\frac{H}{TU_*}\right)^2 \frac{\partial}{\partial y} v_{rms}^2$$

$$+ \frac{1}{Ri}\frac{\partial}{\partial z}(v_{rms} w_{rms}) + \bar{u} = \frac{\partial \bar{p}}{\partial y} , \quad (39)$$

$$3a\, w_{rms}\frac{\partial}{\partial z} w_{rms} = -2b_{rms} , \quad (40)$$

in the derivation of which continuity equation (7) used. The dimensionless numbers brought out by scaling are:

- the ratio of entrainment rate to the friction velocity:

$$\frac{H}{TU_*} \sim 5\ 10^{-4},$$

- the velocity ratio: $\frac{U}{V} \sim 0.2$,

- the Rossby number: $Ro = \frac{V}{f_o L} = (f_o T)^{-1} \sim 10^{-3}$, (41)

- the Richardson number: $Ri = \frac{HB}{V^2} \sim 250$, (42)

- the coefficient: $a = \frac{2mU_*}{RoRiV} \sim 1$. (43)

The coefficient a is called the mixing parameter.

As the front sharpens, the derivatives $\partial\bar{u}/\partial y$ and $\partial\bar{b}/\partial y$ increase with time by an order of magnitude (Roden, 1980). These non-dimensional terms are thus extimated to be of the order of ten. On the other hand, since the mixed layer is well mixed, $\partial\bar{b}/\partial z$ and $\partial\bar{v}/\partial z$ are very small terms. Neglecting all the small terms, the above equations reduce to:

$$\frac{\partial \bar{b}}{\partial t} + \bar{v}\frac{\partial \bar{b}}{\partial y} = -\frac{\partial}{\partial z}(w_{rms} b_{rms}) , \quad (44)$$

$$\bar{v} = \frac{\partial}{\partial z}(u_{rms} w_{rms}) , \quad (45)$$

$$\bar{u} = -\frac{\partial \bar{p}}{\partial y} \quad , \tag{46}$$

$$3a w_{rms} \frac{\partial}{\partial z} w_{rms} = -2 b_{rms} \quad , \tag{47}$$

and are applicable in the mixed layer only. Equations (45) and (46) express that $\bar{v}$ is a pure Ekman drift and that $\bar{u}$ is geostrophically balanced by the cross-front pressure gradient. These solutions for $\bar{u}$ and $\bar{v}$ were anticipated earlier in order to evaluate the scales of $\bar{w}$ and rms fluctuations. It is therefore shown here *a posteriori* that the hypotheses made on $\bar{u}$ and $\bar{v}$ are correct.

6. BULK MODELS: CASES OF CONVERGENCE AND CONFLUENCE

Considerable simplifications result from assuming a homogeneous mixed layer. A closed set of equations is obtained from (44) to (47) by assuming that $\bar{b}$ and $\bar{v}$ are constant, $b_{rms}\, w_{rms}$ and $u_{rms}\, w_{rms}$ linear, and w_{rms}^3 quadratic with depth. Boundary conditions are:

- no surface buoyancy flux: $w_{rms}\, b_{rms} = 0$
- surface stress = wind stress: $u_{rms}\, w_{rms} = -\tau$
- w_{rms} = friction velocity (Chapter three): $w_{rms} = -|\tau|^{\frac{1}{2}}$

} at $z = 0$,

- jump condition (34): $w_{rms}\, b_{rms} = \dot{h}\delta$
- jump condition (35): $u_{rms}\, w_{rms} = 0$
- negligible residual w_{rms} (Chapter three): $|w_{rms}| << |\tau|^{\frac{1}{2}}$

} at $z = -h$,

where τ is the wind stress $\tau_x(y)$, scaled by $\rho_o U_*^2$; δ is the buoyancy jump across the thermocline, function of y and t:

$$\delta = b_-(-h) - \bar{b} \ .$$

After replacement of linear and quadratic laws and after elimination of $\bar{v}$ and w_{Ek} by (23) and (27), ($\bar{v} = -\tau/h$, $w_{Ek} = -\partial\tau/\partial y$ or zero), the prognostic equations for $\bar{b}$ and h can be written:

in the <u>case of convergence</u>

$$\frac{\partial \bar{b}}{\partial t} = \frac{\tau}{h}\frac{\partial \bar{b}}{\partial y} + a\,\frac{|\tau|^{3/2}}{h^2} \ , \qquad (48)$$

$$\frac{\partial h}{\partial t} = \frac{d\tau}{dy} + a\,\frac{|\tau|^{3/2}}{h\delta} \ , \qquad (49)$$

where

$$\delta = y + h - t\frac{d\tau}{dy} - \bar{b} \ ; \qquad (50)$$

in the <u>case of convergence</u>

$$\frac{\partial \bar{b}}{\partial t} = \frac{\tau}{h}\frac{\partial \bar{b}}{\partial y} + a\,\frac{|\tau|^{3/2}}{h^2} \ , \qquad (51)$$

$$\frac{\partial h}{\partial t} = a\,\frac{|\tau|^{3/2}}{h\delta} \ , \qquad (52)$$

where

$$\delta = y + h - \bar{b} \ . \qquad (53)$$

Equations (48) and (51) express that the time rate of change of the mixed-layer buoyancy is due to advection by the Ekman meridional flow and to mixing with newly-entrained fluid from below. Equations (49) and (52) express that the time rate of change of the mixed-layer depth is due to the Ekman downwelling, if any, and to deepening by turbulent erosion. The wind stress, $\tau(y)$, acts as the forcing on the system. The mixing parameter, a, given by (43), depends upon the global physical characteristics of the problem. *This coefficient controls the entrainment rate ... the smaller (larger) a, the less (more)*

intense is the entrainment of stratified fluid in the mixing process, and the slower (faster) is the mixed-layer deepening.

7. NUMERICAL RESULTS

The governing equations (49) to (50) and (51) to (53) are coupled and highly non-linear. Moreover, coefficients depend upon y through the wind-stress forcing τ. The search for an analytical solution is thus hopeless. However, it is very easy to implement a numerical scheme to integrate the governing equations step by step in time, starting from an imposed initial state.

For the numerical calculations, the wind-stress field is chosen to be:

$$\tau(y) = \tanh y \ ,$$

positive for $y>0$ and negative for $y<0$ (Figure 29). A frontal zone is thus expected near $y = 0$. The meridional extent of the basin, in which the equations are solved, is chosen to be:

$$-2 \leq y \leq 2 \ .$$

The initial conditions consist of an initially homogeneous mixed layer of non-zero depth ($h = 0.5$), in order to avoid an initially infinite Ekman flow. The buoyancy gradient is chosen to be in the horizontal and vertical directions, as required by scaling. The ocean stratification horizontal length scale is thus equal to the wind-stress length scale, as it is observed (Roden, 1980). The mathematical expression of the initial buoyancy field results

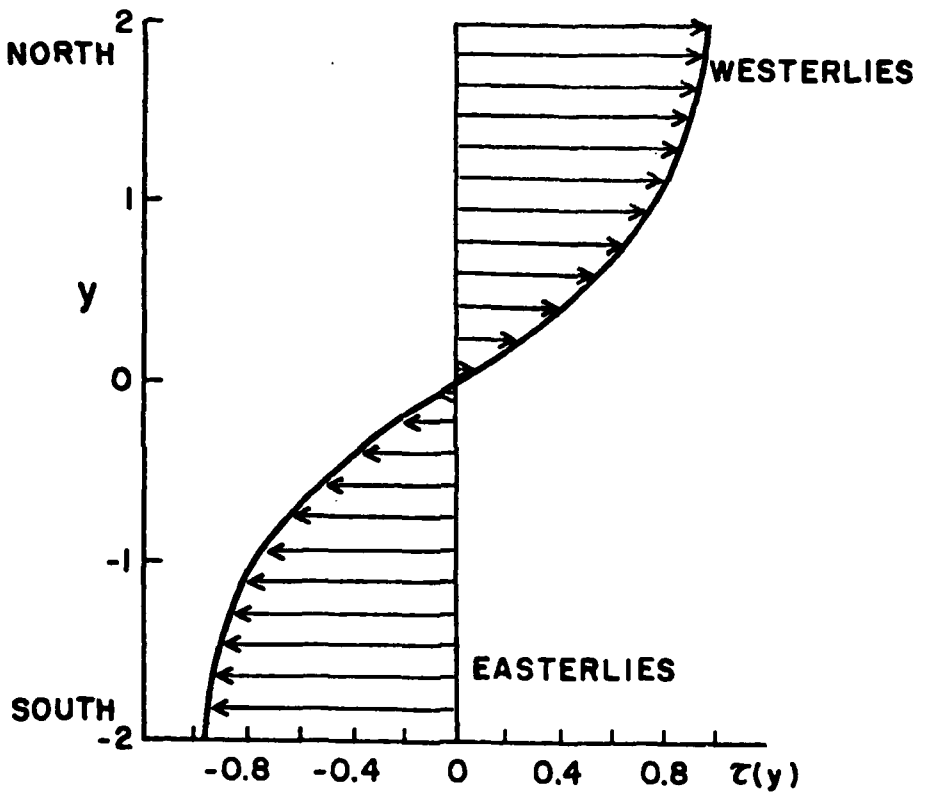

Figure 29. Imposed wind-stress field.

from (2).

$$\bar{b} = y - z \ , \qquad \text{for } z<-0.5 \ , \ -2\leq y\leq 2 \ ,$$

$$\bar{b} = y + 0.25 \ , \qquad \text{for } -0.5<z\leq 0 \ , \ -2\leq y\leq 0 \ .$$

The initial meridional section corresponding to those initial conditions is presented in figure 30.

The problem requires a boundary condition on $\bar{b}$ on each side of the region of interest to characterize the buoyancy of the water newly advected in the basin. These conditions are chosen to be:

$$\frac{\partial \bar{b}}{\partial y} = 1 \quad \text{at } y = -2 \text{ and } y = +2 \ ,$$

expressing that, outside of the region of interest, the water does not feel the presence of the front and conserves its initial horizontal buoyancy gradient.

The results are divided into two classes: the case of *convergence* and the case of *confluence*. For each class, various runs were executed in order to compare the combined effects of mixing and advection.

Figures 31, 32 and 33 show three cross-front sections of the buoyancy field in the case of *convergence*, for increasing values of the mixing parameter a. For these cases, a global Ekman downwelling given by (27), is superimposed on the system. This Ekman downwelling is symmetric about the front and is maximum at the front where the wind-stress curl is the greatest. The resulting deformation field in the stratified fluid is increasing linearly in time. Figures 31 and 32 are plots corresponding to t = 1.6, i.e., about 6 months after the winds start to blow. In figure 33, the

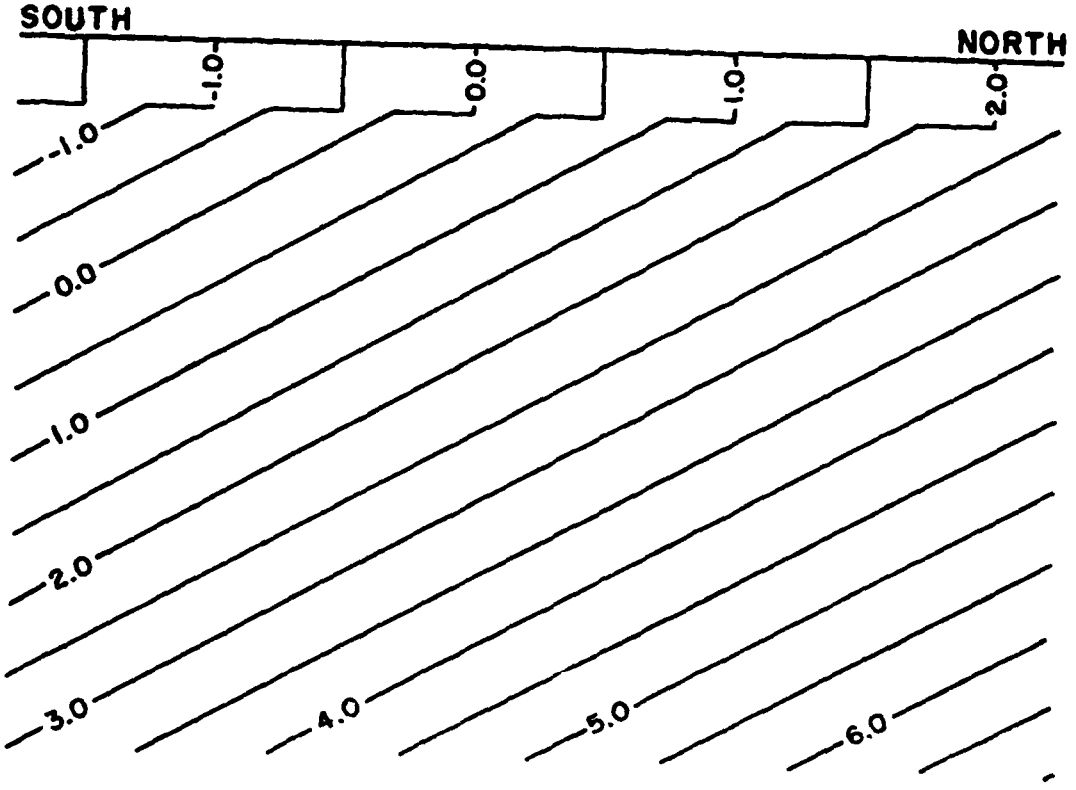

Figure 30. Initial buoyancy field.

Ekman downwelling is less apparent, because the cross-section is made at an earlier time (t = 0.16, i.e., about 18 days after the winds start to blow).

For a small value of the mixing parameter (Figure 31), the erosion of the underlying stratification can be significant only for a very weak density jump across the pycnocline. On the southern side of the front, negative buoyancy advection from the south increases the density jump across the pycnocline and thus prevents any erosion. The mixed layer deepens only be Ekman downwelling without entraining new fluid in the mixing process. On the northern side of the front, positive buoyancy advection from the north decreases the density jump across the pycnocline and favors entrainment of stable fluid. Entrainment is limited, however, since the mixing parameter is small. The mixed layer is somewhat deeper north of the front. Because mixing is not important on either side of the front, the buoyancy field in the mixed layer is governed mainly by advection, i.e., the buoyancy gradient is almost symmetric about the front. Therefore, as shown in figure 31, the asymmetry of the front is most pronounced in the pycnocline strength, while mixed-layer depth and buoyancy profile are quasi-symmetric.

Figure 32 shows a similar section of the buoyancy field for a greater value of the mixing parameter. Mixing is more pronounced away from the front, where the wind-stress magnitude is greater. The mixed-layer depth thus has a minimum at the middle of the front where the wind stress vanishes. In a real oceanic situation,

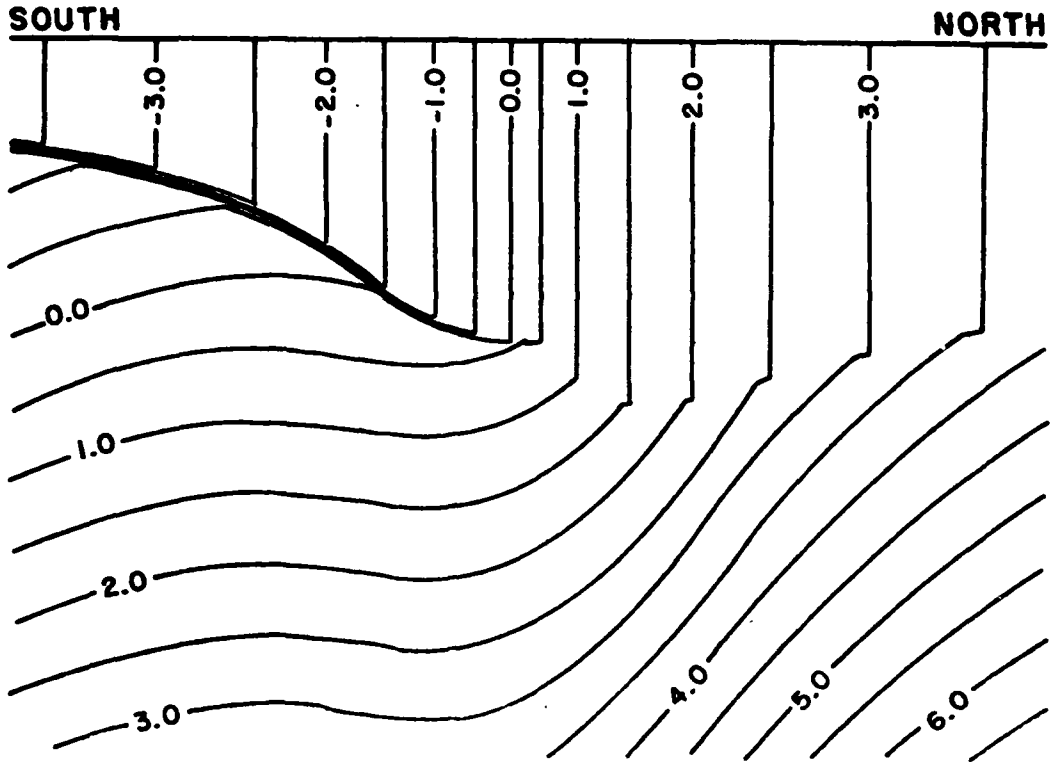

Figure 31. Cross-front section of the buoyancy field in the case of convergence, for t = 7.60 and a = 0.1.

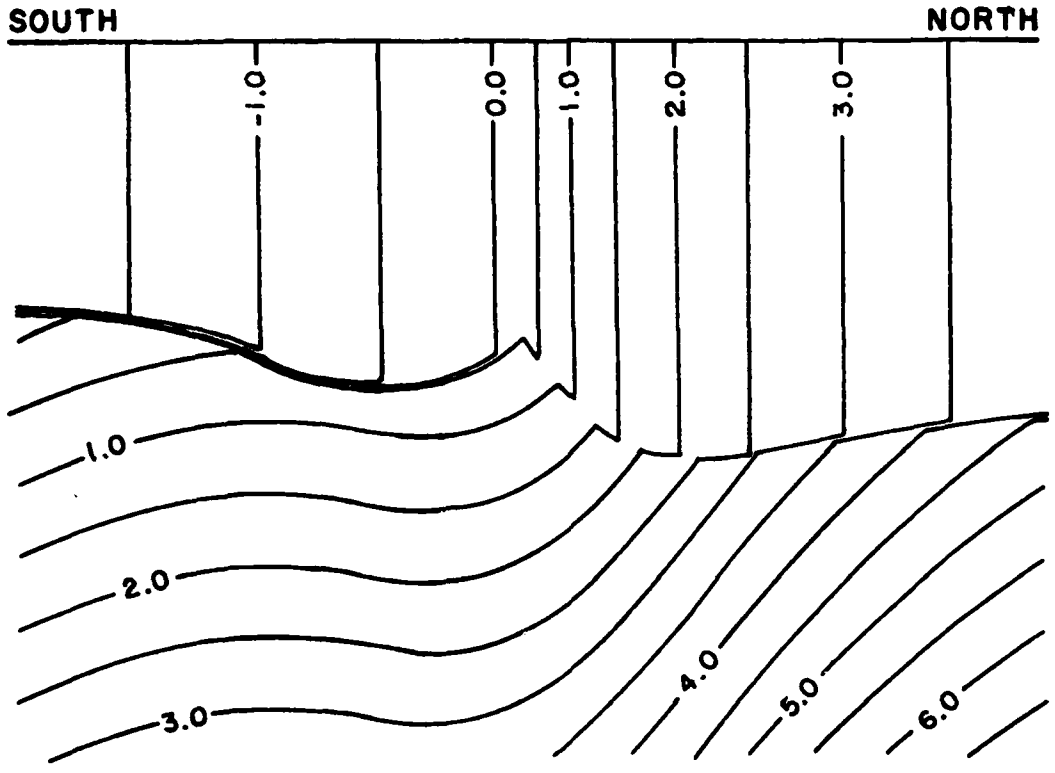

Figure 32. Cross-front section of the buoyancy field in the case of convergence, for t = 1.60 and a = 1.0.

winds fluctuate about a mean value. These fluctuations increase turbulent mixing and not advection, since mixing is non-linearly dependent upon the wind stress. Including such fluctuations in the forcing would therefore reduce the minimum mixed-layer depth at the front. Mixing is maximum away from the front, while the Ekman downwelling is maximum at the front; these two effects thus compete. As shown on figure 32, the result is a maximum mixed-layer depth on both sides of the front. On the southern side of the front, negative buoyancy advection increases the pycnocline strength. Nevertheless, entrainment is effective and tends to increase the mixed-layer buoyancy. Advection and mixing oppose each other, and the buoyancy field in the mixed layer is almost identical to the one of the initial state. On the northern side of the front, positive buoyancy advection decreases the pycnocline strength and favors entrainment. The mixed layer deepens faster in the north. Mixing increases the mixed-layer buoyancy and thus reinforces the positive buoyancy advection from the north, leading to the formation of a large frontal buoyancy gradient. The resulting horizontal profile of the mixed-layer buoyancy is very asymmetric: the southern side is characterized by a weak gradient, almost identical to the one of the initial state, while the northern side is characterized by a strong frontal horizontal gradient.

Figure 33 shows a cross-front section of the buoyancy field for a large value of the mixing parameter. An increasing mixing parameter leads to an increasing rate of entrainment. The mixed

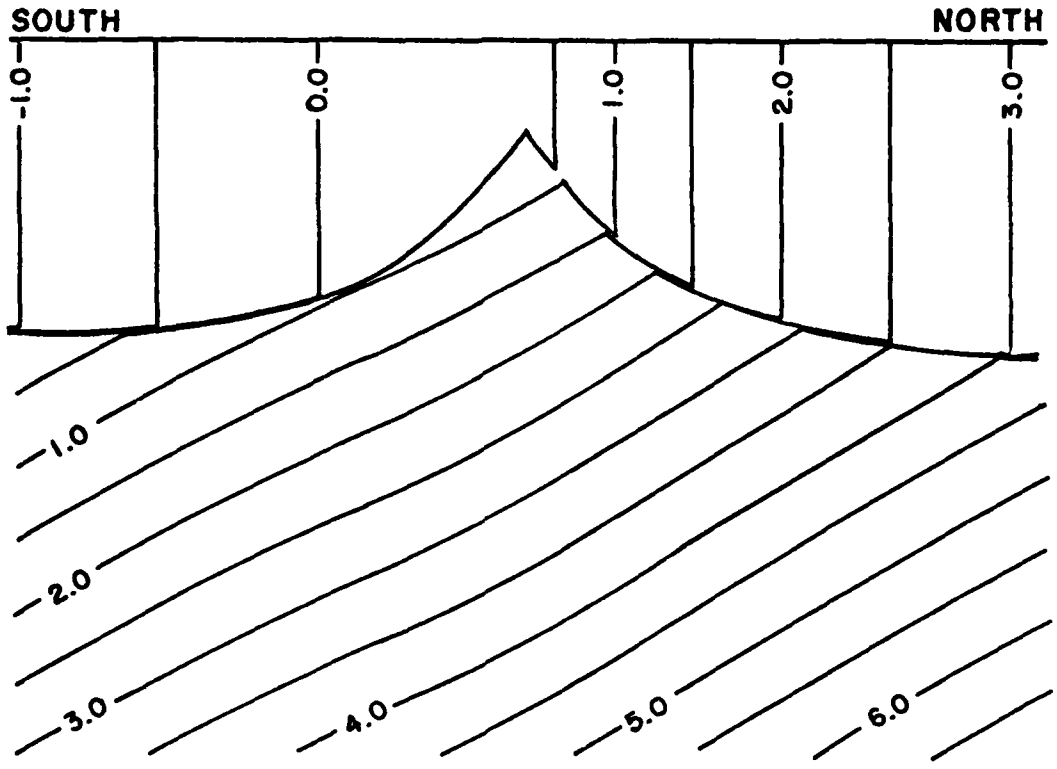

Figure 33. Cross-front section of the buoyancy field in the case of convergence, for t = 0.16 and a = 10.

layer becomes rapidly so deep that the physical occurence of such a situation is doubtful. However, it is interesting to study the modifications brought out in this extreme case. Mixing is now so intense that it controls the deepening of the mixed layer. Hence the mixed-layer depth is symmetric about the front. On the southern side of the front, the density increase due to mixing takes over the density decrease due to advection from the south. The lines of constant buoyancy move southward, away from the front. *Frontolysis* occurs on the southern side. On the northern side, however, mixing and advection reinforce each other, and a front appears. Since advection is not very effective compared to mixing, the front is a result of differential mixing rather than of differential advection.

Figure 34 is a summary of the cross-front profiles of the mixed-layer buoyancy shown in the three previous figures. The dashed line represents the initial linear profile. For a small value of the mixing parameter ($a = 0.1$), the profile is highly distorted by northward advection in the south and southward advection in the north. The profile is almost symmetric about the center of the front ($y = 0$, $\bar{b} = 0.25$). The gradient at the center is five times greater than the initial gradient, revealing the presence of a well-defined front. For a greater value of the mixing parameter ($a = 1.0$), the profile is totally asymmetric: linear and almost identical to the initial profile in the south, and distorted by southward advection in the north. The maximum gradient at the center of the front is near the one for $a = 0.1$,

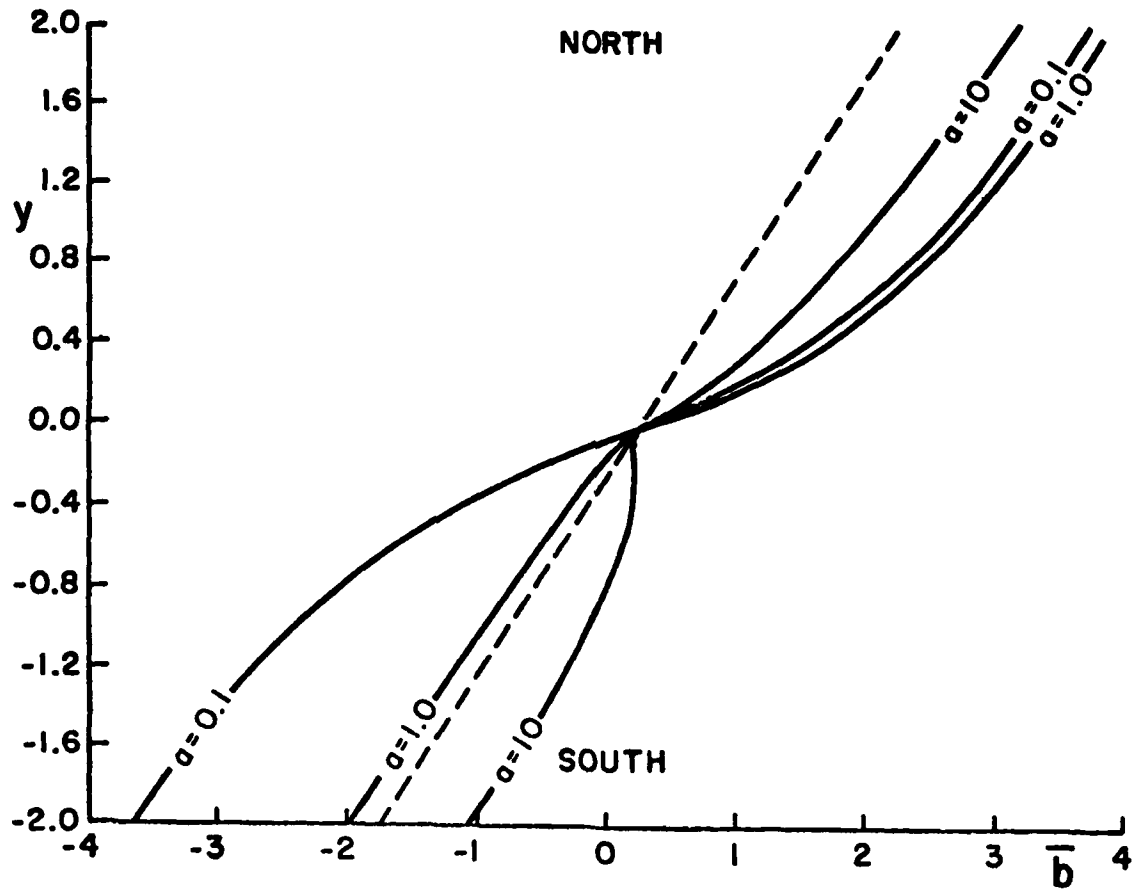

Figure 34. Cross-front variation of the mean buoyancy in the mixed layer in the case of convergence, for three different values of the mixing parameter a. For a = 0.1 and 1.0, values are plotted at t = 1.60. For a = 10, values are plotted at t = 0.16. The dashed line represents the initial profile.

but the region of large gradients is reduced by two, revealing a weaker front. For a large value of the mixing parameter (a = 10.), the buoyancy profile is displaced southward everywhere as a result of mixing only. The buoyancy gradient is almost zero on the southern edge but large on the northern edge of the front. The frontal zone is not a consequence of advection but rather a result of non-mixing in a region where the wind stress vanishes.

The time evolution of the mixed-layer depth on both sides of the front is shown in Figure 35, for the three values of the mixing parameter. As expected, the greater the mixing parameter, the deeper the mixed layer. For times greater than 0.3 (about one month), the mixed layer deepens at a constant rate. On the southern side of the front (y = -0.5), the rate of increase almost coincides with the rate of deepening by Ekman downwelling. The reason is clear: due to negative buoyancy advection, the buoyancy jump across the pycnocline becomes so strong after a month that it prevents any further mixing. On the northern side of the front (y = 0.5), the rate of increase is larger because of the tendency of positive buoyancy advection to reduce the pycnocline strength. The rate of deepening is remarkably constant with time, although there is no reason *a priori* for such behavior. For a = 0.1, the asymmetry between north and south appears around t = 0.2 (about 20 days), when the pycnocline strength is substantially reduced on the northern side such that mixing becomes noticeable. For a = 1.0 and 10, the asymmetry appears sooner, and the incipient deepening is well separated from the Ekman downwelling.

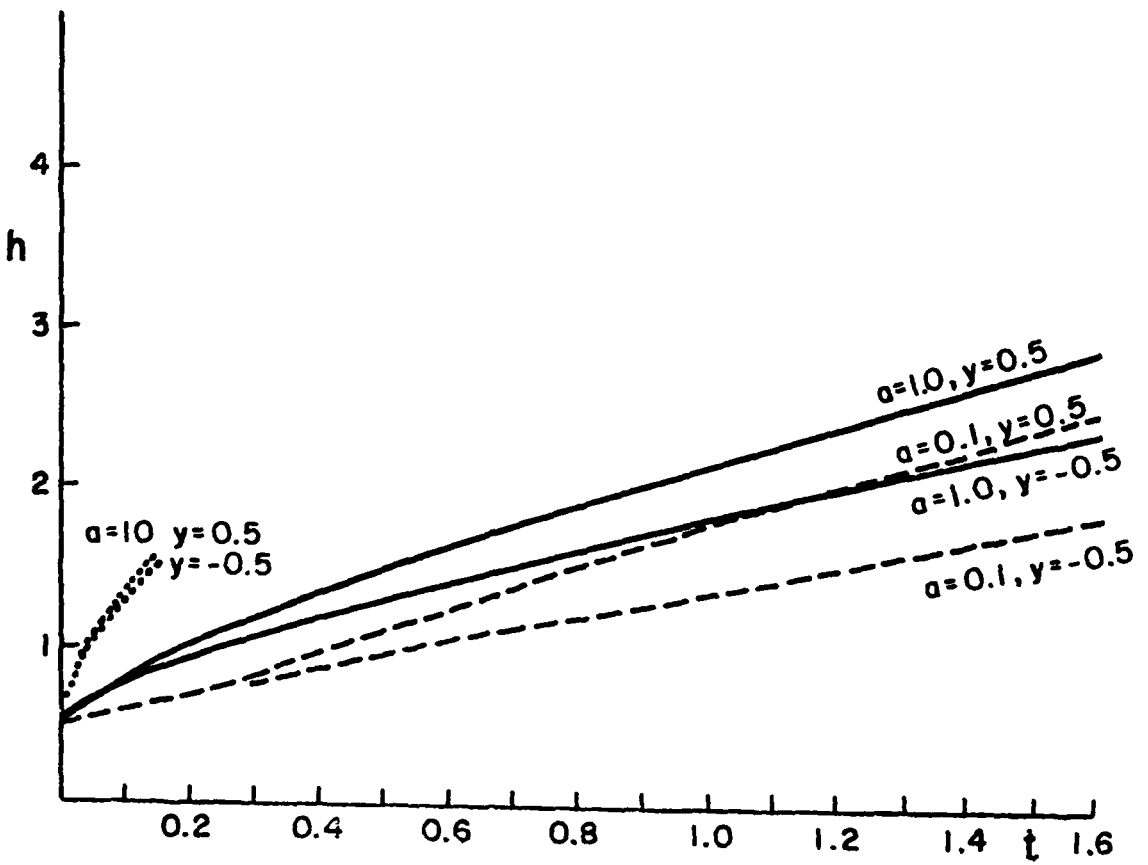

Figure 35. Evolution of the mixed-layer depth on both sides of the front ($y = \pm 0.5$) in the case of convergence, for three different values of the mixing parameter a.

AD-A093 101 FLORIDA STATE UNIV TALLAHASSEE MESOSCALE AIR-SEA INT--ETC F/G 8/3
MIXING, CONVECTION, AND ADVECTION IN THE UPPER OCEAN.(U)
NOV 80 B CUSHMAN-ROISIN N00014-75-C-0201
UNCLASSIFIED 171 NL

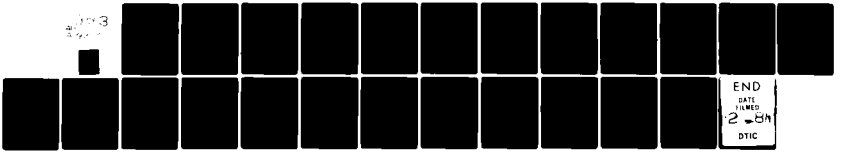

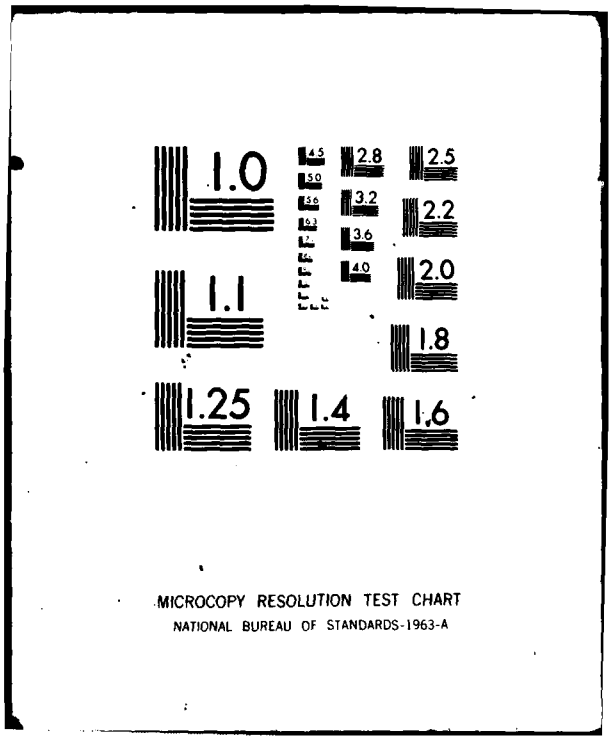
1.0
1.1
1.25
1.4
1.6
1.8
2.0
2.2
2.5
2.8
3.2
3.6
4.0
4.5
5.0
5.6
6.3
MICROCOPY RESOLUTION TEST CHART
NATIONAL BUREAU OF STANDARDS-1963-A

Figures 36, 37 and 38 show three cross-front sections of the buoyancy field in the case of *confluence*, for the same values of the mixing parameter. They are to be compared with Figures 31, 32 and 33, respectively. The interior is at rest at all times. For a small value of the mixing parameter (Figure 36), the pycnocline strength and the mixed-layer depth greatly differ on both sides. On the southern side, negative-buoyancy advection has largely increased the buoyancy jump across the pycnocline and prevented any erosion of the stratified fluid. On the northern side, positive-buoyancy advection has swept out the pycnocline almost totally and favored a moderate deepening (small mixing parameter). For a greater value of the mixing parameter (Figures 37 and 38), the asymmetries of pycnocline strength and of the mixed-layer buoyancy becomes more asymmetric.

Figure 39 is a plot of the cross-front profiles of the mixed-layer buoyancy of the three previous figures. Comparison with Figure 34 reveals that the frontal gradients of buoyancy are greater by about a factor of three in the case of confluence. But, the profiles exhibit qualitatively the same shapes.

The time evolution of the mixed-layer depth on both sides of the front in the case of confluence is shown on Figure 40, for the three values of the mixing parameter. Comparison with Figure 35 reveals that the rate of mixed-layer deepening is reduced in the case of confluence, as a result of the absence of the Ekman downwelling. Because the mixed layer is shallower in the case of confluence, the cross-front Ekman drift is larger and advection

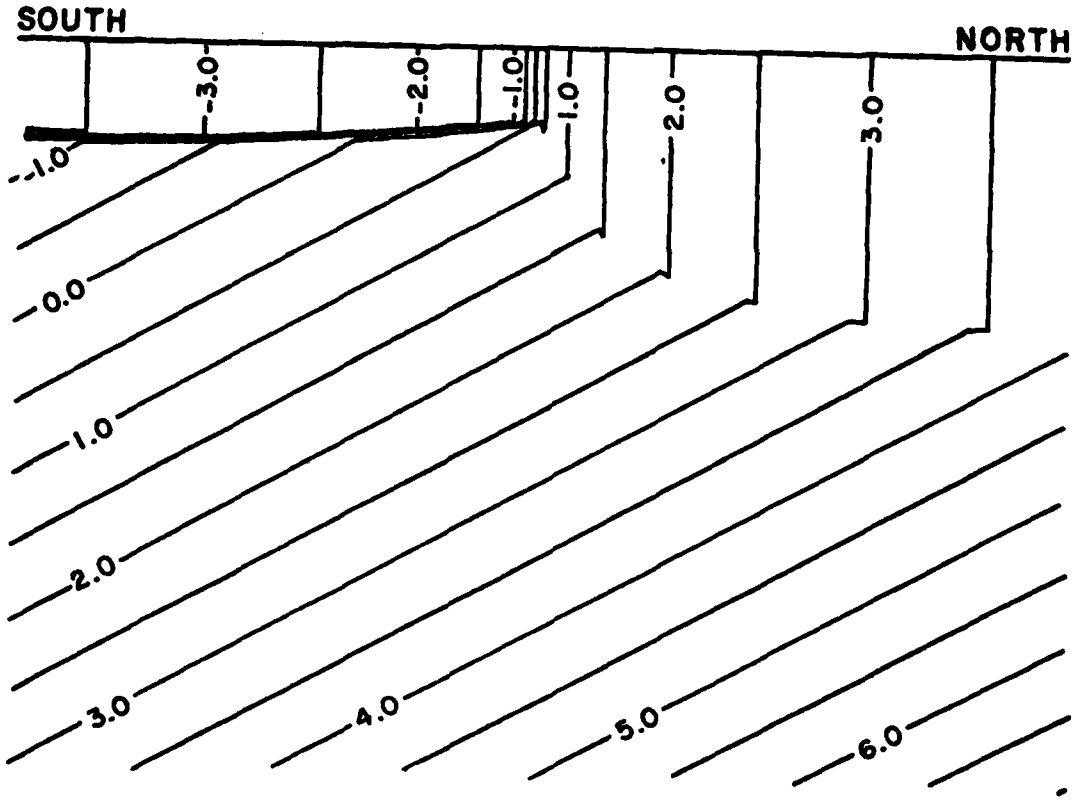

Figure 36. Cross-front section of the buoyancy field in the case of confluence, for $t = 1.60$ and $a = 0.1$.

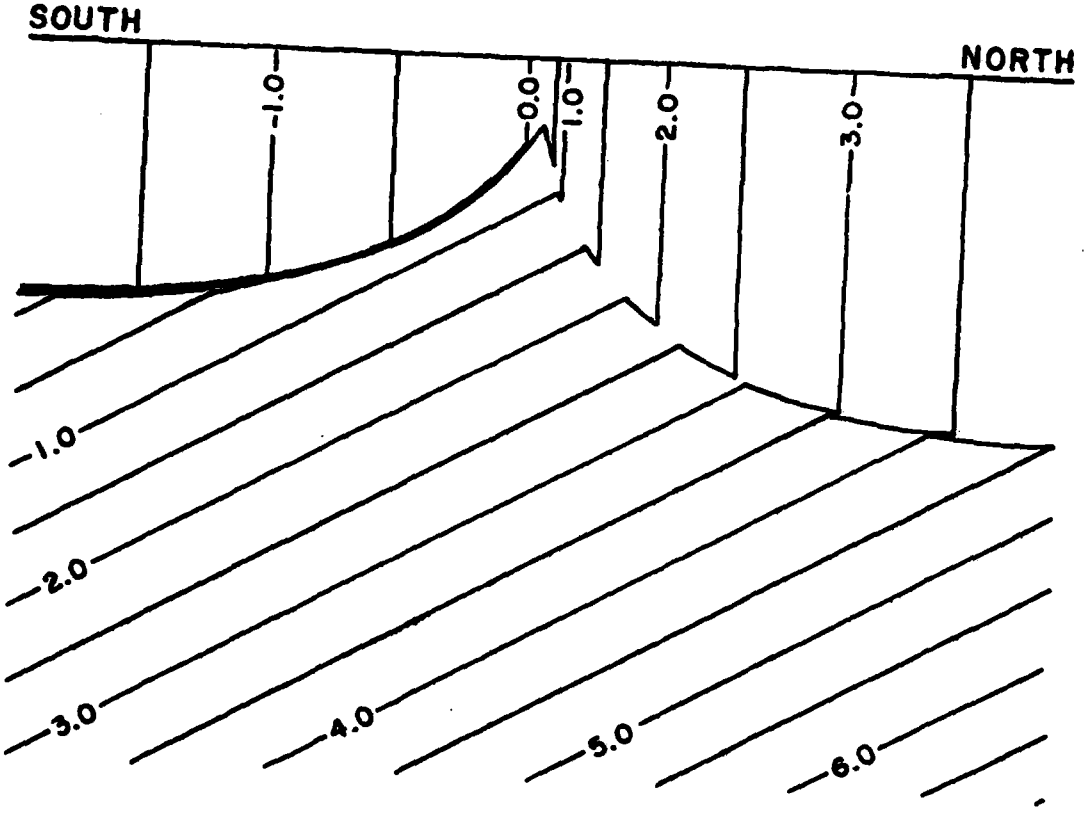

Figure 37. Cross-front section of the buoyancy field in the case of confluence, for t = 1.60 and a = 1.0.

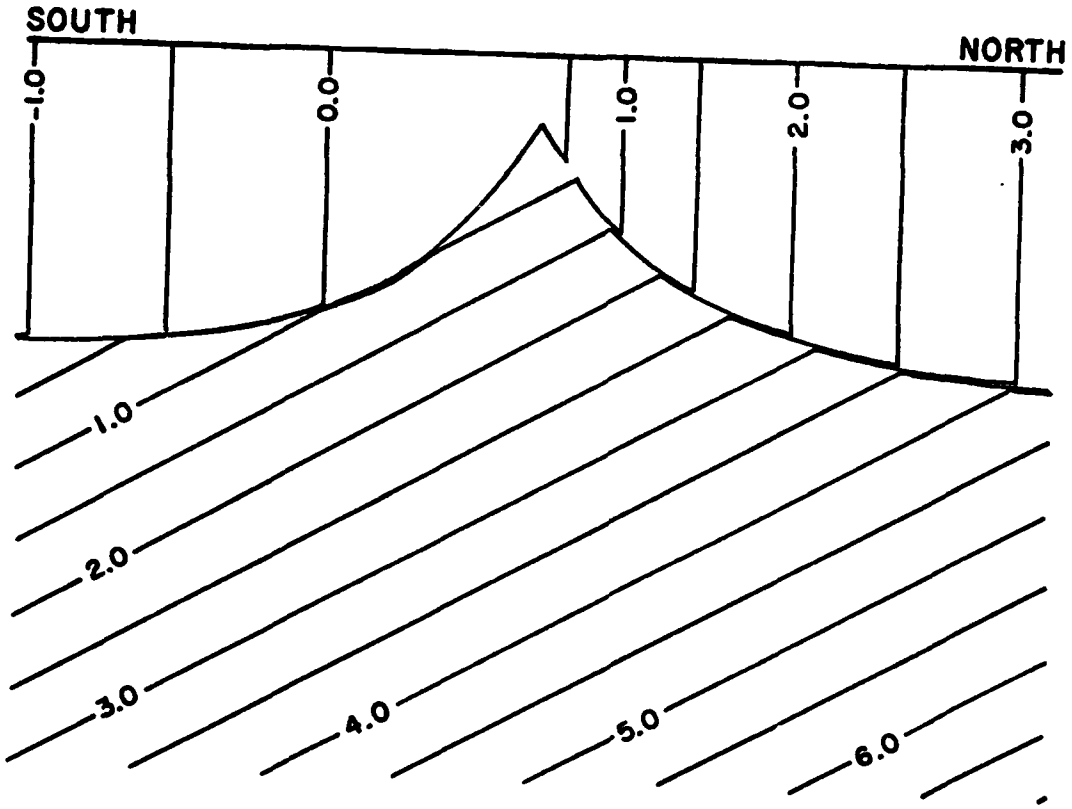

Figure 38. Cross-front section of the buoyancy field in the case of confluence, for t = 0.16 and a = 10.

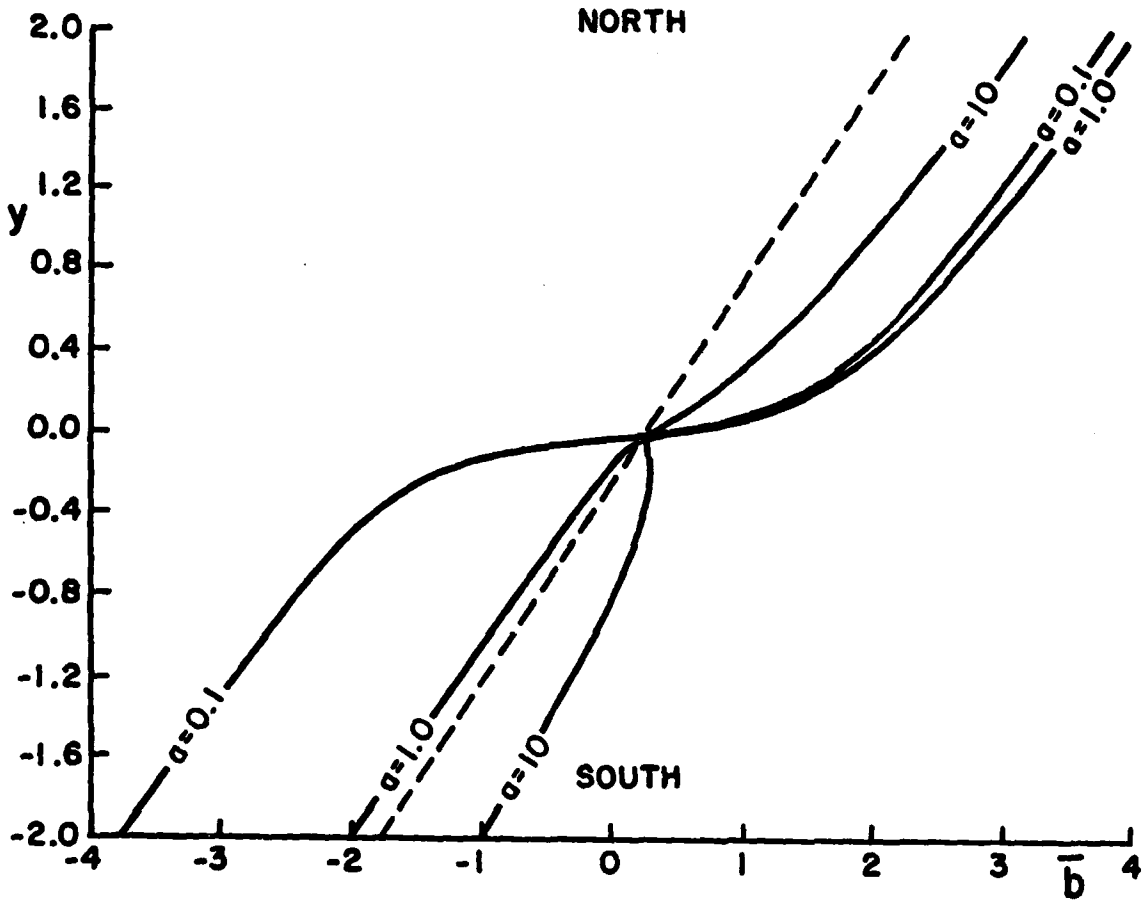

Figure 39. Cross-front variation of the mean buoyancy in the mixed layer in the case of confluence, for three different values of the mixing parameter a. For a = 0.1 and 1.0, values are plotted at time t = 1.60. For a = 10, values are plotted at time t = 0.16. The dashed line represents the initial linear profile.

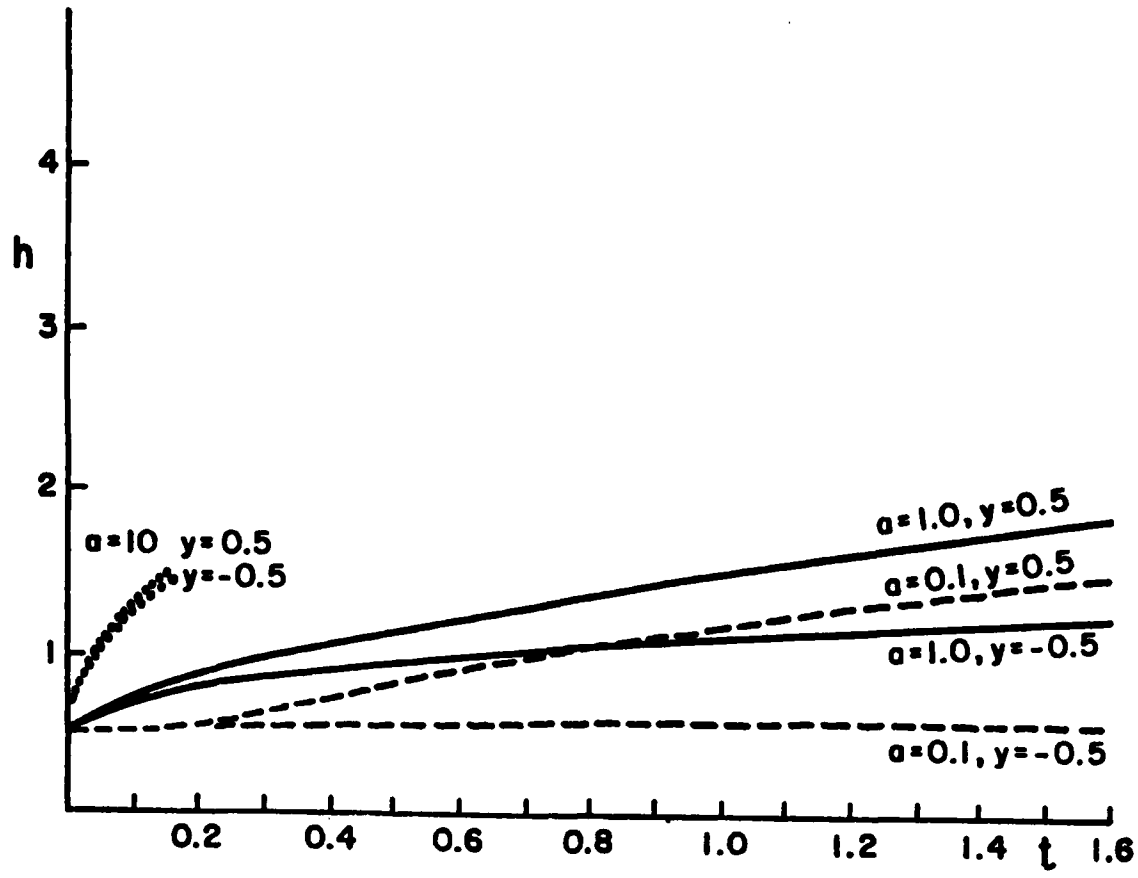

Figure 40. Evolution of the mixed-layer depth on both sides of the front ($y = \pm 0.5$) in the case of confluence, for three different values of the mixing parameter a.

is more important. This explains why the horizontal buoyancy gradients are greater in the case of confluence.

8. SUMMARY AND DISCUSSION

A bulk model for the study of advective and mixing effects in the upper ocean was constructed from a one-dimensional mixed-layer model. The aim of the work was to investigate the formation of a frontal zone by convergence of Ekman transports, as observed in the central North Pacific. The β-effect and dissipation were neglected. Temperature and salinity were combined to form a single thermodynamic variable, called the buoyancy. Scaling showed that the long-front velocity is in geostrophic balance with a cross-front pressure gradient and is unimportant. The cross-front velocity is an Ekman drift, driven by the surface wind stress, and converges toward the region of zero wind stress, producing frontogenesis. Continuity of mass near the front requires that water masses either downwell (*convergence*) or escape laterally (*confluence*). This distinction leads to two cases, each treated separately. Moreover, the wind stress is capable of *advection* and *mixing*. Emphasis was put on the interaction of these two effects.

The model reduces to two coupled highly non-linear prognostic equations for the buoyancy and mixed-layer depth. Numerical solutions were obtained by quadrature in time. The main results are: (i) the front is never symmetric, (ii), in the case of

weak mixing, the asymmetry is most pronounced in the pycnocline strength and in the mixed-layer depth, while the buoyancy field is almost symmetric about the center of the front, (iii), in the case of strong mixing, the asymmetry is most pronounced in the buoyancy field and frontolysis may occur, (iv), after about one month, the Ekman downwelling resulting from convergence strongly controls the rate of deepening, and (v) frontal density gradients are about three times larger in the case of confluence than in the case of convergence.

The relative importance of mixing to advection is measured by a mixing parameter, which results from scaling. It is related to the Rossby and Richardson numbers. In the case of large-scale oceanic fronts as those in the North Pacific Ocean, this mixing parameter is of order one, implying that wind mixing is as important as wind-driven advection. Zero-mean fluctuations superimposed on the mean wind-stress field would change mixing but not advection. These can thus be modelled by increasing the value of the mixing parameter. For very large values of the mixing parameter, frontolysis occurs on the side of low-density advection and strongly weakens the front.

Since dissipation was neglected, the solution of the present model does not reach a steady state; a front is forming and sharpening endlessly with time. The model therefore does not yield any length scale for the width of the frontal zone. However, when the front is sufficiently sharp, dissipation will play a dominant role and force the system to a steady state. Hence the

length scale for the width of the front is believed to be controlled by dissipation.

Finally, since there is no advection where the wind stress vanishes, a coastal wall can be placed at the middle of the front, without altering the solution. Results of convergence are thus applicable to a coastal downwelling, forced by a longshore wind stress increasing offshore. If the mixing parameter is of order one, it is observed that the maximum downwelling does not occur at the coast but somewhat offshore (Figure 32).

CHAPTER SIX

SUMMARY AND DISCUSSION

A new theory of mixing and convection is developed and then applied to three cases: (i) the deepening of the wind-mixed layer, (ii) penetrative convection due to surface cooling, and (iii) upper-ocean frontogenesis by convergence of Ekman transports.

The theory of the model (Chapter 2) is based on the concept of a two-fluid system: *thermals* carrying the information from the boundaries of the system toward the interior, and *anti-thermals* forming the return flow required by continuity of mass. The governing equations are derived from the general dynamical theory developed by Kelly (1964), Green and Naghdi (1965), and Truesdell (1969). Pairs of equations are written for two interacting Boussinesq fluids in a rotating frame, and interaction terms are parametrized in order to adapt the theory to geophysical situations. Each pair meets an Invariance Principle as a consequence of reciprocity in the roles played by thermals and anti-thermals. Each pair is transformed into an average equation for which interaction terms cancelled and a very simple equation linking the two fluid properties. An important parameter of the model is the fraction, f, of area occupied by thermals to the total area. A dynamic saturation equilibrium between thermals and anti-thermals is assumed. This implies a constant value of f throughout the system. Considerable simplification is obtained by assuming that the response time of turbulence is much less than the time scale of

evolution of the overall system. This assumption is realized in all geophysical situations and is a generalization of various assumptions previously stated by Denman (1973), Niiler (1975), Niiler and Kraus (1977), and Garwood (1977) for the upper ocean, and by Lilly (1968), Tennekes (1973), and Lenschow *et al.* (1980), for the atmospheric boundary layer. The model neglects dissipation, and its validity extends to any convective situation where molecular viscosity and diffusivity may be neglected.

The theory is first applied to the study of the deepening of the wind-mixed layer (Chapter 3). The one-dimensional and frictionless model neglects the turbulence production by the mean-flow shear in the thermocline. The potential-energy increase required for deepening is thus supplied by the turbulence input at the surface (turbulent erosion model). A non-similar analytical solution is found in the case of a well-mixed layer bounded below by a sharp thermocline, treated as a boundary layer. That solution is valid if the frictional Richardson number, Ri, defined as the ratio of the total mixed-layer buoyancy to the square of the vertical-velocity scale, is much greater than unity. The model predicts an entrainment rate proportional to Ri^{-1}, and a ratio of thermocline thickness to mixed-layer depth of the order of $Ri^{-3/4}$. The thermocline shallows as $h^{-1/2}$, as the mixed-layer depth, h, increases with time. The vertical structure throughout the mixed layer and thermocline is given by the analytical solution. Vertical profiles of mean values and vertical fluxes are calculated. The comparison of these profiles with those obtained by turbulence-

closure numerical models is favorable.

The same model is applied to the study of penetrative convection in the upper ocean due to surface cooling (Chapter 4). The model is still one-dimensional, but dissipation is included, since dissipative effects are more important when the mixing region is deeper. An analogous non-similar analytical solution is found in the case of a well-mixed layer bounded below by a sharp thermocline. That solution is valid if the Richardson number, Ri, is much greater than unity. The model predicted a deepening rate proportional to $Ri^{-3/4}$, a constant thermocline thickness, and a ratio of thermocline thickness to mixed-layer depth proportional to $Ri^{-3/4}$. If the surface heat flux is constant, the mixed layer deepens in time as $t^{1/2}$. The vertical structure throughout the mixed layer and thermocline is given by the analytical solution. The agreement of mean temperature and vertical fluxes with laboratory experiments is excellent. Moreover, the results of the present analytical calculations are comparable to that of turbulence-closure numerical models.

Advective effects and their interactions with mixing were studied in a case of upper-ocean frontogenesis (Chapter 5). A bulk model including both advection and mixing is derived based on the one-dimensional model developed in Chapter 3. Continuity of mass near the front requires that water masses either downwell (*convergence*) or escape laterally (*confluence*). This distinction led to a study of these two different cases, each treated separately.

Interactions between advection and mixing result in important cross-front asymmetries in properties such as mixed-layer depth, thermocline strength, and/or mixed-layer density. These asymmetries have been observed (Roden, 1976 and 1980). Results also show that there exists a critical time scale within which mixing dominates and beyond which advection controls frontogenesis. For a mixed layer about one hundred meters thick, this time scale is of the order of one month. Strong mixing is shown to be able to induce frontolysis on the front side of light-water advection. Frontal density gradients are about three times larger in the case of confluence than in the case of convergence. Dissipation is neglected, and the model does not reach a steady state. Hence, the length scale for the width of the front (believed to be controlled by dissipation in a steady state) is not provided by the model.

Although the theory presented in chapter two is very general, the subsequent applications are restricted by various simplifying assumptions, such as absence of dissipation, large Richardson number, and decoupling between wind mixing and surface cooling. The scope of this work is to present a better understanding of the fine structure of turbulence in the upper ocean. This understanding could only be acheived by a clear presentation of analytical solutions corresponding to various particular cases. The author is aware of the limitations brought by those simplifying assumptions and of the resulting restricted applicability of the mathematical formulae presented herein. More general and more accurate results can be sought by numerical solutions of the general equations pro-

posed in chapter two.

The applicability of the general theory of chapter two is based on the assumption of a saturation equilibrium between thermals and anti-thermals, which leads to assigning a constant value to f, the fraction of area occupied by thermals to the total area. Although this assumption is supported by physical arguments and various observations, it may fail in particular situations like the incipient deepening of convection or in restricted regions such as those very near the surface or at the bottom of the thermocline. A discussion of possible variations of f was presented in an appendix to chapter three. It was concluded that, if such a region of non-constant f exists, it is very limited and does not affect the overall behavior of the system. On the other hand, the good agreement of the results with observations and with previous models, despite various other simplifications, is very encouraging.

This work also ignores the presence of internal gravity waves generated by turbulence. Although waves are important as a mechanism capable of extracting kinetic energy from the system, the study of their effects on mixing and convection is a recent subject of research, one which is in its early stage of development, and no acceptable parametrization has yet been proposed for geophysical situations.

The model can be applied to various other cases related to geophysical fluids. The coupled problem of wind mixing and surface cooling/heating can be investigated as a direct application of the results presented in chapters three and four. The model is also

directly applicable to convection in the atmospheric boundary layer under a cloud-topped inversion. Moisture can be incorporated in the formalism without major problems. A dual application of the model can be that of convection in the lower atmospheric layers above mixing and convection in the upper oceanic layers. Surface air and sea temperatures and surface heat flux would then be the unknowns in the problem. An intersting case would be that of double penetrative convection, in the atmosphere and the sea, past mid-fall and during winter when the water is warmer than the air.

REFERENCES

Ball, F. K., 1960: Control of inversion height by surface heating. *Quart. J. R. Met. Soc.*, 86, 483-494.

Betts, A. K., 1973: Non-precipitating cumulus convection and its parametrization. *Quart. J. R. Met. Soc.*, 99, 178-196.

Carson, D. J., 1973: The development of a dry inversion-capped convectively unstable boundary layer. *Quart. J. R. Met. Soc.*, 99, 450-467.

Deardorff, J. W., 1974: Three-dimensional numerical study of the height and mean structure of a heated planetary boundary layer. *Boundary-Layer Meteorol.*, 7, 81-106.

Deardorff, J. W., G. E. Willis and D. K. Lilly, 1969: Laboratory investigation of non-steady penetrative convection. *J. Fluid Mech.*, 35, 7-31.

Denman, K. L., 1973: A time-dependent model of the upper ocean. *J. Phys. Oceanogr.*, 3, 173-184.

Denman, K. L., and M. Miyake, 1973: Upper layer modification at Ocean Station *Papa*: Observations and simulation. *J. Phys. Oceanogr.*, 3, 185-196.

de Szoeke, R. A., and P. B. Rhines, 1976: Asymptotic regimes in mixed-layer deepening. *J. Mar. Res.*, 34, 111-116.

Dillon, T. M., and T. M. Powell, 1979: Observations of a surface mixed layer. *Deep-Sea Res.*, 26A, 915-932.

Garwood, R. W., Jr., 1977: An oceanic mixed layer model capable of simulating cyclic states. *J. Phys. Oceanogr.*, 7, 455-468.

Gill, A. E., and J. S. Turner, 1976: A comparison of seasonal thermocline models with observation. *Deep-Sea Res.*, 23, 391-401.

Grant, D. R., 1965: Some aspects of convection as measured from aircraft. *Quart. J. R. Met. Soc.*, 91, 268-281.

Green, A. E., and P. M. Naghdi, 1965: A dynamical theory of interacting continua. *Int. J. Engng. Sci.*, 3, 231-241.

Halpern, D., 1974: Observations of the deepening of the wind-mixed layer in the northeast Pacific Ocean. *J. Phys. Oceanogr.*, 4, 454-466.

Heidt, F. D., 1977: The growth of the mixed layer in a stratified fluid due to penetrative convection. *Boundary-Layer Meteorol.*, 12, 439-461.

Kaimal, J. C., J. C. Wyngaard, D. A. Haugen, O. R. Coté and Y. Izumi, 1976: Turbulence structure in the convective boundary layer. *J. Atm. Sci.*, 33, 2152-2169.

Kantha, L. H., O. M. Phillips and R. S. Azad, 1977: On turbulent entrainment at a stable density interface. *J. Fluid Mech.*, 79, 753-768.

Kato, H., and O. M. Phillips, 1969: On the penetration of a turbulent layer into a stratified fluid. *J. Fluid Mech.*, 37, 643-665.

Kelly, P. D., 1964: A reacting continuum. *Int. J. Engng. Sci.*, 2, 129-153.

Kim, J. W., 1976: A generalized bulk model of the oceanic mixed layer. *J. Phys. Oceanogr.*, 6, 686-695.

Klein, J. P., 1980: Modélisation des mécanismes turbulents dans les couches marines superficielles. Thèse de doctorat d'Etat, Université d'Aix, Marseille II France, 167 pp.

Kraus, E. B., and J. S. Turner, 1967: A one-dimensional model of the seasonal thermocline. II. The general theory and its consequences. *Tellus*, 19, 98-105.

Kullenberg, G., 1977: Entrainment velocity in natural stratified vertical shear flow. *Estuarine and Coastal Mar. Sci.*, 5, 329-338.

Kundu, P. K., 1980a: A numerical investigation of mixed-layer dynamics. *J. Phys. Oceanogr.*, 10, 220-236.

Kundu, P. K., 1980b: Consequences of self-similarity in stress-driven entrainment experiments. Submitted to *J. Fluid Mech.*

Lenschow, D. H., 1970: Airplane measurements of planetary boundary layer structure. *J. Appl. Meteor.*, 9, 874-884.

Lenschow, D. H., 1973: Two examples of planetary boundary layer modification over the Great Lakes. *J. Atm. Sci.*, 30, 568-581.

Lenschow, D. H., 1974: Model of the height variation of the turbulence kinetic energy budget in the unstable planetary boundary layer. *J. Atm. Sci.*, 31, 465-474.

Lenschow, D. H., and W. B. Johnson, 1968: Concurrent airplane and balloon measurements of atmospheric boundary-layer structure over a forest. *J. Appl. Meteor.*, 7, 79-89.

Lenschow, D. H., J. C. Wyngaard and W. T. Pennell, 1980: Mean-field and second-moment budgets in a baroclinic, convective boundary layer. *J. Atm. Sci.*, 37, 1313-1326.

Lilly, D. K., 1968: Models of cloud-topped mixed layers under a strong inversiton. *Quart. J. R. Met. Soc.*, 94, 292-309.

Linden, P. F., 1975: The deepening of a mixed layer in a stratified fluid. *J. Fluid Mech.*, 71, 385-405.

Long, R. R., 1978: The growth of the mixed layer in a turbulent stably stratified fluid. *Geophys. Astrophys. Fluid Dyn.*, 11, 1-12.

MacVean, M. K., and J. D. Woods, 1980: Redistribution of scalars during upper ocean frontogenesis: a numerical model. *Quart. J. R. Met. Soc.*, 106, 293-311.

Manton, M. J., 1975: Penetrative convection due to a field of thermals. *J. Atm. Sci.*, 32, 2272-2277.

Mellor, G., and P. A. Durbin, 1975: The structure and dynamics of the ocean surface mixed layer. *J. Phys. Oceanogr.*, 5, 718-728.

Moore, M. J., and R. R. Long, 1971: An experimental investigation of turbulent stratified shearing flow. *J. Fluid Mech.*, 49, 635-655.

Niiler, P. P., 1975: Deepening of the wind-mixed layer. *J. Mar. Res.*, 33, 405-422.

Niiler, P. P., 1977: One-dimensional models of the seasonal thermocline, *The Sea*, Vol. 6, *Marine Modeling*, Goldberg et al., Eds., Wiley, 97-115.

Niiler, P. P., and E. B. Kraus, 1977: One-dimensional models of the upper ocean. *Modelling and Prediction of the Upper Layers of the Ocean*, E. B. Kraus, Ed., Pergamon Press, 143-172.

Piacsek, S. A., 1968: Numerical experiments on convective flows in geophysical fluid systems, *Proc. Seventh Symp. on Naval Hydrodynamics*, Rome, Italy, 753-783.

Pollard, R. T., P. B. Rhines and R. O. R. Y. Thompson, 1973: The deepening of the wind-mixed layer. *Geophys. Fluid Dyn.*, 4, 381-404.

Price, J. F., 1979: On the scaling of stress-driven entrainment experiments. *J. Fluid Mech.*, 90, 509-529.

Price, J. F., C. N. K. Mooers and J. C. Van Leer, 1978: Observation and simulation of storm-induced mixed-layer deepening. *J. Phys. Oceanogr.*, 8, 582-599.

Priestley, C. H. B., 1959: *Turbulent transfer in the lower atmosphere*. University of Chicago Press, 130 pp.

Roden, G. I., 1976: On the structure and prediction of oceanic fronts. *Naval Res. Rev.*, 29, (3), 18-35.

Roden, G. I., 1980: On the subtropical front zone north of Hawaii during winter. *J. Phys. Oceanogr.*, 10, 342-362.

Roden, G. I., and D. F. Paskausky, 1978: Estimation of rates of frontogenesis and frontolysis in the North Pacific Ocean using satellite and surface meteorological data from January 1977. *J. Geophys. Res.*, 83, 4545-4550.

Roisin, B., 1979: Penetrative convection: modelling with discrete convecting elements. *Geophysical Fluid Dynamics,* Woods Hole Oceanogr. Inst. WHOI-79-84, 1-28.

Scorer, R. S., 1978: *Environmental aerodynamics,* Ellis Horwood Limited, John Wiley, 488 pp.

Spiegel, E. A., and G. Veronis, 1960: On the Boussinesq approximation for a compressible fluid. *Astrophys. J.*, 131, 442-447.

Telford, J. W., and J. Warner, 1964: Fluxes of heat and vapor in the lower atmosphere derived from aircraft observations. *J. Atm. Sci.*, 21, 539-548.

Tennekes, H., 1973: A model for the dynamics of the inversion above a convective boundary layer. *J. Atm. Sci.*, 30, 558-567.

Truesdell, C., 1969: *Rational Thermodynamics. A Course of Lectures on Selected Topics.* McGraw-Hill, 208 pp.

Turner, J. S., 1969: A note on wind mixing at the seasonal thermocline. *Deep-Sea Res.*, Suppl. Vol. 16, 297-300.

Turner, J. S., 1973: *Buoyancy Effects in Fluids,* Cambridge Univ. Press , 367 pp.

Turner, J. S., and E. B. Kraus, 1967: A one-dimensional model of the seasonal thermocline. I. A laboratory experiment and its application. *Tellus,* 19, 88-97.

Warn-Varnas, A. C., and S. A. Piacsek, 1979: An investigation of the importance of third-order correlations and choice of length scale in mixed layer modelling. *Geophys. Astrophys. Fluid Dyn.*, 13, 225-243.

Warner, J., and J. W. Telford, 1967: Convection below cloud base. *J. Atm. Sci.*, 24. 374-382.

Willis, G. E., and J. W. Deardorff, 1974: A laboratory model of the unstable planetary boundary layer. *J. Atm. Sci.*, 31, 1297-1307.

Wyngaard, J. C., O. R. Coté and Y. Izumi, 1971: Local free convection, similarity, and the budgets of shear stress and heat flux. *J. Atm. Sci.*, 28, 1171-1182.

Yamada, T., and G. Mellor, 1975: A simulation of the Wangara atmospheric boundary layer. *J. Atm. Sci.*, 32, 2309-2329.

Zeman, O., and J. L. Lumley, 1976: Modelling buoyancy driven mixed layers. *J. Atm. Sci.*, 33, 1974-1988.

Zilitinkevich, S. S., D. V. Chalikov and Y. D. Resnyansky, 1979: Modelling the oceanic upper layer, *Oceanol. Acta*, 2, 2, 219-240.

VITA

Benoit Cushman-Roisin was born December 17, 1954, in Wellin, Belgium. In July, 1978, he received the degree of Physicist Civil Engineer, Summa Cum Laude, at the University of Liège, Belgium. In partial fulfillment of that degree, he wrote a thesis on three-dimensional models of marine circulation. He began his doctoral program in the Geophysical Fluid Dynamics Institute at the Florida State University in the Fall of 1978. During the Summer of 1979, he participated in the Geophysical Fluid Dynamics Summer Institute at the Woods Hole Oceanographic Institution.

In 1973, Benoit Cushman-Roisin received an award of the Mathematical Association of America, in 1978, a CRB Fellowship of the Belgian American Educational Foundation, and, in 1979, a Pre-doctoral Fellowship of the Woods Hole Oceanographic Institution.

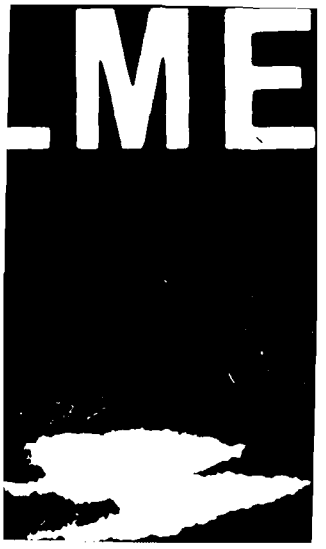
LME